Copyright Warning & Restrictions

The copyright law of the United States (Title 17, United States Code) governs the making of photocopies or other reproductions of copyrighted material.

Under certain conditions specified in the law, libraries and archives are authorized to furnish a photocopy or other reproduction. One of these specified conditions is that the photocopy or reproduction is not to be "used for any purpose other than private study, scholarship, or research." If a, user makes a request for, or later uses, a photocopy or reproduction for purposes in excess of "fair use" that user may be liable for copyright infringement,

This institution reserves the right to refuse to accept a copying order if, in its judgment, fulfillment of the order would involve violation of copyright law.

Please Note: The author retains the copyright while the New Jersey Institute of Technology reserves the right to distribute this thesis or dissertation

Printing note: If you do not wish to print this page, then select "Pages from: first page # to: last page #" on the print dialog screen

INFORMATION TO USERS

This manuscript has been reproduced from the microfilm master. UMI films the text directly from the original or copy submitted. Thus, some thesis and dissertation copies are in typewriter face, while others may be from any type of computer printer.

The quality of this reproduction is dependent upon the quality of the copy submitted. Broken or indistinct print, colored or poor quality illustrations and photographs, print bleedthrough, substandard margins, and improper alignment can adversely affect reproduction.

In the unlikely event that the author did not send UMI a complete manuscript and there are missing pages, these will be noted. Also, if unauthorized copyright material had to be removed, a note will indicate the deletion.

Oversize materials (e.g., maps, drawings, charts) are reproduced by sectioning the original, beginning at the upper left-hand corner and continuing from left to right in equal sections with small overlaps. Each original is also photographed in one exposure and is included in reduced form at the back of the book.

Photographs included in the original manuscript have been reproduced xerographically in this copy. Higher quality 6" x 9" black and white photographic prints are available for any photographs or illustrations appearing in this copy for an additional charge. Contact UMI directly to order.

UMI

A Bell & Howell Information Company
300 North Zeeb Road, Ann Arbor, MI 48106-1346 USA
313/761-4700 800/521-0600

ABSTRACT

PARTICLE DEPOSITION ON SURFACE IN A DIVERGENT CHANNEL FLOW

by
Ding Sun

Particle trajectory and deposition of two phase gas-solid flows in a convergent or divergent two-dimensional channel are investigated numerically in a wide range of parameters. For the fluid phase, a two dimensional, incompressible laminar fluid flow is considered in the analysis. The particle phase is a diluted suspension. The effects of inertia, gravity, viscous force and electrostatic image force are included in the computational model.

Both convergent and divergent channel flow are solved by the finite element method based on the software FIDAP. The flow separations will appear in a divergent channel and their separation positions are obtained in the computation. The governing equations of particle motion are built upon the Lagrangian trajectory method and are solved with the forth- order Runge-Kutta method. A computer simulation procedure is developed to find the trajectory of each particle entering a channel. Particle depositions are calculated based on the distance for a particle to reach the wall. Many computations for deposition are performed on combinations of different parameters, such as charge parameter Q, gravity parameter G, and inertia parameter S.

The ranges of parameters are θ=2.5° to 7.5°, S=0.01 to 100, G=0.01 to 100, Q=0.00001 to 10000, Re=100, and L/h_o=40.

Results under the influence of inertia, viscous, gravity and image forces indicate that particle trajectory in a channel is dependent upon these combined effects. A closer initial particle position to the channel wall may not mean a faster moving to the wall.

Either in a convergent channel or a divergent one, the maximum longest deposition distance keeps the range of Q/G=0.1 to 1, and their deposition distance curves are almost the same after Q/G<0.001. The influence due to varying image forces and gravity is important to the particle deposition fraction. Generally, Q/G is greater or equal to 10, the gravity effect to deposition can be neglected, while the charge effect to deposition fraction can also be neglected at Q/G<0.001. The deposition decreases with increasing S for all Q and G. The particle deposition fraction increases always with increasing X displacement and the channel angle effect to the deposition fraction is smaller as compared with other effects. As small divergent channel cases, the back flow effect can also be neglected in limited channel length ranges.

PARTICLE DEPOSITION ON SURFACES IN A DIVERGENT CHANNEL FLOW

by
Ding Sun

A Dissertation
Submitted to the Faculty of
New Jersey Institute of Technology
In Partial Fulfillment of the Requirements for the Degree of
Doctor of Philosophy

Department of Mechanical and Industrial Engineering

October 1995

APPROVAL PAGE

PARTICLE DEPOSITION ON SURFACES IN A DIVERGENT CHANNEL FLOW

Ding Sun

1995

Dr. Rong Yaw Chen, Thesis Advisor — Date
Professor of Mechanical Engineering, NJIT

Dr. John Droughton — Date
Professor of Mechanical Engineering, NJIT

Dr. Ernest Geskin — Date
Professor of Mechanical Engineering, NJIT

Dr. Robert Kirchner — Date
Professor of Mechanical Engineering, NJIT

Dr. Mengchu Zhou — Date
Assistant Professor of Electrical Engineering, NJIT

BIOGRAPHICAL SKETCH

Author: Ding Sun

Degree: Doctor of Philosophy in Mechanical Engineering

Date: October 1995

Undergraduate and Graduate Education:

- Doctor of Philosophy in Mechanical and Industrial Engineering
  New Jersey Institute of Technology,
  Newark, NJ, 1995
- Doctor of Science in Engineering
  Shanghai Jiao Tong University, China, 1987
- Master of Science in Engineering
  Shanghai Jiao Tong University, China, 1984
- Bachelor of Science in Engineering
  Harbin Shipbuilding Engineering Institute, China, 1981

Major: Mechanical Engineering

Presentation and Publications:

Chen, R. Y., Chiou, H. C., and D. Sun,
"Deposition of Particles in a Convergent Channel"
Powder Technology, 1995

Chen, R. Y. and D. Sun,
"Particle Deposition on Surfaces in a Divergent Channel Flow"
The 6th International Symposium on Gas-Solid Flows

South Carolina, August, 1995

This dissertation is dedicated to my parents

ACKNOWLEDGEMENT

The author would like to express his sincere gratitude to his advisor, Dr. Rong-Yaw Chen, who provided many valuable suggestions, magnificent guidance and continuous encouragement throughout the course of the entire investigation.

The author wishes to express his many thanks to Drs. J. V. Droughton, E. Geskin, R. Kirchner and M. Zhou for serving as members of committee, having kindly read through the original manuscript and providing valuable suggestions. The author also would like to thank the valuable members of the Mechanical Engineering Department for their help and continuous support. Additionally, sincere thanks to Mr. Weiting Huang for his help in this study.

The author would like to extend a special thanks to his immediate family. Many thanks go to his father and mother, and to his wife Mingming Ge and lovely son for their generous dedication and firm support.

TABLE OF CONTENTS

TABLE OF CONTENTS
(Continued)

LIST OF TABLES

LIST OF FIGURES

LIST OF FIGURES
(Continued)

Figure **Page**

LIST OF FIGURES
(Continued)

Figure **Page**

LIST OF FIGURES
(Continued)

LIST OF FIGURES
(Continued)

Figure **Page**

LIST OF FIGURES
(Continued)

LIST OF FIGURES
(Continued)

Figure **Page**

LIST OF FIGURES
(Continued)

Figure **Page**

LIST OF FIGURES
(Continued)

LIST OF SYMBOLS

Symbol

a	particle radius
Br	Brown number
C_D	drag coefficient of a particle
D	diameter of a particle
D_p	particle diffusivity
E	electric field strength
f_x, f_y	particle image force components
F_D	viscous drag force
F_e	electric force
F_L	lift force
g	gravity acceleration constant
G	dimensionless gravitational force parameter
Gc	coefficient of Cunningham slip correction
h_o	half the channel width
H	half of the dimensionless channel width
Kn	Knudsen number
m	mass of a particle
Ma	Mach number
n	number of image pairs
N	total number of image pairs
p	fluid pressure
q	electric charge per particle
Q	dimensionless image force parameter

LIST OF SYMBOLS
(continued)

Symbol

q_n	distance between the point charge to the primary image n
$q_{n'}$	distance between the point charge to the secondary image n'
r,s	natural coordinates
Re	Reynolds number of fluid
Re_p	Reynolds number of particle
Ri	weighted residuals of Galerkin method
S	dimensionless inertia parameter
Sc	Schmidt number
t	time variable
T	dimensionless time variable
u,v	x, y components of fluid velocity
u_p,v_p	x, y components of particle velocity
u_o	inlet velocity of fluid
U,V	dimensionless X, Y components of fluid velocity
U_p,V_p	dimensionless X, Y components of particle velocity
U_o	dimensionless inlet velocity of fluid
V	electric potential
w_o	relative velocity between particle and fluid
x_m	horzontal distance from the charge point to the center of image circle
x,y	horizontal and vertical coordinates
X,Y	dimensionless horizontal and vertical coordinates
y_o	inlet particle
y_l	inlet particle coordinate where particles deposit on the lower channel wall
y_u	inlet particle coordinate where particles deposit on the upper channel wall

LIST OF SYMBOLS
(continued)

Symbol

Y_l dimensionless inlet particle coordinate where particles deposit on the lower channel wall

Y_u dimensionless inlet particle coordinate where particles deposit on the upper channel wall

Y_o dimensionless inlet coordinate

Greek Letters

ε_o permitivity of free space

$\varepsilon_u, \varepsilon_F$ tolerance of convergence criterion

θ polar angle coordinate of inlet point

ρ gas density

ρ_p particle density

α_o angle between the center line and the line from the charge to the center

α_n half the angle subtended by the chord connecting the charge to image n

$\alpha_{n'}$ half the angle subtended by the chord connecting the charge to image n'

β_n angle between y-axis and the chord connecting the charge to the primary image n

$\beta_{n'}$ angle between y-axis and the chord connecting the charge to the primary image n'

μ viscosity of the fluid flow

ν kinematic viscosity

λ_i mean free path of particles

λ_g mean free path of gas

φ column vector of the interpolation function of fluid velocity

ψ column vector of the interpolation function of fluid pressure

Ω_E element domain

CHAPTER 1

INTRODUCTION

1.1 Fundamental and Practical Application

The micron-size particle or aerosols suspension in a fluid flow plays an important role in a wide variety of industrial and natural situations. They may be found in atmospheric processes, manufacturing, air pollution control technology, and in many other areas. Aerosol technology for practical purposes covers a broader range of application. Some examples in industry are:

Dust collectors --- The devices that have been manufactured for particulate control represent a wide variety of approaches. Mechanical devices for gravitational or inertial separation are mechanical collectors, including gravity or momentum settlers and cyclones; electrical forces for deposition are utilized by electrostatic precipitators; filtration of materials through fibrous mats or packed beds are utilized in filtration and wet scrubbers.

Fluidized beds --- A fluidized bed is simply a volume of inert particles, e.g., fine coal, which are supported by a grate-like air distributor. When air is blown through the bed mass, the solid particles are lifted and suspended by the air. The particles can move freely, and the bed behaves like a fluid. Fluidized beds are frequently used in industry to promote heat transfer or chemical reactions.

Pneumatic conveyors --- Bulk of solids can be transported by suspension in a gas or liquid. Long pipelines have been built for the transport of powdered coal, cement, and other suitable materials. When the velocity and turbulence level in a flow are high enough, they work against gravity to keep the particles suspended.

Clean room technology --- Clean rooms are used in manufacturing industries such as semiconductor, printed circuit board, computer disk drive, aerospace, medical device and pharmaceutical industries to provide a low contaminant environment. Since the

products are quite sensitive to sub micron particles, particulate contamination has a major impact on the production rate. The contaminant particle sources in a clean room need to be identified and properly controlled to improve the quality of the clean room.

Spray injection equipment --- Combustion of powdered coal is a well-known technique in which the fine powder must be injected into a combustion chamber by means of a carrier gas. The use of devices to disperse quantities of pesticides for agricultural or public health applications almost always utilizes two phase flows in the form of sprays or suspended powders. Solid rocket propellants often contain fine metal powders to improve performance.

Therefore, knowledge of the behavior of particle suspensions is of considerable importance in technology, and investigation of particle suspensions has received much attention.

Motion of aerosols in an air stream occurs in most of the above applications. Transport of aerosol particles by flowing air is usually accompanied by the process of particle deposition upon surfaces bounding the flow stream. The cases where particle deposition plays an important role are encountered in air pollution problems, clean room technology as well as inhalation toxicology. The problem of removing aerosols from gas has become important because of stringent environmental regulations to reduce health hazards, limit nuisance dust, and recover valuable products, and in particular, the recent need of microelectronics and computer manufacturing industries to control micro-contamination processes.

A wide variety of commercial equipment used for collecting aerosols relies on aerosols depositing on surfaces which are then cleaned or removed. Typical examples, as stated above, are fibrous filters and electrostatic precipitators which use plane or cylindrical surfaces to capture the aerosol particles. In each device, the deposition process always presents a model of the fluid flow field around the object or target.

1.2 Basic Concepts of Particle Dynamics

Studies of particle dynamics in a fluid have followed two methods of approach:

1. Treating the dynamics of single particles and then trying to extend to a multiple particle system in an analogous manner as in kinetic theory. The general equation of motion is based on treatments of particle dynamics by Basset, Boussinesq, and Oseen[43] and is essentially an application of Newton's second law:

$$\left(\frac{\pi D^3 \rho_p}{6}\right)\frac{du_p}{dt} = \left(\frac{\pi D^3 \rho_p}{6}\right)\left(\frac{3C_D\rho}{4D\rho_p}\right)\left|u-u_p\right|\left(u-u_p\right) - \left(\frac{\pi D^3}{6}\right)\frac{\partial p}{\partial x} + \frac{1}{2}\left(\frac{\pi D^3}{6}\right)\rho\frac{d}{dt}\left(u-u_p\right) + \left(\frac{3D^2}{2}\right)\sqrt{\pi\rho\mu}\int_{t_0}^{t}\frac{\left(du/dt'\right)-\left(du_p/dt'\right)}{\sqrt{t-t'}}dt' + external\,force$$

where p, t, and x represent the gas pressure, the time and position coordinates, respectively; t' is the integration variable and is the time of the start of the motion, D is the diameter of the particle and C_D is the drag coefficient.

2. Considering the particulate phase as a continuum and applying integral balances in order to derive the field and constitutive equations leads to a continuum mechanics description of multiphase flow. For a simple case when a flow is an incompressible, two-dimensional and steady laminar flow upon introduction of particles to the fluid phase, the governing equations will be:

$$\frac{\partial u}{\partial x} + \frac{\partial v}{\partial y} = 0$$

$$u\frac{\partial u}{\partial x} + v\frac{\partial u}{\partial y} = -\frac{1}{\rho}\frac{dp}{dx} + \frac{\mu}{\rho}\frac{\partial^2 u}{\partial y^2}$$

$$u_p \frac{\partial u_p}{\partial x} + v_p \frac{\partial u_p}{\partial y} = \bar{F}(u - u_p) + \frac{D_p}{\rho_p} \frac{\partial}{\partial y}\left(\rho_p \frac{\partial u_p}{\partial y}\right)$$

$$u_p \frac{\partial v_p}{\partial x} + v_p \frac{\partial v_p}{\partial y} = \bar{F}(v - v_p)$$

$$u \frac{\partial \rho_p}{\partial x} + v \frac{\partial \rho_p}{\partial y} = D_p \frac{\partial^2 \rho_p}{\partial y^2}$$

where:

$$\bar{F} = F^*\left[9(\bar{\mu}/2a^2)\rho_p\right]\left[1 + (\rho/2\bar{\rho}_p)\right]^{-1}$$

$$F^* = (C_D/24)\left[2a(\bar{\rho}|\bar{v} - \bar{v}_p|)/\bar{\mu}\right]$$

D_p: particle diffusivity

a: radius of a particle

For the dynamics of single particles, the first formulation appears to have been derived in the 19th century. The continuum mechanics of multi-phase flow began by 1960. Now, both of the methods have been studied extensively. Gas-solid flows involve many different phenomena such as particle-fluid interaction, particle-particle interaction, particle-wall interaction and the effect of the existing force field. The importance of these effects vary in relation to each other. Hence, the two methods are restricted to specific application cases, respectively. The solution of motion of the single particle equations is not the way to determine the behavior of a cloud of particles. However, continuum mechanics is unfortunately restricted to cases where the continuum approximation are valid, i.e., for small size and low inertia particles, and where some external force fields can be ignored, e.g., electrostatic image force field. It is also limited to giving the general phase configuration solutions of multiphase flow, and is not able to trace the trajectories of single particles.

1.3 Aerosol Particles

The particle size of interest for gas-solid flows ranges from a fraction of a micrometer to several millimeters. Several typical sizes are indicated below:

Table 1.1 Typical Particle Size

Material	Approx. size(μm)
Tobacco smoke	0.01 - 1
Oil smoke	0.03 - 1
Coal dust	1 - 100
Fly dust	1 - 200
Fog	2 - 80

The shapes of particulate matter are, in general, non-spherical. The spherical shape is a special case or an idealization of irregular shapes. Model particles are treated as smooth, inert, rigid spheres in near-thermodynamic equilibrium with their surrounding. The particle concentration is very much less than the gas molecule concentration. In such an idealized model, the typical ranges of the parameter for particles found in atmospheres are included in following table:

Table 1.2 Particle Parameter Ranges

	Particles	Gas	Atmospheric aerosols	Air (sea level)
Number density(cm^{-3})	n_i	n_g	10^2-10^5	10^{19}
Mean temperature(^oK)	T_i	T_g	$T_g \approx T_i$	240 - 310
Mean velocity(cm/s)	v_i	v_g	10^{-2}-10^3	0 -10^3
Mean free path(cm)	λ_i	λ_g	$> 10^2$	6×10^{-6} (N_2)

Table 1.2(Continued) Particle Parameter Ranges

Particle radius(cm)	a_i	a_g	10^{-6}-10^{-3}	1.9×10^{-8} (N_2)
Particle mass (g)	m_i	m_g	10^{-18}-10^{-9}	4.6×10^{-23}(N_2)
Particle charge(units	$\pm q$	weakly		weakly ionized
of elementary charge)		ionized		single charge
Aerodynamic length	L_i	L_g	$L_i \approx a_i$	$L_g \to \infty$

The subscript i refers to the ith class, and g refers to the gas. Generally, the idealization requires that the size(radius) $a_g/a_i<1$ and mass ratio $m_g/m_i<<1$.

Moreover, in the dynamics of two phase flow there are four dimensionless parameters to be used to describe particle behaviors. The four basic parameters for aerosols in the single-particle regime[38] are:

Knudsen number --- $Kn = \lambda_g / a_i$

Mach number --- $Ma = |v_i - v_g| / \bar{q}_g$

Schmidt number --- $Sc = a_i^2 n_g \lambda_g$

Brown number --- $Br = \bar{q}_i / \bar{q}_g$

Here, $\bar{q}_g$ and $\bar{q}_i$ are the mean thermal speeds of gas and particle, respectively. There is a relationship between the Reynolds number ($Re = v_i a_i / v_g$) and Ma, Kn. It is $Re \approx 4\,Ma / Kn$. The Knudsen number Kn specifies the extent to which the system departs from that given by continuum dynamics. The Schmidt and Brown numbers Sc and Br indicate the degree of importance of thermal agitation of the particles.

1.4 The Scope of this Work

The objective of this study is to analyze the deposition rate of particles on the surface in a channel flow. Since the deposition is a complex phenomenon that involves a variety of

factors, in order to predict the performance of deposition effectively, the complete flow mechanism of the particulate phase has to be examined, the significance of parameters involved has to be identified, and a mathematical model to simulate the flow and deposition process has to be developed.

Since micro-size particles (0.01 μm ~ 100 μm) with a dilute suspension in a flow are the main concern of this work, their presence in the fluid is assumed to have no effect on the fluid phase. Incompressible, two-dimensional and laminar flow will be taken into consideration for the present investigation. Most of the previous works in this field concentrated only on fully developed flows in a parallel horizontal or parallel vertical channel. Therefore, this work will concentrate on an angled channel flow case, especially on the divergent one. The laminar fluid phase from developing to fully developed flow will be solved numerically by the finite element method, using sophisticated CFD software FIDAP on the sun work-station. In addition, the situation of the flow with separation in a divergent channel will be investigated, and the separation point will be determined.

Many practical problems involving suspension of particles are at relatively low particle number density. The particulate concentration in this work will be a dilute suspension phase in a range of 10^{-5} per cubic centimeter. The forces that affect the motion of particles in the situation are inertia, gravity, viscous force and electrostatic force. In particular, the effect of the electrostatic force due to the charge borne by particles on the deposition efficiency has lately attracted much attention. This is due to the fact that aerosol deposition experiments often yield higher deposition than that based on calculation of gravitational setting. Practically all aerosols or particles, natural or artificial, are electrostaticly charged. The charged force may arise in two ways: (1) by the mutual electrostatic repulsion between particles, and (2) by the charge induced on the walls, which is called the image force. When the particle number density is sufficiently low, the predominant effect is due to the image force.

This study stems from investigating the motion of particles on the principle of the Basset-Boussinesq-Oseen method under the coupled effects of above all forces. Then the resulting governing equations with association of boundary condition are solved numerically using the Runge-Kutta method of fourth order algorithm. The deposition rate can, therefore, be assessed on the solved trajectory of particles. These numerical works are carried out on an IBM486 by use of the advanced Quick-BASIC language. All results will be summed and also the characteristics of the rate of deposition curves for different flow parameters, together with the effect of channel angle, will be discussed in depth.

CHAPTER 2

LITERATURE SURVEY ON THE DEPOSITION OF PARTICLES IN TWO PHASE FLOW

A brief literature review in the chapter is made in order to have a better understanding of previous investigations. The difficulties of both analytical and experimental investigations have led to a large number of publications of many facets of gas-particle flow. For example, the books by Fuchs[33] and Soo[62] each list some 900 references. Clearly, it is not possible here to cover all aspects. This review is restricted to the studies on the internal flow of suspensions and deposition of suspended particles from laminar and turbulent flows.

In this field, the work of some early papers was reviewed in the book by Fuchs[33]. In 1957, Friedlander and Johnstone[32] conducted an experimental study of the rate of deposition of dust particles on the wall of a tube with an analysis of the mechanism of particles transport in a turbulent stream. They found that when a stream of gas carrying suspended particles flow in turbulent motion past a surface, the particles are deposited due to the radial fluctuating component of velocity. They also found that the net rate of deposition depends on both the rate of transport of the particles to the wall and the rate of re-entrainment; the second effect was reduced to a minimum by allowing only a single layer of particles to accumulate on the surface and by taking precautions to ensure adherence of all particles that struck the wall.

Stukel and Soo[67] experimentally investigated the hydrodynamics of a suspension with particles suspended in turbulent flow over the inlet of a channel formed by two parallel-plates made for various flow velocities, plate gap widths, and mass flow ratios of solids to air. Their study was undertaken to further the understanding of the aerodynamics of air pollution control equipment.

Experiments were carried out in a 12 inch by 12 inch subsonic wind tunnel with maximum tunnel speed of up to 120 ft/sec., place gap widths of 1/4, 1 and 2 inch, and mass flow ratios of particles to air varied from 0.01 to 0.1 lb. particles/lb air. They determined the particle and air velocities, the particulate mass flow and density distributions, and the particle size distribution as affected by the flow response.

It was found that for the nature of the developing turbulent boundary layer of dilute suspensions, the density of particles is higher at the wall than at the core because of the presence of charge on the particles induced by surface contacts. Furthermore, as analogous to rarefied gas motions, a particle slip velocity brought about by the lack of particle to particle collisions in the suspension at the wall was also observed. They, thus, concluded that similarity laws for the scaling of equipment for air pollution control should include the momentum transfer parameter and the electroviscous parameter in addition to the Reynolds number. The electroviscous number is especially important where the particles possess large charge-to-mass ratios.

The occurrence of deposition due to field forces was studied by Soo and Rodgers[63]. They defined a sticking probability, σ, which depends on material properties. This sticking probability is related to the force of adhesion of particles to a surface. It was found that $\sigma = 1$ when all particles drifting to the wall stick to or settle at the wall; and $\sigma = 0$ for complete re-entrainment.

Corn[21] showed that the electrical forces include contact potential difference and dipole effect, space charge and electronic structure. He also found that the effect of gravity alone produces settling, but the fact that a particle may again become re-entrained gives $\sigma < 1$. There is another sticking probability σ_w which concerns adhesion of particles at the immediate vicinity of the wall. Opposite to settling is the lifting of a particle in the shear flow of a fluid. This leads to a re-distribution of density of particle clouds and erosion of a bed of deposited particles.

The general case of a fully developed pipe flow of suspension in a turbulent fluid in gravitational and electric fields and a shear flow field was analyzed by Soo and Tung[64][65]. The influencing parameters that defined the state of motion include: pipe flow Reynolds number, Froude number, diffusion-response number, electro-diffusion number, momentum-transfer number and particle Knudson number. Additional considerations are diffusion and setting under field forces, the sticking probability of a particle at the wall and that to a bed of similar particles. Although they claimed that the method of solution could be extended to a laminar flow field, they did not carry out any study on laminar flow.

Hughmark [39] studied the deposition from a turbulent gas stream. He did an experiment to estimate the particle velocity as a function of the stopping distance, which is defined as the distance that a particle with a given initial velocity will move through a stagnant fluid. And, he claimed that data for 0.8μ particles in 0.54cm diameter pipe are not shown because these data are not in agreement with the other particle data. Also he added that the assumptions of equal particle and gas diffusion, stopping distance, and particle velocity equal to fluctuating velocity appear to be consistent with the experimental data.

Peddieson[48] discussed the theoretical prediction of the performance of dust collectors. A state of multi-phase flow exists in such devices. Furthermore, he[49] studied the motion of a dust carrier gas suspension in the vicinity of a sphere or a circular cylinder, which has been of interest for several engineering situations. Examples are the collection and sampling of dust for the purpose of monitoring and controlling air pollution. A knowledge of the rate of dust collection by a single isolated element can be used to estimate the rate of collection of the bed as a whole. Also, the heads of various sampling devices often take the form of spheres or cylinders.

The flow of a dust gas through an infinitely long pipe was studied by Crooke and Walsh[22]. A set of linear partial differential equations were derived to represent two dimensional flow, and solutions to these equations were obtained for rectangular and

circular geometry. They examined both steady-state and transient cases. They developed a method for the construction of solutions for the flow of a viscous, incompressible gas with suspended dust particles when the flow domain possesses special geometry. They did not consider any change in the number density of the particles, i.e., the caase of no particle deposition

Deposition of aerosol particles in a long channel due to diffusive and electrostatic charge effects was investigated theoretically by Chen[11]. The diffusion equation and the Poisson equation for flow of aerosol particles with electrostatic charge force were solved with an integral method based on gas flow with a uniform or parabolic velocity profile. He found that the inverse of the centerline particle density increased linearly with the product of the electrostatic parameter and the axial distance for the flow near the channel inlet. The centerline particle density, the penetration and the electric field force decreased exponentially with the axial distance for flow far from the channel inlet.

From the concept of the particle trajectory function, Pich[50] derived an equi-penetration curve of particles at the inlet plane. The particles below the equi-penetration curve are considered deposited on the wall surface. The deposition efficiency is found by integrating the product of particle velocity and the area between the equi-penetration curve and the boundary of the channel wall.

Wang[71] further developed the concept of particle trajectory in an inclined channel in a laminar flow. Analytical solutions for gravitational deposition of particles were derived for the uphill and downhill flows. At zero inclination, i.e., in a horizontal tube, Wang obtained the same solution as that derived by Pich[50]. In an uphill flow with parabolic velocity profile, the axial component of particle velocity at the entrance region is negative; hence, these particles are not able to enter the tube. In the calculation of particle deposition, those particles are not included while in a downhill flow, this situation does not happen since the axial components of particle velocity in the entrance region are all positive. It was found that the deposition is dependent upon the sedimentation parameter,

which is the product of the particle terminal velocity, the diameter of tube, and the angle of inclination.

According to Wang's study, the use of the trajectory function provides a simple way for calculating the flow rate of particles through any area. This is particularly useful in the analysis of the deposition in the inclined channels of which the inlet and outlet cross-sections are not vertical.

Taulbee and Yu[69] investigated theoretically the simultaneous diffusion and sedimentation of aerosol particles in two dimensional channels for both uniform and fully developed flow. They found that the fractional penetration depends on a parameter $q'' = H*V_g/D$ where h is the channel half height, V_g is the setting velocity of a particle and D is the Brounian diffusion coefficient. The results showed that for $q'' < 0.1$, the particle loss was practically due to diffusion alone, while for $q'' > 200$, the deposition is mainly due to setting. The deposition due to the combined mechanism in the range $0.1 < q'' < 200$ is significantly smaller than the algebraic sum of deposition due to two independent mechanisms.

Some theoretical analysis and investigations on deposition in the entrance of a channel and in a diffuser were conducted by Eldighidy, Chen, and Conparin[26]. Under the effects of diffusion, electrostatic repulsive force and adhesive force, the results showed that the electrostatic charge inference plays an important role in the deposition of particles. They also found that the surface adhesion has a smaller effect on the rate of deposition than the electric charge. Moreover, it was found that the rate of deposition is greatly affected by the divergence angle of the diffusers. The rate of deposition increases as the diffuser angle increases; particularly, the rate of deposition increased rapidly in the presence of electric charge. However, the effect of electrostatic image force was not investigated in these analyses.

Yu and Chandra[74] analyzed charge repulsive force and image force in consideration of electrostatically charged particles suspended in a fluid. They showed that,

at 1.0E05 particles per cubic centimeter, the space charge force can only lead to a small effect on the deposition and the predominant effect is due to image forces exerted on the particles. In the image model, the interactive forces between particles is neglected and the deposition is independent of the particle density. They investigated theoretically the deposition of charged particles by their image forces from laminar flows in rectangular and cylindrical channels. It was found that the image force contributes approximately the same amount of deposition as the gravitational force does, when particles of 1 μm diameter and 100el./particle were breathed into human lung with 1000cc tidal volume and 12 respiration per minute. Their numerical calculations were based on the analysis of limiting trajectories of particles.

Ingham[40] consider the deposition of a steady flow of suspensions due to electrostatic charge field force near the entrance of a cylindrical tube. Neglecting the axial diffusions in the steady state transport equation and Poisson's equation for electrostatic field, he solved these equations analytically.

Considering diffusion, electrostatic charge field force, and gravitational force, Chen and Gelber[13] studied the particle deposition in a parallel plate with laminar flow. Variations in deposition were determined by using a dimensionless parameter (charge-diffusion parameter) which is a ratio of the space electrostatic charge effect to the diffusion effect. They found that when this parameter was greater than 50, the diffusion effect may be neglected. When gravity acting in the direction of flow was considered, a velocity ratio (terminal velocity of the particle to the mean velocity of the fluid flow) was introduced. The space electrostatic charge field force effect and the gravity effect were considered in this case, and the velocity profile was either uniform or fully developed.

Chen et al[14] extended the study to include the effect of particle inertia on the deposition of aerosol in a parallel plate channel. Highly charged fine particles of sizes less than 20 micrometers had been analyzed numerically for both uniform and fully developed flows using a trajectory method. They considered the deposition to be primarily due to

space charge alone and the image and gravity forces were not included in the analysis. They also defined a charge-inertia parameter n (ranging from 0 to 1) to characterize the flow deposition phenomena. They found that for n less than 0.1, the effect of inertia forces may be neglected and that the fraction of deposition near the entrance of the channel deviated substantially from the result that neglected the inertia effect.

The number of studies on the motion of aerosol particles and their deposition on surfaces has largely increased from mid of 1980s due to their numerous industrial applications. One recent example is the analysis of particle deposition rate on wafers for controlling the micro contamination in micro-electronics industry. Cooper[19] summarized the state of understanding of the micro-contamination control in the semiconductor industry, and provided a review of the needed micro-contamination control research for microelectronics industries. The research is needed in: source determination, transport modeling, aerosol characterization, deposition mechanisms, surface particle characterization and some more. Then, Cooper et al[20] reported the progress in analyzing particle deposition rates on wafers.

Douglas and Ilias[24] investigated the deposition of aerosol particles on cylinders in turbulent crossflow. Their work was based on the concept of eddy diffusivity and tested by comparing theoretical results with experimental data of Douglas in 1980. The numerical solution of the model equations requires the assumption of an eddy diffusivity profile within the boundary layer and a velocity profile at the outer edge of the boundary layer. In this work, the normalized eddy diffusivity profile near the cylinder surface was assumed to have the same shape as the eddy diffusivity profile near a flat plate. The velocity components were obtained from the solution of the boundary layer equation for two velocity specifications at the outer edge of the boundary layer, but their turbulent diffusion model tends to overestimate the measured collection efficiencies.

Fichman et al.[29] proposed a model of particle deposition in turbulent flow to a smooth surface based on the calculation of particle trajectories only. The model was based

on the calculation of particle trajectories in the wall region, using a detailed description of the flow in this region. The deposited particles were assumed to come from the space between two eddies. To calculate deposition, the limiting particle trajectory in the developed flow field must be calculated. This was done by solving the Lagrangean equations of particle motion, which include the lift force perpendicular to the flow direction, resulting from the shear flow in the streamline direction. It was shown that the lift force is important in the deposition process.

Aerosol particle deposition in numerically simulated channel flow was carried out by McLaughlin[46]. He used a pseudospectral computer program to simulate the three-dimensional, time-dependent flow field, then to compute the trajectories of rigid spherical particles in a turbulent channel flow. He assumed that the channel is vertical so that gravity cannot directly cause the deposition of particles on the walls. The particles are assumed to be sufficiently small and widely separated so that their influence on the fluid velocity field can be ignored. He found that when the particles are assigned random initial locations with initial velocities that are equal to the local fluid velocity, the particles tend to accumulate in the viscous sublayer. At the edge of the viscous sublayer, the particles that deposit on the wall typically possess normal components of velocity that are comparable in magnitude to the intensity of the normal component of the velocity in the core of the channel, i.e., of the order of magnitude of the friction velocity. A shear-induced lift force having the form derived by Saffman for laminar flow is found to have virtually no effect on particle trajectories, except within the viscous sublayer where it plays a significant role both in the inertial deposition of particles and in the accumulation of trapped particles.

The problem of aerosol deposition in two-dimensional laminar stagnation flow under the combined effect of inertial impaction, interception and gravity is investigated by Ramarao and Tien[55]. Analytically expressions for particle trajectories were obtained by ignoring the boundary layer effect near the deposition plane. With the inclusion of the boundary layer effect, particle trajectory can only be determined numerically. Their main

findings are that aerosol flux is uniform along the deposition plane which is true regardless of whether the boundary layer effect is included or not, the inclusion of the boundary layer in determining deposition tends to increase the deposition flux and this effect decreases with the increase of particle size but increases with the increase of α. α is a constant and is characteristic of the flow field. They also showed that under certain limiting conditions the analysis yields results identical to those of previous investigations.

Chen et al[15] derived the image force equation for the two-dimensional convergent channels by using the concept of image circle. The deposition analysis due to the image force alone for the 15°, 10°, and 5° of convergent channel was studied for the uniform flow. They concluded that in comparison with the parallel-plate channel, the depositions were found to be smaller near the entrance in the convergent channels, but they increase as the axial distance is increased.

A two-dimensional steady state two-phase hydrodynamic model was developed by Arastoopour et al[2] based on multiphase flow equations of continuum mechanics, to describe dilute gas-solids flow behavior in a vertical pipe. Their model considered the particles to be the same size and their boundary layers as a separate continuum phase. Furthermore, viscous dissipation forces and phase interaction forces are incorporated. They found that a gas-solids drag force plays an important role in describing two-phase flow behavior. They pointed out that more fundamental research is needed to obtain a suitable expression capable of describing the interactive forces between gas and particulate phase at different regimes. Soo[61] in the Canadian Chemical Engineering Conference presented a detailed review on the theoretical studies of multiphase flow by continuum mechanics.

Motion of small suspended particles in a turbulent channel flow was studied by Abuzeid, Busuaina and Ahmadi[1], using Lagrangian simulation technique. The effect of Reynolds number, turbulence intensity and particle diameter was investigated. Their results showed that turbulence fluctuations and Brownian motion have significant effects

on the particle deposition process. The results also showed that turbulence fluctuations remain significant regardless of particle diameter, while Brownian effects become negligible as the particle diameter becomes greater than 1 μm. The turbulence intensity is shown to be directly proportional to the deposition rate. The results also showed that as the Reynolds number increases, the deposition rate increases as well.

Li and Ahmadi[44] further extend their studies. Effects of Brownian diffusion, Saffman lift force, gravity and particle-surface interactions were included in their computational model. Several simulations for deposition of particles of various sizes were performed and the corresponding deposition velocities are evaluated. The effect of particle rebound from surface on particle deposition rate is also studied. They showed that gravitational effect significantly increases the deposition velocity for particles larger than 2 μm, in the vertical channel, the minimum deposition rate occurs for particle diameters in the range of 1,0-5.0 μm, for the horizontal channel. The gravitational effect shifts the position of minimum to the 0.1-0.5 μm size range. Rebound effects become noticeable for particles larger than 10 μm.

Chen, Chiou and Sun[12] investigated the deposition of particles in a convergent channel numerically in a wide range of parameters. A laminar fluid flow of uniform and developing velocity profile is used in the analysis, and the effects of inertia, gravity, viscous force and image force are included in the computational model. The governing equations were built upon a trajectory method to find the trajectory of each particle entering the channel. The deposition was based on the distance for a particle to reach the wall. Many computations for deposition were performed with combinations of different parameters.

Further investigation in our work would be to study theoretically the deposition of particles from a laminar flow in a divergent channel due to inertia, gravity, viscous and image forces.

CHAPTER 3

ANALYSIS OF LAMINAR SUSPENSION FLOW IN AN ANGLED CHANNEL

The deposition of gas-particles or droplets from a suspension flow to channel walls has been the central subject of a number of theoretical treatments. The present work will focus on the analysis of the deposition of aerosol particles on the internal walls of a laminar, angled channel flow. In this chapter, the work will aim at a comprehensive study of all the physical effects occurring during the process of particle deposition, understanding of the dilute gas-particle flow patterns, and further development of formulation to predict such particle behavior on the proposed model. Although many of the practical two phase systems are turbulent, depositions in low Reynolds number flow are the subject of considerable literature as seen on the chapter 2. A laminar flow will be dealt with in the research. This is because it will lead to a relatively rigorous mathematical solution and a feasible method that can be extended to a corresponding turbulent flow system with minimal modification. With a dilute suspension, the interactions between particles are ignored in the gas particle system.

3.1 Dynamics of Single Particles

3.1.1 Motion Equations

Finding the path of the aerosol particle lends much information to the flow behavior of gas-particle systems. Few measurement techniques can deal with the individual particle trajectory and its velocity. Numerical simulation offers another path for such analysis. Compared with experimental approach, the different aspect about finding the trajectory of the particle is that the basic equation defining such behavior is nonlinear, requiring a numerical solution.

An analysis of particle deposition to surfaces in a laminar flow is made based upon the calculation of particle trajectories. The particle trajectory is computed using the Lagrangian solution of the particle equations of motion in the laminar flow field.

On the consideration of variety of factors, the Lagrangian equations of particle motion for a small rigid particle in a non-uniform channel flow can be expressed as follows. This equation stemmed from Basset-Boussinesq-Oseen equation, now including the Saffman lift force, Brownian force, and gravity force.

$$\begin{aligned}\left(\frac{\pi D^3\rho_p}{6}\right)\frac{du_p}{dt} &= \left(\frac{\pi D^3\rho_p}{6}\right)\left(\frac{3C_D\rho}{4D\rho_p}\right)|u-u_p|(u-u_p)\\ &-\left(\frac{\pi D^3}{6}\right)\frac{\partial p}{\partial x}+\frac{1}{2}\left(\frac{\pi D^3}{6}\right)\rho\frac{d}{dt}(u-u_p)\\ &+\left(\frac{3D^2}{2}\right)\sqrt{\pi\rho\mu}\int_{t_0}^{t}\frac{(du/dt')-(du_p/dt')}{\sqrt{t-t'}}dt'\\ &+6.46\mu a^2\left[\left(\frac{1}{\nu}\right)\left|\frac{du_x}{dy}\right|\right]^{1/2}(u_x-u_{px})\hat{y}\\ &+\frac{\pi D^3}{6}(\rho-\rho_p)g\hat{y}\\ &+n_i(t)\frac{\pi D^3\rho_p}{6}\\ &+external\,force\end{aligned} \tag{3.1.1}$$

The basic physical meaning of each term from the left of equation (3.1.1) is:

term 1 = inertia force

term 2 = drag force

term 3 = pressure gradient force

term 4 = apparent mass force

term 5 = Basset force

term 6 = Saffman lift force

term 7 = Buoyancy and gravity force

term 8 = Brownian force

External forces in the equation, generally, should include electrostatic forces; electromagnetic radiation (photophoretic) forces, and thermal gradient (thermophoretic) forces.

In the equation, the x-axis is along the centerline of the channel, y is perpendicular to the centerline and opposite to gravity. u_p is the velocity of the particle, u is the velocity of the undisturbed fluid evaluated at the center of the particle, t is the time, D is the diameter of the particle, ρ and ρ_p are the density of the particle and the density of the fluid, d/dt denotes a time derivative following the particle, and ν is the kinematic viscosity of the fluid. The dynamic viscosity is denoted by μ. The equation of motion is, practically, based on two Reynolds numbers. One is related to a particle and the other to the flow field of a channel. In terms of dimensional parameters, the two Reynolds numbers are:

$$\mathrm{Re}_p = w_o a / \nu \quad \text{and} \quad \mathrm{Re} = u_o h / \nu \tag{3.1.2}$$

where a is the radius of the particle, h is the half channel width at the entrance, w_0 is a velocity that is characteristic of the relative motion between the particle and the undisturbed fluid; u_0 is velocity of the flow. The channel flow is two-dimensional, therefore, the equation (3.1.2) should be written both for x and y directions. The Reynolds number Re_p is based on the magnitude of the relative velocity, or :

$$Re_p = (\rho D/\mu)\left[w_{ox}^2 + w_{oy}^2\right]^{1/2} \tag{3.1.3}$$

All terms in the equation are derived on the assumption that the particle is a small rigid sphere. If a non spherical or irregularly shaped solid particle is applied, the uniform motion and consistent orientation of such a particle can not be assured. It is almost impossible for a theoretical analysis.

The equation (3.1.1) is so complex for a solution that a couple of assumptions will be taken into account. For typical conditions of gas-particle flow, the density ratio ρ/ρ_p is of the order of 10^{-3}. It means that the density of a particle is sufficiently great compared to the gas that virtual mass effects are unimportant. This assumption will be used to apply order of magnitude examination of some terms in our analysis.

3.1.2 Force Analysis

On the left hand side of the equation (3.1.1), term 1 is equal to the product of mass and acceleration of the particle. It represents the force necessary to accelerate the particle, i.e., inertia force, which is present in the unsteady flow situation.

On the right hand side of the equation (3.1.1), term 2 is the drag force. It contains the drag coefficient C_D that is a function of the Reynolds number of a particle. When Re_p is less than about one, the drag is obtained analytically by Stokes laws:

$$\text{Stokes drag:} \quad F_D = 3\pi D\mu(u-u_p) \tag{3.1.4}$$

$$\text{Drag coefficient:} \quad C_D = 24/Re_p \tag{3.1.5}$$

where, the definition of the drag coefficient is:

$$C_D = \frac{F_D}{(\pi a^2)\left(\frac{1}{2}\rho u^2\right)} \tag{3.1.6}$$

For example, choosing: $a = 1\ \mu m = 1\times10^{-6}$ m, $w_o = 0.1u_o$

$Re=100$, $u_o = 2.896$ m/s

Then: $Re_p=0.02$

Here, $w_o = (10\% \sim 15\%)u_o$ is based on experiments of Zhu and Soo[75].

For higher Reynolds number Re_p, Some more investigations of C_D based on experiments have been done by Kemp[42], Rutnam[52], and Puri[53].

In our cases of laminar channel flows, the drag coefficients will definitely be less than 100, hence C_D is given by:

$$\begin{aligned} C_D &= \frac{24}{Re_p} && \text{for } Re_p < 1 \\ C_D &= \frac{24}{Re_p}\left(1+\frac{3}{16}Re_p\right)^{1/2} && \text{for } 1 \le Re_p \le 100 \end{aligned} \tag{3.1.7}$$

For atmospheric air, the molecular mean free path λ is of the order of 0.1μm. The assumption of continuum flow thus becomes invalid for extremely small particles or for low gas density, then the drag force on the particle must be corrected for slippage of gas at the particle surface. Cunningham slip correction Gc is applied to the drag coefficient, which depends on the Knudsen number $Kn=\lambda/D$.

$$Gc = 1+1.257Kn+0.400Kn\exp(-1.10Kn^{-1}) \tag{3.1.8}$$

To correct the drag coefficient, the C_D is divided by the term Gc.

The force acting on the particle on term 3 is led to by the pressure gradient in the fluid. For a gas flow, the pressure gradient is given by:

$$-\frac{\partial p}{\partial x}=\rho\frac{Du}{Dt}=\rho\left(\frac{\partial u}{\partial t}+u\frac{\partial u}{\partial x}\right) \tag{3.1.9}$$

When a particle is accelerated relative to a surrounding fluid, it sets up a two dimensional flow around it which possesses kinetic energy. Therefore, work must be supplied to move the particle in addition to that which is required to accelerate it alone. This extra energy requirement shows up as an additional force on the particle which is term 4. For a sphere, it behaves as if it possessed an additional "apparent mass" equal to one half of the fluid which it displaces. It acts to reduce the velocity lag.

For particles suspended in gases, the density ratio of 10^{-3} usually makes the effect of term 3 and term 4 negligible.

Since viscous effects, such as boundary layer growth, are governed by diffusion equations, the instantaneous flow field is a function of the entire previous history of the particle motion. For laminar flow, Basset obtained the result in term 5. The Basset force is rather awkward to calculate and its significance is not readily ascertained. Klinzing[43] gives three examples to indicate its magnitude. For typical density ratio of 10^{-3} the Basset force becomes smaller than 10% of Stokes drag. We will neglect its effect, too.

Saffman lift force is induced by velocity gradient in shear flow. It is term 6. The magnitude of lift force F_L to drag force F_D is given by

$$\frac{|F_L|}{|F_D|}\propto\left(\frac{a^2(du/dy)}{\nu}\right)^{1/2} \tag{3.1.10}$$

Hence for small particles, the lift force due to its passage through a shear layer can be neglected when a^2(du/dy)/ν is small. McLaughlin[46] points out that even within the

viscous sublayer the Saffman lift term is still quite small compared to the normal component of the Stokes drag force.

In term 7, g is the acceleration of gravity and equal to -9.807 m/s^2. The buoyancy term should be small compared to the Stokes drag term for a sufficiently small particle.

Brownian diffusion force plays an important role in the concentration distribution of a cloud of particles. But when the two-phase flow is dilute, its effect will be of little importance.

In the term of external forces, electrostatic force often is a significant factor. Practically, all aerosols or particles, natural or artificial, are electrostatically charged. When particles capture free ions from the air, they become charge carriers. Particles may also acquire charge when they impact each other and the wall. The electrification of particles can be great in gas-solid systems. The large charges on small particles are related to the large surface/volume ratio that is present for these fine materials. The electrostatic force has the same magnitude as gravity in many cases[10]. It will be an important factor in this research. The photophoretic force or thermophoretic force will not be included in the work. Shchukin[60], Turner[69] and Ye[72] have done work on them.

3.1.3 Governing Equations

Based on above force analysis, practically, the efficiency of deposition of particles in a divergent channel flow with a dilute suspension will be mainly due to inertia, viscous, gravity and charge forces. To get the basic governing equations, the assumptions are summed up as following:

(1) Incompressible, steady flow

(2) Two-dimensional, laminar flow

(3) Dilute suspension

(4) Interaction between particles is negligible

(5) Density ratio ρ/ρ_p is of the order of 10^{-3}

(6) Particles behave like a sphere of radius "a"

(7) Thickness of the deposition layer is much smaller than the channel width

(8) Negligible temperature effects

Assuming the flow incompressible is a good approximation for compressible fluids at very low Mach numbers.

A rectangular Cartesian coordinate system is employed as shown below, in which the x-axis is along the center-line of the channel and the y-axis is opposite to the direction of gravity.

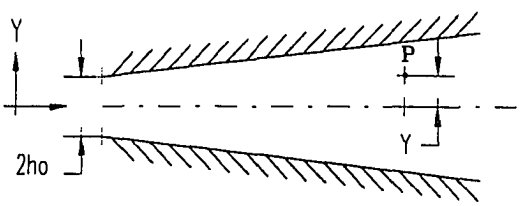

Figure 3.1.1 Coordinate System for a Divergent Channel

Referring to the figure 3.1.1, the width of the divergent channel at entrance(x=0) is $2h_0$. Further downstream(x>0), the divergent channel half width h is larger than h_o and is a

function of x. On the above consideration, the governing equations for a particle in a divergent channel flow are as follows:

$$m\frac{du_p}{dt} = k(u-u_p)+f_x \tag{3.1.11}$$

$$m\frac{dv_p}{dt} = k(v-v_p)-mg+f_y \tag{3.1.12}$$

Where m is the mass of the particle, the subscript p denotes a particle, and u and v are velocities of the fluid in the x and y directions. The f_x and f_y denote the electrostatic force components in the x and y directions, respectively. The equations include the effects of inertia, viscous, gravity and charge forces.

The second order differential equations can be rewritten in the form of two equivalent first order differential equations when we let:

$$u_p = \frac{dx}{dt} \quad v_p = \frac{dy}{dt} \tag{3.1.13}$$

In this work, this divergent channel walls are considered to be conducting and to be properly grounded. For a dilute suspension of particle number densities less than 10^5 particle per cm^3, the dominant effect of the electrostatic force on deposition is due to the image force.

A particle with charge q in a conducting channel will induce a certain amount of opposite charge on the nearby surface of the conducting plates. The total electric potential is partly due to q directly and partly to this induced charge. The basic equations to depict the electric field are:

$$\vec{F} = q\vec{E} \tag{3.1.14}$$

$$\vec{E} = -\nabla V \tag{3.1.15}$$

$$\nabla^2 V = -\frac{q}{\varepsilon_o} \tag{3.1.16}$$

where $\vec{F}$ is electric force, $\vec{E}$ is electric field strength and V is electric potential. $\nabla^2 V = -q/\varepsilon_o$ is known as Poisson's equation. ε_0 denotes the permittivity of space in the electrostatic theory.

From the mathematical point of view, our problem is to solve Poisson's equation with a single point charge q located at (x, y) subject to boundary conditions. But our problem can be classed as a problem that can be solved by method of images. The uniqueness theorem plays a crucial role. It guarantees that there is only one function which is our solution. In the method of images a single point charge near a grounded conducting plane can be treated by construction of its mirror image charges. This will guarantee that the plane will be at potential zero and be precisely the conditions of our original problem. For this configuration, its potential can be easily written down, and is exactly the same as our problem.

Based on the principle, for a channel which is made of two parallel plates placed $2h_0$ apart with walls that are conducting and grounded, the image forces on a charged particle can be expressed as:

$$f_x = 0$$

$$f_y = \frac{q^2 h_o y}{4\pi\varepsilon_o}\left\{\frac{1}{\left(h_o^{\,2} - y^2\right)} + \sum_{n=1}^{\infty}\frac{2n+1}{\left[(2n+1)^2 h_o^{\,2} - y^2\right]^2}\right\} \tag{3.1.17}$$

The same approach is applied for an angled channel while the image circle concept is introduced. When two conducting planes intersect at an angle 2θ, the image of a point charge particle is finite and confined on a circle, which is the image circle. This image circle is defined by having its center at the extended intersecting point of the two conducting planes, and the distance from this intersecting point to the point charge particle is the radius. The total number of pairs of images(N) is equal to $\pi/(2\theta)$. Hence, the formulas of image forces of an angled channel are derived as:

$$f_x = \frac{-q^2}{4\pi\varepsilon_0}\left\{\sum_{n=1}^{N}(-1)^n \frac{\sin\beta_n}{q_n^{\,2}} + \sum_{n=1}^{N-1}(-1)^n \frac{\sin\beta_{n'}}{q_{n'}^{\,2}}\right\} \tag{3.1.18}$$

$$f_y = \frac{-q^2}{4\pi\varepsilon_0}\left\{\sum_{n=1}^{N}(-1)^n \frac{con\beta_n}{q_n^{\,2}} - \sum_{n=1}^{N-1}(-1)^n \frac{con\beta_{n'}}{q_{n'}^{\,2}}\right\} \tag{3.1.19}$$

where:

$$N = \frac{\pi}{2\theta}$$

θ: the half convergent channel angle

q: the charge per particle

ε_0: the permitivity of space

β_n: angle between the y-axis and the chord connecting the charge to image n'

$\beta_{n'}$: angle between the y-axis and the chord connecting the charge to the secondary image n'

q_n: distance between the point charge to the primary image n

$q_{n'}$: distance between the point charge to the secondary image n'

A detailed meaning and proof of the above formulas appear in [15].

In this work, electrostatic charge is assumed uniformly distributed on the surface of a particle so that it works like a point charge. The above equations work on convergent channel cases and need to change the sign of f_x in the divergent channel case. A modification formula is applied to the equations to have them applicable for our practical divergent channel.

3.2 Steady Flow Through an Angled Channel

3.2.1 Fluid Dynamics Equations

The basic principles of fluid dynamics are the well known conservation of mass and conservation of momentum. The first one leads to the continuity equation, and the second one to the momentum equations or Navier Stokes equations. When we consider that the fluid is Newtonian, the flow is homogeneous, isotropic, incompressible, and limit to the case of a 2-dimensional and steady channel flow, the equation of continuity can be written as:

$$\frac{\partial u}{\partial x}+\frac{\partial v}{\partial y}=0 \tag{3.2.1}$$

and the momentum equations take the form:

$$u\frac{\partial u}{\partial x}+v\frac{\partial u}{\partial y}=-\frac{1}{\rho}\frac{\partial p}{\partial x}+\upsilon\left(\frac{\partial^2 u}{\partial x^2}+\frac{\partial^2 u}{\partial y^2}\right) \tag{3.2.2}$$

$$u\frac{\partial v}{\partial x}+v\frac{\partial v}{\partial y}=-g-\frac{1}{\rho}\frac{\partial p}{\partial y}+\upsilon\left(\frac{\partial^2 v}{\partial x^2}+\frac{\partial^2 v}{\partial y^2}\right) \tag{3.2.3}$$

Terms on the left hand side are the convection terms. The pressure gradient is the first term on the right hand side, the second term is known as the diffusion term and g is the gravity term.

These equations, though simplified, are still a formidable system of nonlinear partial differential equations. No general analytical method yet exists. In particular, analytical difficulties arise if the angled channel is a divergent one. A divergent channel flow does not become fully developed, separation, back flow, and unsteadiness complicate the flow pattern.

In recent years, major advances in computer technology and computational mechanics have made it possible to construct numerical models of fluid dynamics. Some solution methods are based on the finite element method(FEM), which has a relatively short history in computational fluid mechanics and is becoming a powerful tool. The great advantage of FEM over other methods is its inherent flexibility in treating arbitrarily complex flow domains and boundary conditions.

3.2.2 Finite Element Analysis

The finite element method is a numerical method for solving a system of governing equations over the domain of a continuous physical system. Elements subdivide the domain, and these elements assemble through interconnection at a finite number of points on each element. Then this assembly provides a model of the continuum region of interest.

(1) Formulation

Since the Eulerian description of fluid motion is used in the field equations, the elements are assumed to be fixed in space. Within each element, the dependent variables u_i and p are interpolated by functions of compatible order, in terms of values to be determined at a set of nodal points. The velocity, pressure and temperature fields within each element are approximated by,

$$u_i(x,\ t) = \varphi^T U_i(t)$$
$$p(x,\ t) = \psi^T P(t) \tag{3.2.4}$$

where U_i and P are column vectors of element nodal point unknowns and φ and ψ are column vectors of the interpolation functions.

Substituting these interpolation functions into the field equations as well as boundary condition yields a set of equations of the form:

Momentum: $f_1(\varphi, \psi, U_i, P) = R_1$

Continuity: $f_2 = (\varphi, U_i) = R_2$

where R_i is the residual resulting from the use of those approximation equations. The Galerkin method of weighted residuals seeks to reduce the error(residual) R_i to zero. This is achieved by making:

$$\int_{\Omega_E} (f_1 \cdot \varphi) d\Omega = \int_{\Omega_E} (R_1 \cdot \varphi) d\Omega = 0 \tag{3.2.5}$$

$$\int_{\Omega_E} (f_2 \cdot \psi) d\Omega = \int_{\Omega_E} (R_2 \cdot \psi) d\Omega = 0 \tag{3.2.6}$$

where, Ω_E is the element domain.

The application of the Galerkin procedure to the field equations results in a system of algebraic equations of the form:

$$[K][\Phi] = [F] \tag{3.2.7}$$

where, [K] is the stiffness matrix, [Φ] is the column vector of unknowns and [F] is the source term which includes the effects of body forces and boundary conditions.

(2) Element

A nine node quadrilateral element has been used for the computations. In terms of normalized or natural coordinates of the element, i.e., r and s, the velocitys are approximated using biquadratic interpolation functions, given by:

$$\varphi = \begin{bmatrix} \frac{1}{4}rs(1-r)(1-s) \\ -\frac{1}{4}rs(1+r)(1-s) \\ \frac{1}{4}rs(1+r)(1+s) \\ -\frac{1}{4}rs(1-r)(1+s) \\ -\frac{1}{2}s(1-s)(1-r^2) \\ \frac{1}{2}r(1+r)(1-s^2) \\ \frac{1}{2}s(1+s)(1-r^2) \\ -\frac{1}{2}r(1-r)(1-s^2) \\ (1-r^2)(1-s^2) \end{bmatrix} \tag{3.2.8}$$

The pressure approximations used with the element are bilinear. The pressure values for the bilinear approximation are located at the four points of 2×2 Gaussian integration. Its interpolation functions are given by,

$$\psi = \begin{bmatrix} \frac{1}{4}(g-r)(g-s)/g^2 \\ \frac{1}{4}(g+r)(g-s)/g^2 \\ \frac{1}{4}(g+r)(g+s)/g^2 \\ \frac{1}{4}(g-r)(g+s)/g^2 \end{bmatrix} \tag{3.2.9}$$

$$g = 2\sqrt{1/3} \tag{3.2.10}$$

(3) Boundary Conditions

It is required to provide appropriate boundary conditions u, v on the boundary of the computational domain, as shown on the following figure.

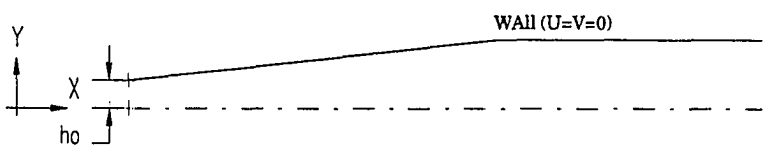

$$\partial U / \partial x = 0$$
$$\partial V / \partial x = 0$$

$$\partial U / \partial y = 0 \quad V = 0$$

Figure 3.2.2 Boundary Conditions for FEA Computational Domain

The inlet plane is positioned upstream of the regions of interest in area where the flow field is unperturbed from any nearby obstacles. The velocity distribution is prescribed uniform at the inlet.

On the solid wall, rigid, no-slip boundary conditions are applied, hence velocities are prescribed zero.

At the symmetry plane, the gradient of u is set to zero in the y direction and v is set to zero, too.

For the outlet profile boundary, the fully-developed parabolic velocity profile is applied in the axial direction.

(4) Algorithm and convergence criteria

A segregated implicit algorithm is employed for the numerical solution of the set of discretized equations resulting from the application of the Galerkin finite element method to the field equations. The discretized implicit equations associated with each primary flow variable are assembled in smaller sub-matrices. Mixed velocity-pressure formulation is used. At the beginning, an approximation of the pressure is obtained from the solution of the Poisson type pressure matrix using the latest available value of the field variables. The criteria are applied to terminate the iteration in solving the equations. According to the relative error of the solution vector $\hat{u}_i$ at iteration i, a convergence criterion is:

$$\frac{\|\Delta\hat{u}_i\|}{\|\hat{u}_i\|} < \varepsilon_u \tag{3.2.11}$$

$$\Delta\hat{u}_i = \hat{u}_i - \hat{u}_{i-1} \tag{3.2.12}$$

where ε_u denotes a given tolerance. $\|\ \|$ means an appropriate norm.

The second convergence criterion is based on the residual vector to check the tendency of errors as $\hat{u}_i$ tends to u. It is

$$\frac{\|R(\hat{u}_i)\|}{\|R_o\|} < \varepsilon_F \tag{3.2.13}$$

where R_0 is a reference vector, usually $R(\hat{u}_o)$. These two criteria provide an effective overall convergence criterion for solutions.

Based on the equations, boundary conditions and the principles for solution, flow computation programs have been built upon the FIDAP package, as shown in Appendix. The dimensionless length of a channel is X=40. In the X direction, they are divided into 51 segments and 21 segments in Y direction. The quadrilateral, 9-node elements of the total number of 1071 are used in the computation.

CHAPTER 4

COMPUTATION OF DEPOSITION FRACTION IN A CHANNEL FLOW

In this chapter, a numerical scheme is presented to study the suspensions of laminar flow in a two dimensional divergent channel, also including some cases in a convergent channel. First, the governing equations of particle motion are solved in dimensionless form to get the particle trajectories. Then, the fraction of deposition of aerosol particles on the channel wall is calculated upon these trajectories. Deposition is due to the effects of the inertia force of the particle, gravity force, electrostatic charge image force on the particle, and viscous force of the fluid.

4.1 Dimensionless Equations

The trajectory of a particle moving in a gas can be estimated by integrating the governing equations of motion for the particle over a time period. The basic definition relates the particle position to its velocity and time as:

$$x = \int_{t_o}^{t} u_p dt' + x_o \tag{4.1.1}$$

$$y = \int_{t_o}^{t} v_p dt' + y_o \tag{4.1.2}$$

In order to simplify the governing equations and make parameter studies, the number of variables involved are reduced. The following dimensionless terms are introduced in the analysis:

$$T = \frac{tu_0}{h_0} \tag{4.1.3}$$

$$X = \frac{x}{h_0};\ Y = \frac{y}{y_0} \tag{4.1.4}$$

$$U = \frac{u}{u_0};\ V = \frac{v}{v_0} \tag{4.1.5}$$

Using the Lagragian approach, a particle at time t is located at (x, y, z). The velocity components are:

$$u_p = \frac{dx}{dt};\quad v_p = \frac{dy}{dt} \tag{4.1.6}$$

Substituting all of these into equations (3.1.11) and (3.1.12) yields:

$$m\frac{u_o^2}{h_o}\frac{d^2X}{dT^2} = ku_o\left(U - \frac{dX}{dT}\right) + \frac{-q^2}{4\pi\varepsilon_0}\left\{\sum_{n=1}^{N}(-1)^n\frac{\sin\beta_n}{q_n^2} + \sum_{n=1}^{N-1}(-1)^n\frac{\sin\beta_{n'}}{q_{n'}^2}\right\} \tag{4.1.7}$$

and

$$m\frac{u_o^2}{h_o}\frac{d^2Y}{dT^2} = ku_0\left(V - \frac{dY}{dT}\right) - mg + \frac{-q^2}{4\pi\varepsilon_0}\left\{\sum_{n=1}^{N}(-1)^n\frac{con\beta_n}{q_n^2} - \sum_{n=1}^{N-1}(-1)^n\frac{con\beta_{n'}}{q_{n'}^2}\right\} \tag{4.1.8}$$

Dividing the whole equations by ku_0 leads to:

$$\frac{mu_o}{h_o k}\frac{d^2X}{dT^2} = U - \frac{dX}{dT} + \frac{-q^2}{4\pi\varepsilon_0 ku_o}\left\{\sum_{n=1}^{N}(-1)^n\frac{\sin\beta_n}{q_n^2} + \sum_{n=1}^{N-1}(-1)^n\frac{\sin\beta_{n'}}{q_{n'}^2}\right\} \tag{4.1.9}$$

and

$$\frac{mu_o}{h_o k}\frac{d^2Y}{dT^2} = V - \frac{dY}{dT} - \frac{mg}{h_o k} + \frac{-q^2}{4\pi\varepsilon_0 k u_o}\left\{\sum_{n=1}^{N}(-1)^n \frac{con\beta_n}{q_n^{\,2}} - \sum_{n=1}^{N-1}(-1)^n \frac{con\beta_{n'}}{q_{n'}^{\,2}}\right\} \quad (4.1.10)$$

Further, using parameters S, G, and Q, the governing equations of particle motion become:

$$S\frac{d^2X}{dT^2} = U - \frac{dX}{dT} + QF_x \quad (4.1.11)$$

$$S\frac{d^2Y}{dT^2} = V - \frac{dY}{dT} - G + QF_y \quad (4.1.12)$$

where, the physical meaning of S, G and Q are:

$$S = \frac{\text{inertia force}}{\text{viscous force}} = \frac{mu_0}{h_0 k} \quad (4.1.13)$$

$$G = \frac{\text{gravity force}}{\text{viscous force}} = \frac{mg}{ku_0} \quad (4.1.14)$$

$$Q = \frac{\text{charge force}}{\text{viscous force}} = \frac{q^2}{4\pi\varepsilon_0 h_0^{\,2} k u_0} \quad (4.1.15)$$

and F_x and F_y are:

$$F_x = -h_o^{\,2}\left\{\sum_{n=1}^{N}(-1)^n \frac{\sin\beta_n}{q_n^{\,2}} + \sum_{n=1}^{N-1}(-1)^n \frac{\sin\beta_{n'}}{q_{n'}^{\,2}}\right\} \quad (4.1.16)$$

$$F_y = -h_o^{\,2}\left\{\sum_{n=1}^{N}(-1)^n \frac{con\beta_n}{q_n^{\,2}} - \sum_{n=1}^{N-1}(-1)^n \frac{con\beta_{n'}}{q_{n'}^{\,2}}\right\} \quad (4.1.17)$$

The equation (4.1.11) and (4.1.12) are our final governing equations in the dimensionless form. Notice that from these equations, the solution depends on the inertia parameter S, charge parameter Q, gravity parameter G, and initial and boundary conditions as well.

The initial conditions are as follows:

at t=0

$x=0$ and $y=y_o$; for $-h_o<y_o<h_o$ (4.1.18)

$$v_p=\frac{dy}{dt}=0; \quad \text{for } -h_o<y_o<h_o \tag{4.1.19}$$

$$u_p=\frac{dx}{dt}=u_o; \quad \text{for } -h_o<y_o<h_o \tag{4.1.20}$$

$$h=h_o \tag{4.1.21}$$

In a similar way, the dimensionless forms of these conditions are:

At T=0

$X=0$ and $Y=Y_0$; for $-1 < Y_0 < 1$ (4.1.22)

$$V_p=\frac{dY}{dT}=0; \text{ for } -1 < Y_0 < 1 \tag{4.1.23}$$

$$U_p = \frac{dX}{dT} = 1; \text{ for } -1 < Y_0 < 1 \tag{4.1.24}$$

$$H = 1 \tag{4.1.25}$$

The boundary conditions of particle motion are:

(1) When a particle reaches the channel wall or Y =1.0 or Y =-1.0, it is considered to be deposited on the wall.

(2)The initial positions of particle are located at the inlet plane, ranging from Y_0 =0.998 to Y_0 =-0.998 with a set of 115 points.

In a divergent channel, the axial image force at the inlet plane is zero and then gradually reach to its theoretical value. Hence, a correction Km is applied to the axial theoretical formula of the image force.

$$K_m = \left(\frac{x - x_o}{x}\right)^{\frac{1}{3}} \tag{4.1.26}$$

where x_o is the axial inlet plane position and x is the axial position of a particle in a channel.

The ranges of parameters that we used to solve these equations in studying the trajectory of the particle suspension are:

θ=7.5°, 5.0°, 2.5°

S=100, 10, 1, 0.1, 0.01

G=100, 10, 1, 0.1, 0.01

Q=10000, 1000, 100, 10, 1, 0.01, 0.001, 0.0001, 0.00001

4.2 Numerical Treatments

Since it is an initial value problem the particle trajectories are obtained by integrating the governing equations, using the forth order Runge-Kutta Method.

4.2.1 Differentiation and Integration

First, for our simultaneous governing equations:

$$\begin{aligned} x'' &= f(x', x, t) \\ y'' &= f(y', y, t) \end{aligned} \tag{4.2.1}$$

We set x' = A, y' = B and then obtain the following system of simultaneous first-order equations:

$$x' = A(x,t) \tag{4.2.2}$$

$$A' = f(A,x,t) \tag{4.2.3}$$

$$y' = B(x,t) \tag{4.2.4}$$

$$B' = g(B,x,t) \tag{4.2.5}$$

where x and y are function of t. Then to integrate them we compute the increments in x and y for the first interval by the forth order Runge-Kutta formulas. The increments for the succeeding intervals are computed in exactly the same way except that x_o, y_o, A_o, B_o, and t_o

are replaced by x_1, y_1, A_1, B_1, and t_1 as the computation proceed, until x_n, y_n, A_n, B_n, and t_n are obtained.

The governing equation (4.1.11) and (4.1.12) are second order differential equations, and can be rewritten as follows.

$$\text{Let: } A=\frac{dX}{dT};\quad B=\frac{dY}{dT} \tag{4.2.6}$$

where A and B are the particle velocities in the x-direction and y-direction. Therefore,

$$\frac{dA}{dt}=\frac{d}{dT}\left(\frac{dX}{dT}\right)=\frac{d^2X}{dT^2} \tag{4.2.7}$$

$$\frac{dB}{dt}=\frac{d}{dT}\left(\frac{dY}{dT}\right)=\frac{d^2Y}{dT^2} \tag{4.2.8}$$

By substituting these into equation(4.2.7) (4.2.8), we have:

$$\frac{dA}{dT}=\frac{U-A+QF_x}{S} \tag{4.2.9}$$

and

$$\frac{dB}{dT}=\frac{V-B-G+QF_y}{S} \tag{4.2.10}$$

Hence, the second-order differential equations are transferred to the first-order differential equations. The four modified equations together with the initial condition are solved by the forth order Runge-Kutta method.

4.2.2 Interpolation of Fluid Flow Velocity

The data of fluid flow in a convergent or divergent channel are obtained at the nodes of a finite element mesh model, therefore, it is necessary to determine the values of flow velocity at a given point among the set of solved data. It is referred to as an interpolation problem. The two dimensional interpolation is required in the numerical integration of solving the governing equations.

The simplest linear polynomial interpolation produces a polygonal path that consists of line segments that pass through the points, while polynomial interpolation for a set of N+1 points is often rather unsatisfactory which graph will wiggle in order to pass through the points. For a low interpolation error, the piecewise cubic splines are employed. It is a kind of piece-together of cubic polynomials with continuity of the first and second derivatives on a larger interval. The form of cubic spline function $S_k(x)$ is as follows:

$$S_k(x)=\frac{m_k}{6h_k}(x_{k+1}-x)^3+\frac{m_{k+1}}{6h_k}(x-x_k)^3 +\left(\frac{y_k}{h_k}-\frac{m_k h_k}{6}\right)(x_{k+1}-x)+\left(\frac{y_{k+1}}{h_k}-\frac{m_{k+1}h_k}{6}\right)(x-x_k) \tag{4.2.11}$$

$$S_k''(x)=S''(x_k)\frac{x-x_{k+1}}{x_k-x_{k+1}}+S''(x_{k+1})\frac{x-x_k}{x_{k+1}-x_k} \tag{4.2.12}$$

$$m_k=S_k''(x_k) \tag{4.2.13}$$

$$h_k=x_{k+1}-x_k \tag{4.2.14}$$

for $x_k \le x \le x_{k+1}$ and k=0,1,2,...,N-1.

The cubic spline $S_k(x)$ has the properties :

(1) $S_k(x_k) = y_k$. The spline passes through each data point.

(2) $S_k(x_{k+1}) = S_{k+1}(x_{k+1})$. The spline forms a continuous function.

(3) $S_k'(x_{k+1}) = S_{k+1}'(x_{k+1})$. The spline forms a smooth function.

(4) $S_k''(x_{k+1}) = S_{k+1}''(x_{k+1})$. The second derivative is continuous.

The m_k is the only unknown coefficient in the spline function. Based on these cubic spline properties, an important relation involving m_{k-1}, m_k, and m_{k+1} is used to find the solution. It is,

$$h_{k-1}m_{k-1} + 2(h_{k-1} + h_k)m_k + h_k m_{k+1} = t_k \qquad (4.2.15)$$

where $t_k = 6(d_k - d_{k-1})$, $d_k = \frac{y_{k+1} - y_k}{h_k}$ for k = 1, 2, ..., N-1, and $m_0 = 0$, $m_N = 0$ for a natural cubic spline.

Using the formula of above cubic spline, the velocity interpolation is made at two times, first in x-direction then in y-direction. The x_k and x represents the position coordinates, and y_k and $S_k(x)$ indicates the velocity components at the known data points and particle point, respectively.

4.2.3 A Closed Form Solution with Q=0

In this section, finally we consider a extreme case. When the channel is parallel one and the image force is negligible, a closed form solution is derived with a parabolic flow profile. It is as follows:

Initial conditions:

At T =0, Y =0, dY/dT =0, X =0 (4.2.15)

and dX/dT =1.5(1-Y_o^2) (4.2.16)

At T> 0, U = 1.5 (1-Y^2) (4.2.17)

Solution:

$$Y(T) = S \cdot G + Y_o - G \cdot T - S \cdot G \cdot Exp(-T/S) \tag{4.2.18}$$

$$\begin{aligned} X(T'') = 1.5G^2S^3\{&4.5 + 6Y_oK \\ &+[K^2(1-Y_o^2) - 4Y_oK - 5]\cdot T'' \\ &+(2+Y_oK)\cdot T''^2 - 1/3T''^3 \\ &-2(2+3Y_oK)\cdot Exp(-T'') - 2Y_oK\cdot T''\cdot Exp(-T'') \\ &+T''^2\cdot Exp(-T'') - 0.5Exp(-2T'')\} \end{aligned} \tag{4.2.19}$$

where K =1/S/G, T'' =T/S

Again, when the inertial effect is negligible, too, i.e. at S =0, the above solutions become:

$$\begin{aligned} Y(T) &= Y_o - G\cdot T \\ X(T) &= 1.5G\cdot T^2(1 - G\cdot T/3) \end{aligned} \tag{4.2.20}$$

Similar results can be seen in [16].

4.3 Calculation of Fraction of Deposition

To determine the fraction of deposition of the particles on the divergent channel wall, the equation of conservation of mass of the particle phase can be written as:

$$Fraction of\ deposition = \frac{\text{total number of particles deposited on the wall}}{\text{total number of particles entering the channel}}$$

$$= \frac{\int_{-h_o}^{y_l} \rho_p u_p dy + \int_{y_u}^{h_o} \rho_p u_p dy}{\int_{-h_o}^{h_o} \rho_p u_p dy} \qquad (4.3.1)$$

Following the concept of limiting trajectories by Pich[50], y_l and y_u in the equation are two critical values of y at the channel entrance x =0, such that the particles entering the channel between y =-h_o and y_l will deposit on the lower channel wall; those entering between y =y_u and h_o will deposit on the upper channel wall; and those entering between y =y_l and y_u will penetrate the divergent channel. The distributions of particles will not be symmetric because of gravity effect on the particles.

The above equation can also be rewritten in dimensionless form as:

$$Fraction of\ deposition = \frac{\int_{-1}^{Y_l} \rho_p U_p dY + \int_{Y_u}^{1} \rho_p U_p dY}{\int_{-1}^{1} \rho_p U_p dY}$$

$$= 1 - \frac{1}{2}(Y_o - Y_l) \qquad (4.3.2)$$

where $Y_l = y_l / h_o$, $Y_u = y_u / h_o$, and $U_p = 1$ at X =0.

CHAPTER 5

RESULTS AND DISCUSSIONS

In this chapter, the particle deposition on the walls both in a convergent and divergent channel due to the effects of inertia force, viscous force, gravity force and electrostatic image force will be discussed. The deposition process upon the combined effects has been solved numerically. In the discussion, the laminar velocity profile for the fluid phase in a convergent or divergent channel is examined briefly and then the particle trajectories for the particle phase are analyzed for understanding the kinetics of particle suspension. Finally, the particle deposition on channel surfaces are studied extensively, since the solution of the problem is a parametric type, and the interest is to find out which parameters affect considerably the rate of deposition of the particle.

As was mentioned in the previous chapters, the range of dimensionless parameters investigated in this analysis are 100, 10, 1, 0.1, and 0.01 for both S (inertia parameter) and G (gravity parameter). Q (image parameter) is ranged from 10000 to 0.00001. The half convergent channel angels investigated in this study are 7.5, 5 and 2.5 degrees.

5.1 Fluid Phase

(1) Convergent channel flow

The results of convergent channel flow are obtained by numerical solution of the Navier Stokes equations and the continuity equation for the symmetric laminar flows. Figure 5.1.1 and 5.1.2 are the displays of the velocity vectors and streamlines of the fluid phase, respectively.

Figure 5.1.3 through Figure 5.1.8 show the axial (U) and vertical (V) velocity distribution of the fluid phase at half convergent channel angles of 2.5, 5.0, 7.5 degrees. In

the reported results, all velocities and distances are non-dimensionlized with respect to inlet average velocity (u_o) and inlet half width (h_o) of the channel.

With a flat inlet velocity profile a sharp gradient of velocity exist at those cross sections near the inlet, and the axial component of velocity fluctuates along various cross sections. As the axial length increases, the velocity profile in each case tends to become parabolic. As the convergent half angle of the channel is increased, the length required for the flow to become fully developed increases as shown on these figures.

For vertical velocity in convergent flow, the values of V are negative, which means that the direction of motion of the fluid elements in the vertical direction is away from the channel wall. And, there is a positive fluctuation of V component around the cross section X=10, which may present the velocity instability character near inlet segments when a flat inlet flow squeezes into the convergent channel.

(2) Divergent channel flow

In this section, results for divergent channel flow will be considered. A typical geometry for this study and boundary conditions has already been discussed in Chapter 4. The main parameters affecting the performance of the fluid phase of a divergent channel are the inlet Reynolds number and the angle of channel expansion. The velocity vectors and streamline at half divergent channel angle of 2.5, 5.0, 7.5 degree are depicted in Figure 5.1.9 through Figure 5.1.11. Figure 5.1.12 to Figure 5.1.17 show the axial and vertical component distributions of flow velocities. All these velocities and distances are non-dimensionlized with respect to inlet average velocity (u_o) and inlet half width (h_o) of the channel.

In a divergent channel, it is clear that the centerline velocity U_c decreases downstream, and the numerical value of the velocity gradient at the wall ($\partial U / \partial Y$) decreases along the x-axis. The flow will separate and lead to a reverse flow in the downstream. Figure 5.1.18 shows the separation point locations of divergent channel flow at the half channel angles of 5.0, 7.5 degrees for various Reynolds numbers in the range of

laminar flow. Moreover, there is no separation happening or taking place in the chosen channel length for a smaller half angle of θ=2.5°. The reason for this may be the fact that as the angle decreases below a certain limit at a fixed Reynolds number, the location of separation point will move downstream much faster than before.

Figure 5.1.18 indicates that with the increase in Reynolds number, the separation will occur early. For any fixed Reynolds number, the separation distance is found to be shorter for the geometry with a larger half angle of channel. For all of these cases when the flow separation takes place, there is a reverse back flow; however, the reverse flow velocity is much smaller as compared with main flow velocity in the given length of channels. When θ=7.5°, the ratio of the maximum reverse velocity with the corresponding largest velocity of main flow is about 0.7%, and the ratio of the maximum reverse flow thickness with the corresponding half channel width is 8%.

Figure 5.1.15, 5.1.16 and 5.1.17 also show the vertical velocity distribution. Here, the values of V are positive. This means that the direction of motion of the fluid elements in the normal direction is away from the centerline. It can be seen that the absolute values of V decrease when increasing along the x-axis.

5.2 Particle Phase

The objective of this section is to study the particle trajectory under the influences of inertia forces, viscous forces, gravity forces and electrostatic image forces. Several cases of particle flow in a convergent or divergent channel are discussed below as typical examples.

5.2.1 Particle Trajectory in Convergent Channel

Figure 5.2.1 to Figure 5.2.6 show the deposition distances of particles in convergent channels. In these figures, Y_o axis represents the initial position of a particle entering the

channel. Deposition distance Xd is defined as the distance that a particle will have traveled before it deposits on the wall.

It is noted that the channel wall itself can be seen as a streamline. If there is no inertia, viscosity, gravity and electrostatic charge, the particle will simply move along with the fluid and exit the channel without hitting the channel wall. Practically, while particles near the channel wall, the vertical component of the fluid phase has a tendency to apply viscous forces on the particles and push them away from the wall, while at the same time induced image force on wall will also attract the particles to the wall. Besides, there are still gravity and inertia. That means that the results will be dependent upon the combined influence. It is not obvious for one to state that the closer the initial particle position is to the channel wall, the faster the particles move to the channel wall.

The case of S=100, G=1, $\theta=2.5^{\circ}$ is shown in the figure 5.2.1. The longest deposition distance is observed as 1.53, 5.66, 17.23, 19.11, 16.43, 16.27 for Q=10000, 100, 1, 0.1, 0.001 and 0.00001 respectively, while the initial position Yo, that a particle entering the channel will have the longest deposition distance, is observed as 0, 0.01, 0.23, 0.66, 0.86 and 0.9. The Yo initial positions are close to the center of the channel for large Q/G ($Q/G \geq 100$), and shift to the upper channel wall with decreasing Q. For a large Q/G the gravity effect on the particle is much smaller in comparison with the image force. The particles entering the convergent channel at the position near the center of the channel will encounter the image force for both the upper and lower walls with almost the same magnitude. For this reason particles near the center travel far downstream before they deposit on the channel wall. Theoretically, the particle with Yo=0 will not deposit on the wall before exiting the channel for the case of G=0. The larger image force Q will lead to a shorter deposition distance, however, maximum distance occurs at the Q/G=0.1. This is due to the effects of force balance, especially between gravity and image forces. When the image force becomes very small, i.e., $Q<0.001$, their deposition distance are almost the same.

The case of S=100, G=100, θ=2.5° indicates the results of gravity effect increment. It is shown on the Figure 5.2.2. The largest deposition distance is 1.17, 3.08, 2.39, 1.97, 1.96, 1.95 for Q=10000, 100, 1, 0.1, 0.001, and 0.00001, where the Yo is located at 0.005, 0.5, 0.94, 0.96, 0.995, 0.998. Compared with Figure 5.2.1, the deposition distance is decreased with increasing gravity for G=1 to 100. It is also observed from the figures, the initial Yo positions shifted closer to the upper wall because of the rise of gravity force. The maximum deposition distance occurs at the Q/G=1. Being similar with Figure 5.2.1 when Q/G <0.001, the curves are nearly overlapping in most segments

Figure 5.2.3 to Figure 5.2.6 are cases of half convergent channel angles of 5° and 7.5°. They have similar tendency of deposition distance in changing various Q/G. For the case of S=100, G=1, θ=5.0° in Figure 5.2.3, the longest deposition distance is observed as 1.96, 4.61, 10.12, 10.75, 11.21, 11.36 for Q=10000, 100, 1, 0.1, 0.001 and 0.00001. The Yo is located at 0, 0.005, 0.2, 0.42, 0.58, 0.62. For the case of S=100, G=1, θ=7.5°, the longest deposition distance is 2.22, 4.2, 7.04, 7.5, 7.7 at Q=10000, 100, 1, 0.1, 0.001 and 0.00001. The Yo is 0, 0.005, 0.12, 0.2, 0.24, 0.24. It is clear that the deposition distance will increase as the convergent angle decreases. In Figure 5.2.5, the dashed lines represent the deposition distance results of uniform flow. In this case, the uniform flow is used instead of the real developing flow in a convergent channel for solving the governing equations of particle movements. It is found that particles tend to travel farther than those of uniform flow, and only those near the walls of the developing flow have a shorter travel distance, but the difference is small, especially for smaller Q and G.

5.2.2 Particle Trajectory in Divergent Channel

The particles traveling through a divergent channel will vary from the cases of a convergent channel. In a convergent channel, the axial component of the image force will tend to push particle downstream, while the same component in a divergent channel will pull these particles backward. The larger the divergent angle, the stronger the backward

force. In addition, back flow will occur in a divergent flow. Figure 5.2.7 to Figure 5.2.25 depict the deposition distance of particles in divergent channels. The Yo axis also represents the dimensionless initial position of a particle entering the channel.

The cases of S=0.01, G=1 and S=0.01, G=100 at half divergent channel angle 5.0° are shown in Figure 5.2.7 and Figure 5.2.8. For Q=10000, 100, 1, 0.1, 0.001 and 0.00001, the longest deposition distances are 0.0095, 0.12, 1.76, 3.91, 3.11, 3.1, and 0.0078, 0.036, 0.04, 0.031, 0.031, 0.03, respectively. Yo is located at 0, 0.01, 0.52, 0.86, 0.95, 0.95 for G=1. Yo is 0.01, 0.5, 0.95, 0.985, 0.99, 0.99 for G=100. When Q decreases at a fixed S and G, the deposition distance increases until Q/G reaches to a value of Q/G=0.1 for both G=1 and G=100. The maximum longest deposition appears at Q/G=0.1. Considering the case of G=1 in Figure 5.2.8, the ratio of the longest deposition distances between Q=10000 and 100 is 12.6 and that of the ratio between Q=100 and Q=1 is 14.7. After Q/G is less than 0.1, the effect of image force is weakened, relatively. The ratio of longest deposition distance between Q=0.1 and 0.001 reduces to only 1.26, while the ratio between Q=0.001 and Q=0.00001 is almost unity in their deposition distance curves. For a much larger Q, i.e., Q=10000 or Q/G>=100, the image force have a dominant influence on the movement of particles, and the initial position Yo of the longest deposition distance is close to the center of the channel. As the Q/G decreases, the effects of gravity parameter will increase so that Yo will shift upward for a maximum deposition distance.

For the case of S=0.01, G=0.01 and θ=5.0°, the curves of deposition distance are truncated as shown in Figure 5.2.9. When both Q and G are small, the particles will travel farther downstream and exit the channel. But the tendency of curves will be similar with Figure 5.2.7 and Figure 5.2.8. Comparing Figures 5.2.7, 5.2.8, and 5.2.9 at Q=1, the ratio of the longest deposition distance is 9.43 between G=0.01 and 1, and is 44.0 between G=1 and 100. In effect, the gravity force affects more than the image force in these cases and the deposition distance decreases drastically as the gravity parameter G is increased.

Observing Figure 5.2.10 through Figure 5.2.15, they only have different inertia parameter S with the above group of Figures 5.2.7, 5.2.8 and 5.2.9. In the cases of S=1, G=1 of the Figure 5.2.11 and S=1, G=100 of the Figure 5.2.12, the longest deposition distances are 0.091, 0.91, 4.97, 9.91, 3.11, 3.09, and 0.076, 0.39, 0.26, 0.23, 0.205, 0.205, respectively, at Q=10000, 100,1, 0.1, 0.001, 0.00001. The Yo appears at 0, 0.01, 0.56, 0.86, 0.95, 0.95 for G=1, and is 0.01, 0.52, 0.95, 0.985, 0.99, 0.99 for G=100. Both of the two cases have a maximum longest deposition distance at Q/G=1. The another group of figures with S=100 also indicates similar situations of the effects of gravity and image force to particles. Their maximum longest deposition distances occur at Q/G=1, too. Comparing the three group of figures with S=0.01, S=1, S=100 at θ=5.0°, it has been found that, the ratio of longest deposition distance in varying S at Q=1, G=1 is 7.5 between S=0.01 and 1, and 12.4 between S=1 and 100, respectively. In effect, the inertia force affects less than the image force and gravity force. For all these cases, the maximum longest deposition distance keeps in the range of Q/G=0.1 to 1, and the deposition distance are nearly the same after Q/G<0.001.

From the figure group of Figures 5.2.19, 5.2.21, 5.2.22(θ=2.5°), and Figures 5.2.13, 5.2.15, 5.2.16(θ=5.0°) to Figures 5.2.22, 5.2.23, 5.2.24(θ=7.5°) at S=100, the influence of the divergent angle to the particle movements is compared. When the divergent angle of a channel increases, the particles will move farther downstream, but not a lot. Particularly, comparing Figures 5.2.7, 5.2.8, 5.2.9(θ=5.0°) with Figures 5.2.16, 5.2.17, 5.2.18(θ=2.5°), at S=0.01, the increments due to the effect of increasing divergent angle are smaller than above S=100 cases. In general, the effect of increasing divergent angle to the particle movement is smaller in contrast with the convergent one[12]. The reversing axis component of the image force and velocity V may play important roles in compensating for the influence of divergent angle increments.

At θ=7.5°, the divergent channel flow has flow separation and a reverse flow layer appears after X=11.6 as shown on Figure 5.1.9 and Figure 5.1.11. Because the reverse

flow layer is thin and the velocity is very small in comparison with main flow, its influence to deposition distance of particles is small. The situation is shown on Figure 5.2.25, in which the fluid flow starts a back flow after the dashed line. A slight reducing tendency of the deposition distance may be seen from these curves of the particle deposition distances in the figure.

5.3 Deposition Fractions of Particles

As described in Chapter 4, the main purpose of this investigation is to determine the deposition fractions of particles on the channel wall due to the viscous, inertia, gravity and electrostatic image forces at various channel angles. Results of this analysis on particle deposition are given in Figure 5.3.1 to Figure 5.3.75. For each of these figures, the deposition fraction of particles is shown at various axial displacement in a channel.

5.3.1 Deposition Due to the Combined Effects of Viscous Force, Inertia Force, Gravity Force and Image Force

Deposition of particles due to the combined effects of the viscous force, inertia force, gravity force and image force is analyzed by varying inertia parameter S, gravity parameter G and charge parameter Q in solving the governing equations of particle movements. The viscous force is inversely proportional to the parameter S, G and Q. Therefore, the effect from the viscosity of the fluid can also be determined.

Figure 5.3.1 to Figure 5.3.25 are results at constant half divergent channel angle of 2.5°. The parameter S and G range from 0.01 to 100 for varying Q from 0.00001 to 10000. It is obvious from these figures that the particle deposition increases with increasing image force Q at a fixed inertia parameter S and gravity parameter G. One example is shown on Figure 5.3.13 for θ=2.5°, S=1 and G=1. The various deposition fraction of particles at increasing Q is obtained for X displacement equaling to 0.5. It is 100%, 98%, and 35% for Q=10000, 100, 1, and 17%, 5.9% and 4.8% for Q being 0.1,

0.001, 0.00001. At X displacement equal to 1, the deposition for Q>100 reaches to 100% and 53%, 17%, 16% for Q=0.1, 0.001 and 0.00001. Comparing Figure 5.3.1 to Figure 5.3.25, it is observed that when image forces acting on particles become quite large (Q>1000), the particles will deposit soon on the channel walls of the entrance region. When the image forces are less than Q=0.001, the influence of image forces is small and the difference between curve Q=0.0001 and curve Q=0.00001 tends to vary little. In these cases some particles will exit the channel. The influence due to varying image forces is important to the particle deposition fraction.

Figure 5.3.1 to Figure 5.3.5 is a group of curves with a range of G=0.01, 0.1, 1, 10, 100 for a fixed value of S=0.01. At X=0.01 of the figures, the deposition fraction is 92%, 92%, 92%, 92%, 93%, and 25%, 25%, 25%, 25%, 22%, and 1.5%, 1.55, 1.6%, 2.6%, 56%, respectively, for Q=1000, 10, and 0.001. It is shown that the deposition will remain almost the same for any value of G($100 \geq G \geq 0.01$) when Q is large, i.e., Q≥1000. However, as Q becomes smaller, the deposition of particle will increase with increasing G. Another example is shown on Figure 5.3.11 to Figure 5.3.15. In Figure 5.3.11 (G=0.01), the deposition at X=0.1 is 93%, 27%, 1.1%, 0.12 for Q=1000, 10, 0.001 and 0.00001, respectively. As the gravity G increase to 1 as shown on Figure 5.3.13, the deposition becomes 93%, 27%, 1.12%, 0.25%, respectively. Then when G=100, the deposition is 93%, 37% for Q=1000, 10, and 24%, 23% for Q=0.001, 0.00001. It is shown that the deposition remain the same for Q=10000 and 1000, but deposition increases greatly for Q=0.00001 as G increases. These data reveals that when Q is large enough (Q≥1000), the deposition will not be affected by the changing of gravity. In effect, when Q/G is greater or equal to 10, the gravity effect to deposition fraction can be neglected. On the other hand, the deposition increases with increasing gravity in a relatively small Q range(i.e. Q/G < 10), while the charge effect to the deposition fraction can also be neglected when Q/G is less than 0.001. It can also be obtained from the other group of curves at a fixed S. For the case of small Q, the increment in gravity force will increase the deposition of the

particles to the lower channel wall resulting in a higher deposition fraction. More particles will deposit on the lower channel wall even faster as the gravity effect becomes greater. Checking the group of curves in Figure 5.3.1 to 5.3.5 at a large X displacement X=1 again, at Q=0.001 the deposition fraction is 7.8%, 9.9%, 51%, 100%, and 100% for G=0.01, 0.1, 1, 10, 100. The influence of the gravity force to deposition fraction gradually becomes stronger as the X displacement increases. When particles move into the entrance region of the channel, the image force from the upper channel wall will balance with the gravity effect due to a stronger image charge effect in a smaller channel width, especially for Q and G at the same order of magnitude. Therefore, the particles will not deposit on the wall until further downstream, where the image effect becomes weaker as the channel width increases.

Figure 5.3.1, 5.3.11 and 5.3.21 show the deposition fraction for inertia parameter S=0.01, 1 to 100 at G=0.01. The deposition at X equal to 0.1 for S=0.01 is 100%, 100%, 38%, 0.76%, and 0.19%, for Q equal to 10000, 100, 1, 0.001 and 0.00001. The deposition is also found to be 100%, 56%, 12%, 0.14%, 0.12% for S=1, and 57%, 12%, 2.5%, 0.11%, 0.01% for S=100. As X increases to 1, the depositions for the above Q parameter are found to be 100%, 100%, 79%, 0.4%, 0.22% for S=0.01, and 100%, 100%, 53%, 0.4%, 0.14% for S=1, and 100%, 55%, 10%, 0.19%, 0.01% for S=100. It is revealed from these data that the deposition decreases with increasing S for all Q. When Q is greater than 0.001, the tendency is even obvious. The same phenomena are also observed for the cases of other G values. The deposition increases with decreasing inertia effect. Increments of inertia effect on the particles consequently increase the particle momentum in the axial direction. It actually helps the particles to prevent deposit on the channel wall at the entrance region and the particles will travel further downstream before they can be attracted to the channel wall by the image force. Therefore, it results in the decrease of particle deposition.

5.3.2 Divergent Channel Angle Effects on the Particle Deposition Along the Axial Distance X

In all cases, the particle deposition fraction increases with increasing X, as shown in Figure 5.3.1 to Figure 5.3.75. From these figures it can be found that, when the gravity effect parameter G≥10, almost all particles will deposit soon on the channel wall; while most of the particles will travel downstream and move out the channel exit at Q≤1000 and G≤0.01.

The channel angle effect to the deposition fraction is small in a divergent channel and has been discussed in section 5.3.2. When both Q and G are large, the deposition fraction is nearly the same for the half divergent channel angles of 2.5, 5.0, 7.5 degree. But for very small Q and G, the clear deposition difference between various divergent channel angles is shown. Comparing Figure 5.3.1 ($\theta=2.5^{o}$) with Figure 5.3.51 ($\theta=7.5^{o}$), the deposition fraction at X=1 for Q=0.00001 and G=0.01 is 2.19% in Figure 5.3.1 and is 1.52% in Figure 5.3.51. The effect of a larger divergent channel angle will decrease the deposition fraction of particles. This effect appears at those cases of a smaller G and Q. Moreover, the effect of the divergent channel angle will be enhanced as the inertia parameter increases as shown on Figure 5.3.21 and Figure 5.3.71 (S=100). Comparing the two figures, the difference of deposition fraction at Q=1 becomes clear. At X=1, G=0.01, Q=1, the deposition is 10.4% for $\theta=2.5^{o}$ and is 7.1% for $\theta=7.5^{o}$. At a larger divergent channel angle and at larger inertia parameters, more particles with small Q and G will exit the channel.

5.3.3 Deposition Fraction at G=0

When the gravity force is perpendicular to the X-Y plane, it has no effect on the deposition of particle to the channel walls. This situation can be considered as G=0 in the analysis. Figure 5.3.76 to Figure 5.3.78 depict the deposition fraction of zero gravity effect at various Q and S. The deposition fractions at X=1 is 100%, 78%, 7% for Q=1000,

1, 0.001 at S=0.01, and are 100%, 49%, 2.9% at S=1 and is 93%, 8.6%, 1.1% at S=100. The deposition fraction decreases much in comparison with those G≠ 0 cases. At G=0, the deposition of particles will depend on Q and S, and at a smaller S and larger Q, a larger deposition fraction will be obtained.

5.4 Deposition Computation for Various Particle Size

In a practical situation, it is easy to compute the parameter S, G and Q from each particle size. Its deposition fraction can be found from the above mentioned deposition figures. A practical particle example is described below:

Consider a fluidic device which has an air fluid phase with the velocity of 30 cm/s, and the half width h_0 equal to 0.1 cm. The particle specific gravity is assumed to be 1, and a charge electron density of 1 electron per 1.18 E-10 cm^2, and μ=1.8E-4 dyne sec/cm^2, ε_0 = 8.85434E-21 Coulomb^2/dyne cm^2. The particle size is 5 μm. Based on the formula in Chapter 4, we have:

q = 26629 electron

m = 5.236×10^{-10} gram

S = 0.093

Q = 0.00032

G = 0.01

In practice, the parameter S and G are proportional to a^2, where a is the radius of a particle. The electrostatic charge on a particle may be considered as proportional to the surface area of the particle, so Q is proportional to a^3. If a particle size is increased by a factor of 10, the S and G will be increased by a factor of 100; while Q will be the product by a factor of 1000. Considering the case of S=0.1, G=0.1, Q=0.001, θ=2.5° as shown in Figure 5.3.7, it is found that the deposition fraction for X=0.01, 0.1 and 1 is 0.58%, 2.8%,

and 9.1%, respectively. When S=10, G=10 and Q=10 as shown in Figure 5.3.19, the deposition for X=0.01, 0.1 and 1 is 2.7%, 12%, and 58%, respectively.

CHAPTER 6

CONCLUSIONS

The problems of aerosol particle deposition in a convergent or divergent channel flow have been investigated in the present study. An incompressible, two-dimensional gas-solid flow with a dilute suspension has been taken into consideration for the investigation.

A laminar fluid phase from developing to fully developed flow has been solved numerically for both convergent and divergent cases by the finite element method. A computational program has been developed by using FIDAP package to get a velocity profile of the fluid phase.

Much effort has been expended to identify the significance of various parameters in the complex phenomena of the gas-solid flow. Motion of small suspended particles in a channel flow under the combined effects of inertia, gravity, viscous force and electrostatic image force are studied using a Lagrangian simulation technique. A digital simulation procedure for studying deposition process of aerosol particle has been developed. Computations in varying the parameters have been made and based on the presented results, the following conclusion may be drawn:

The ranges of parameters are θ=2.5° to 7.5°, S=0.01 to 100, G=0.01 to 100, Q=0.00001 to 10000, Re=100, and L/h_0=40.

(1) For either convergent or divergent channel flow with a flat inlet velocity profile a sharp gradient of velocity exists at those cross sections near channel inlet. As the axial length increases the velocity profile in each case tends to become parabolic. The larger the half angle of a channel, the longer is the length required for the flow to become fully developed.

(2) In a divergent channel, the numerical value of the velocity gradient at the wall decreases along the x-axis. The fluid flow will separate and lead to a reverse flow

downstream. The separation will happen early when the Reynolds number of the fluid flow increases. For any fixed Reynolds number the separation distance is found to be shorter for the geometry with a larger half angle of channel. The speed of the reverse flow after the separation point is much smaller as compared with the main flow speed.

(3) Particle trajectory in a channel is dependent upon the combined influence such as gravity, image force and so on. The closer initial particle position to the channel wall may not mean faster moving to the channel wall. In convergent channel flow cases, the maximum distance occur at the Q/G=0.1 for a smaller G, and for a larger G the maximum distance occur at the Q/G=1. When the image force becomes very small, Q<0.001, those deposition distance curves are nearly overlapping in most segments. In particular, when the uniform flow is used instead of real laminar flow, the difference of deposition distance curves is small, especially for a smaller Q and G.

(4) Similar with convergent cases, the maximum largest deposition distance keeps in the range of Q/G=0.1 to 1 in divergent cases and their deposition distance are almost the same after Q/G<0.001. When the divergent angle of a channel increases, the particle suspension will move farther downstream but not a lot. The effect of increasing divergent angle to the particle movement is smaller in contrast with the convergent one. In divergent channels with small channel angles, though a reverse flow layer appears after the flow separation point, its influence to deposition distance of particles is small due to the fact that the layer of separation is very small for the range of axial distance studied(L/h_o=30).

(5) The influence due to a varying image force is important to the particle deposition fraction. When image forces acting on the particles become quite large(Q>1000), the particles will deposit soon on the channel walls of the entrance region, and the deposition will remain almost the same for any value of G. When the image forces are less than Q=0.001, the influence of image forces is small. In effect, when Q/G is

greater or equal to 10, the gravity effect to deposition can be neglected, while the charge effect to deposition fraction can also be neglected at $Q/G<0.001$.

(6) For the case of small Q, the increment in gravity force will increase the deposition of the particles to the lower channel wall. The more particles will deposit faster on the lower channel wall, as the gravity effect becomes greater. The influence of the gravity force to deposition fraction gradually becomes stronger as the X displacement increases. For Q and G at same order of magnitude, the particles will not deposit on the wall until it reaches further downstream where the image effect becomes weaker. At $G=0$, the deposition fraction decrease much in comparison with those $G\neq0$ cases.

(7) The deposition decreases with increasing S for all Q and G. When Q is greater than 0.001, the tendency is even more obvious.

(8) The particle deposition fraction increases with increasing X displacement. When the gravity effect parameter $G\geq10$, almost all particles will deposit soon on the channel wall, while most of particles will travel downstream and move out the channel exit at $Q\leq1000$ and $G\leq0.01$. The channel angle effect to the deposition fraction is small in a divergent channel. The effect of a larger divergent channel angle will decrease the deposition fractions at those cases with a smaller G and Q. Moreover, the effect of the divergent channel angle will be enhanced as the inertia parameter increases.

A detailed analysis on the deposition of gas-solid suspension in a convergent or divergent channel has been studied in this work. The following may be considered for a future investigation:

(1) Turbulent flow pattern should be investigated. Special attention should be paid to the impulse velocity components.

(2) Investigation may enlarge to a larger channel angle cases as well as an inclined channel.

(3) Some other effects such as lift force, boundary effect etc. may be included in a more detailed model.

APPENDIX FIGURES IN CHAPTER 5

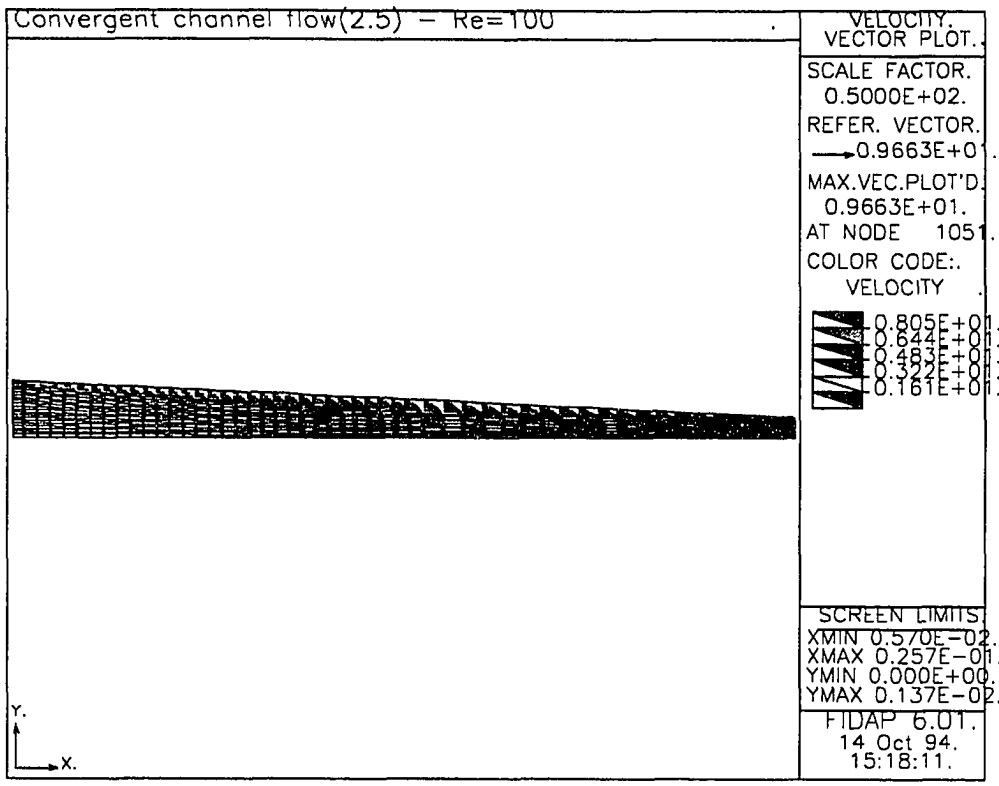

Figure 5.1.1 Velocity Vector Plot of a Convergent Channel

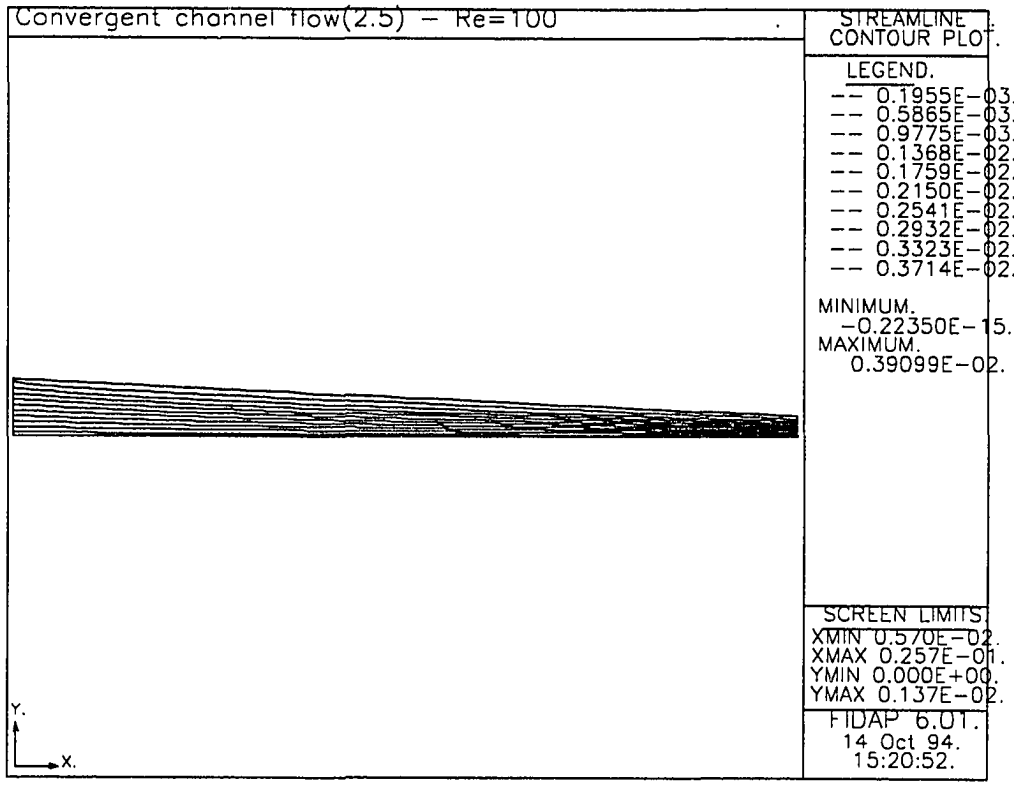

Figure 5.1.2 Streamline Contour Plot of a Convergent Channel

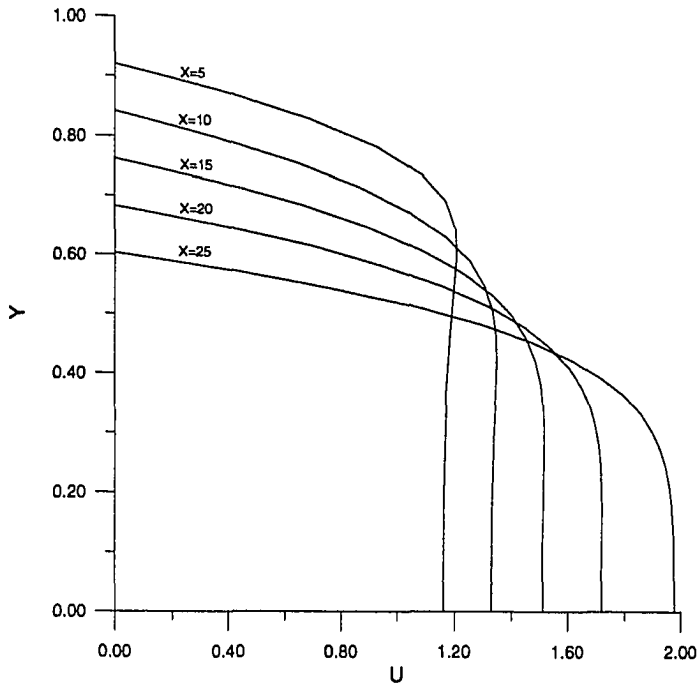

Figure 5.1.3 Velocity Profile at X-direction in the Convergent Channel of $\theta = 2.5^{\circ}$

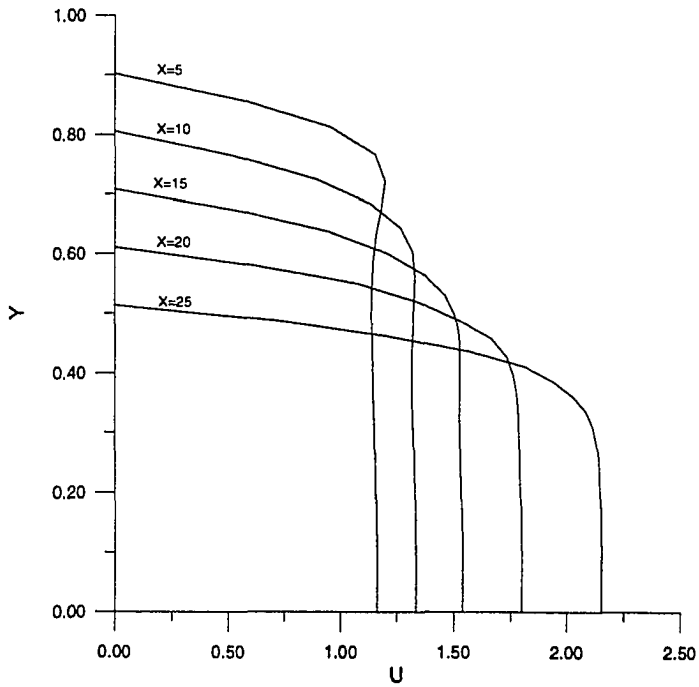

Figure 5.1.4 Velocity Profile at X-direction in the Convergent Channel of $\theta = 5.0^{\circ}$

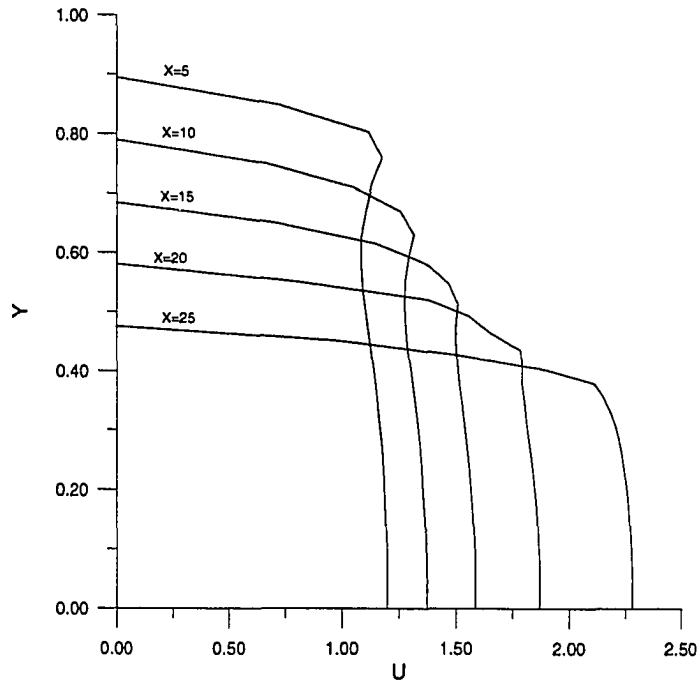

Figure 5.1.5 Velocity Profile at X-direction in the Convergent Channel of $\theta = 7.5^{o}$

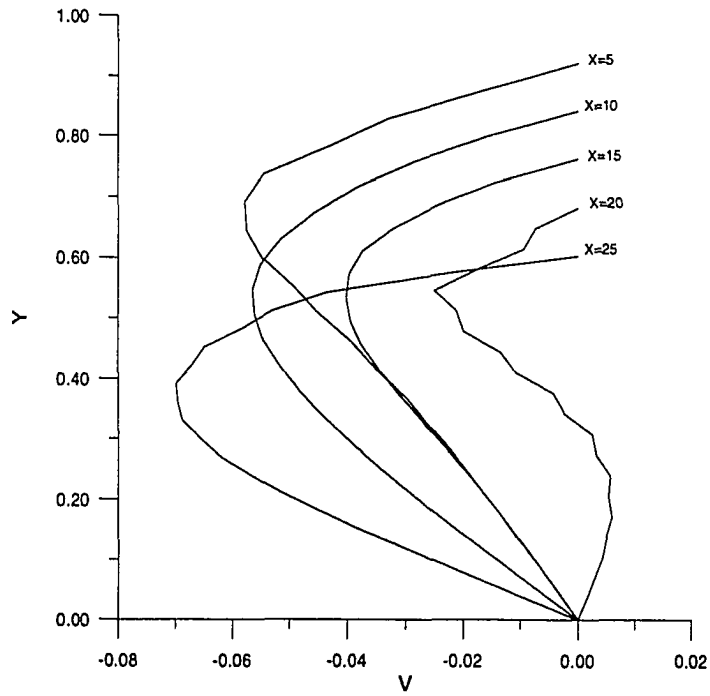

Figure 5.1.6 Velocity Profile at Y-direction in the Convergent Channel of $\theta = 2.5^{o}$

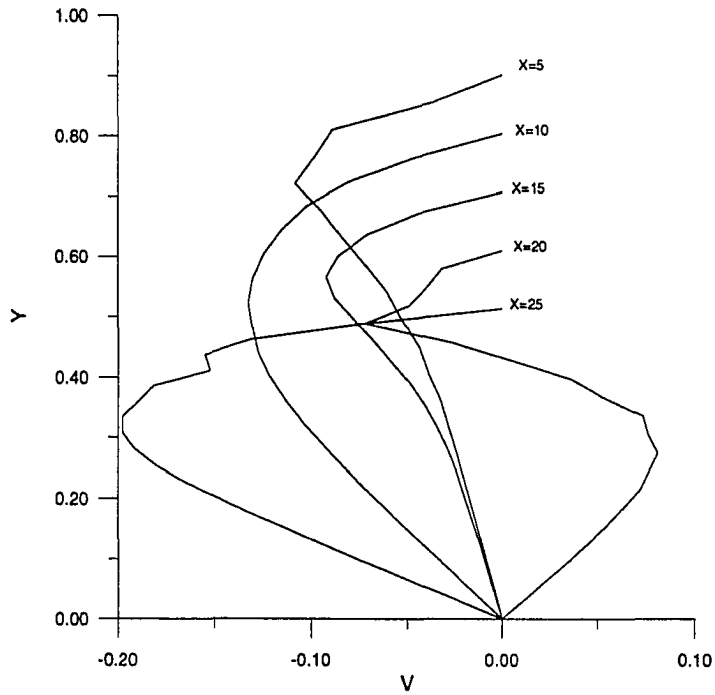

Figure 5.1.7 Velocity Profile at Y-direction in the Convergent Channel of $\theta = 5.0^{o}$

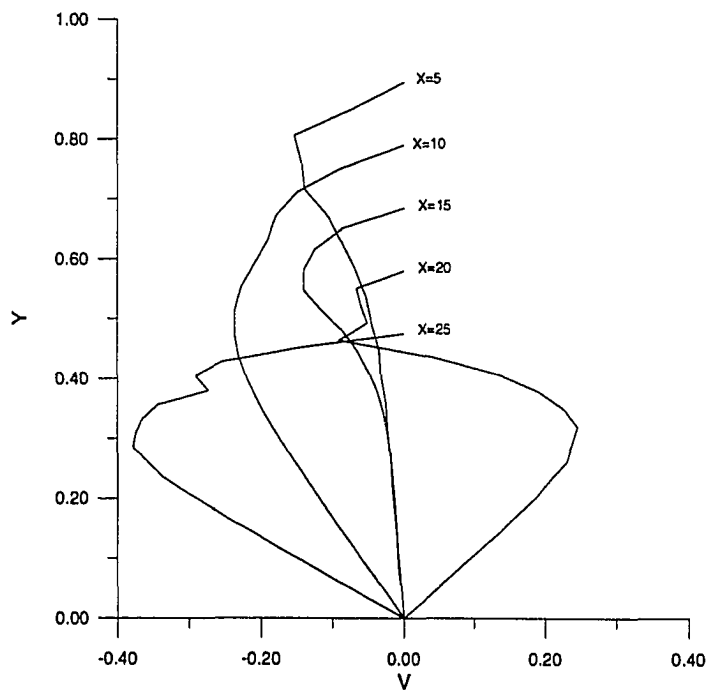

Figure 5.1.8 Velocity Profile at Y-direction in the Convergent Channel of $\theta = 7.5^{o}$

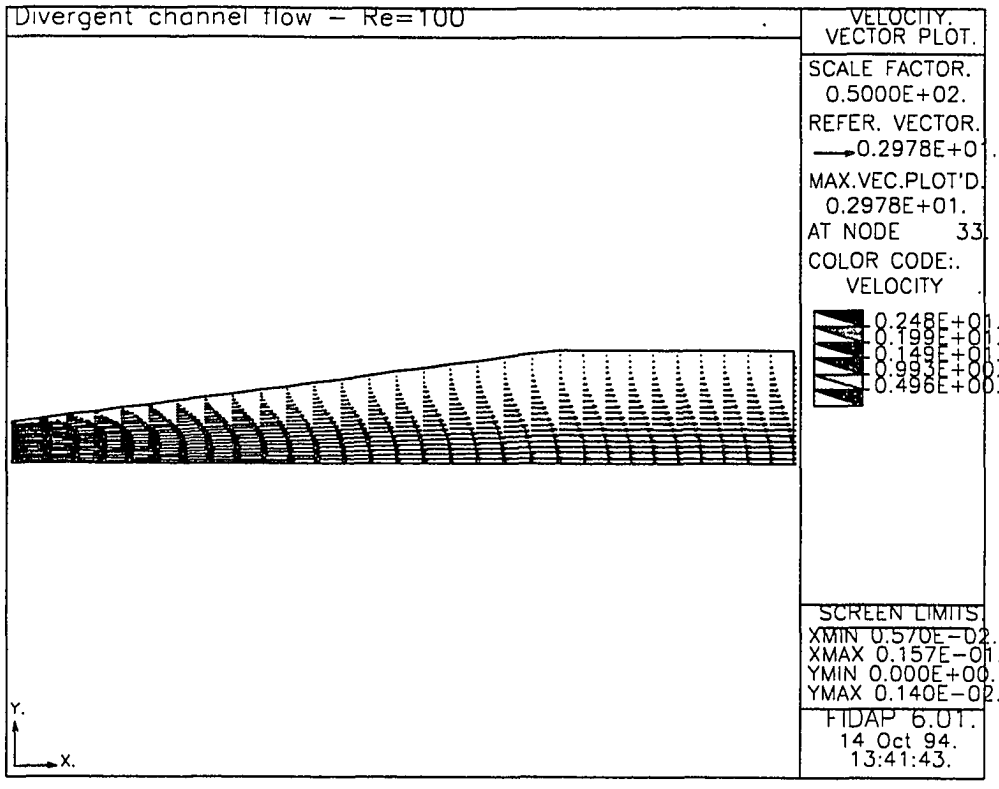

Figure 5.1.9 Velocity Vector Plot of a Divergent Channel

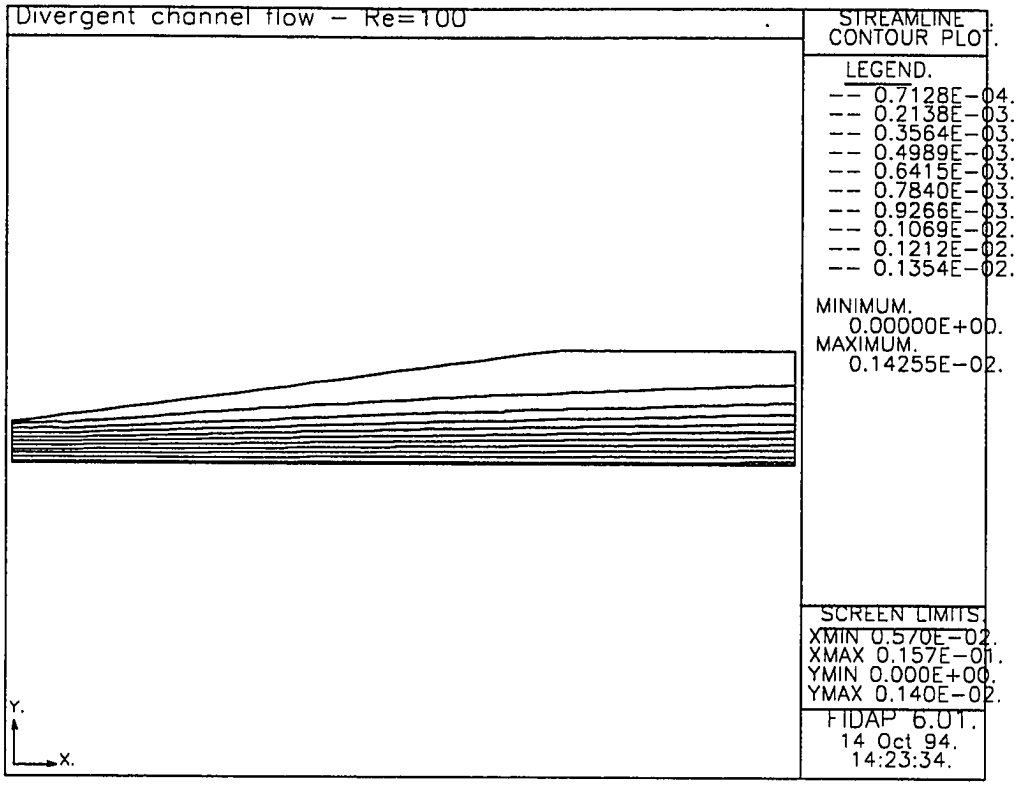

Figure 5.1.10 Streamline Contour Plot of a Divergent Channel

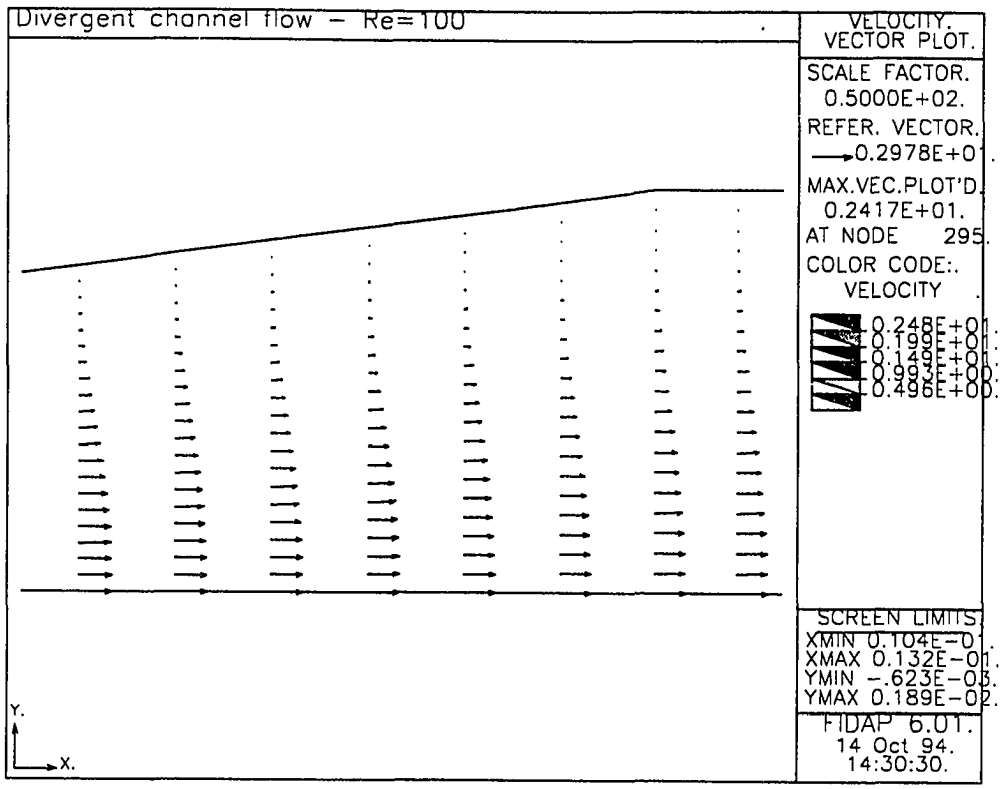

Figure 5.1.11 Local Velocity Vector Plot Around the Separation position

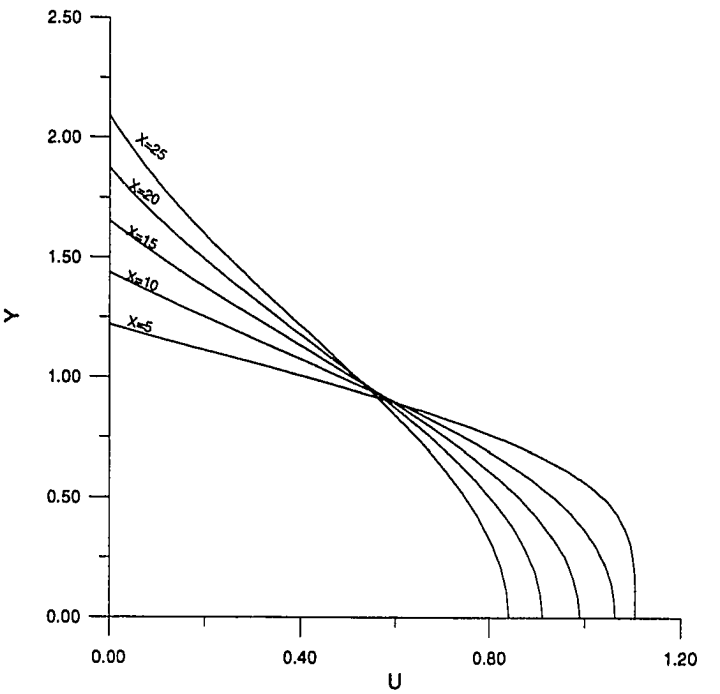

Figure 5.1.12 Velocity Profile at X-direction in the Divergent Channel of $\theta = 2.5^{\circ}$

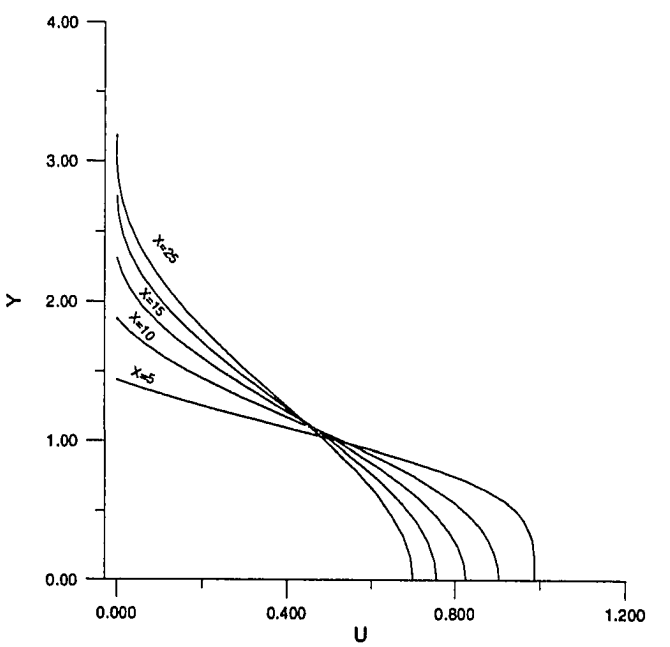

Figure 5.1.13 Velocity Profile at X-direction in the Divergent Channel of $\theta = 5.0^{\circ}$

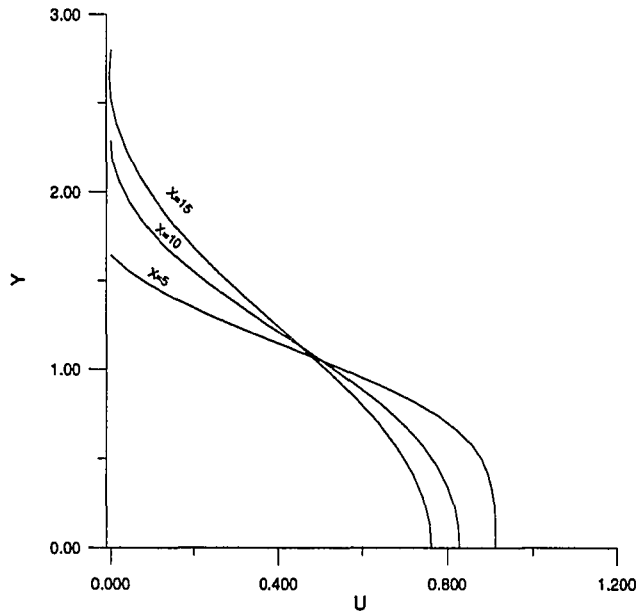

Figure 5.1.14 Velocity Profile at X-direction in the Divergent Channel of $\theta = 7.5^{o}$

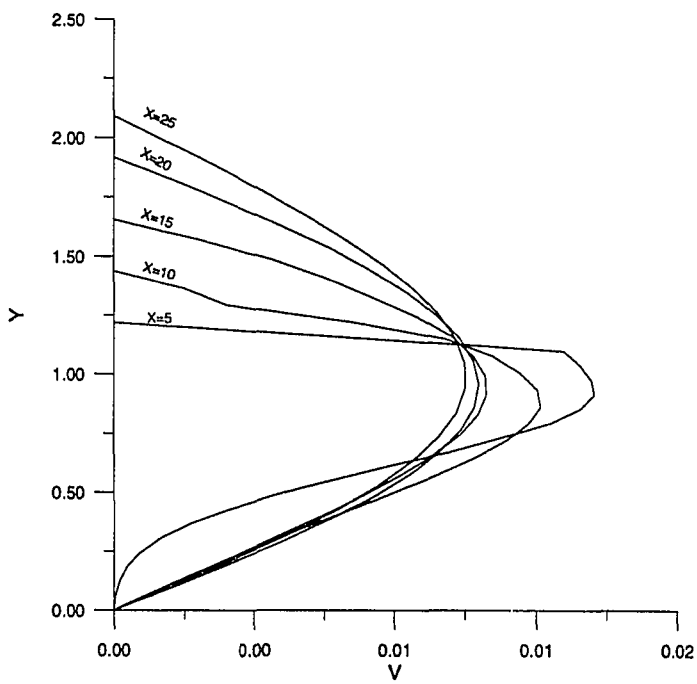

Figure 5.1.15 Velocity Profile at Y-direction in the Divergent Channel of $\theta = 2.5^{o}$

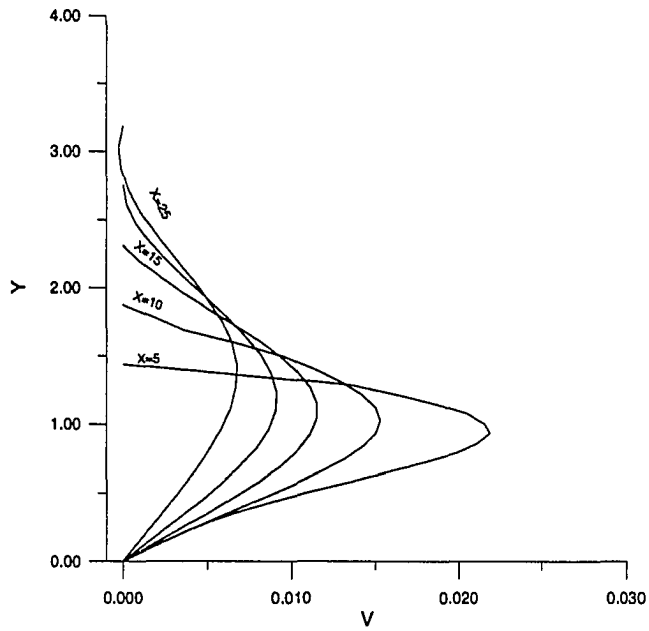

Figure 5.1.16 Velocity Profile at Y-direction in the Divergent Channel of $\theta = 5.0°$

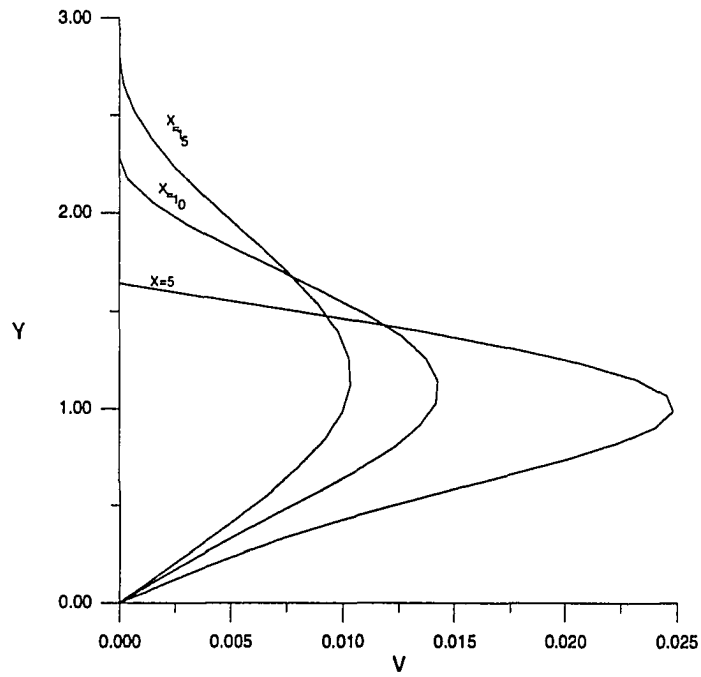

Figure 5.1.17 Velocity Profile at Y-direction in the Divergent Channel of $\theta = 7.5°$

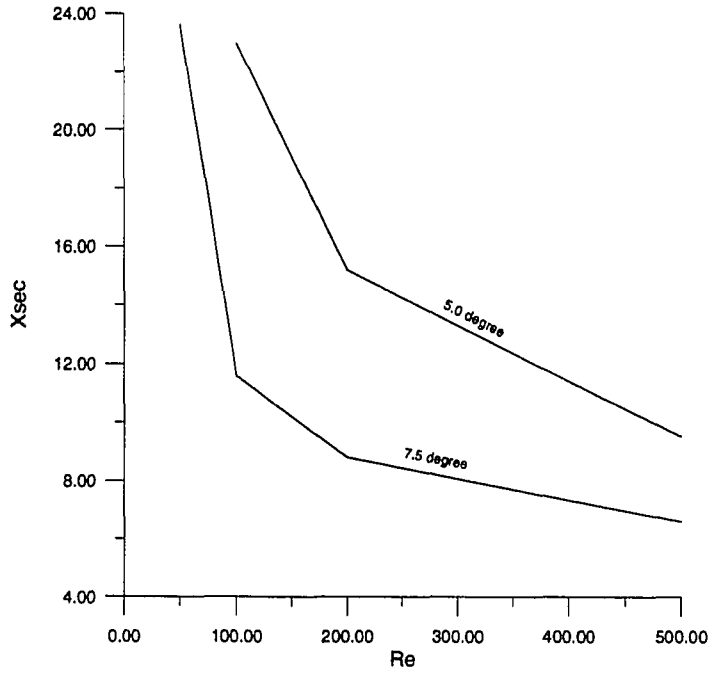

Figure 5.1.18 Flow Separation position in a Divergent Channel

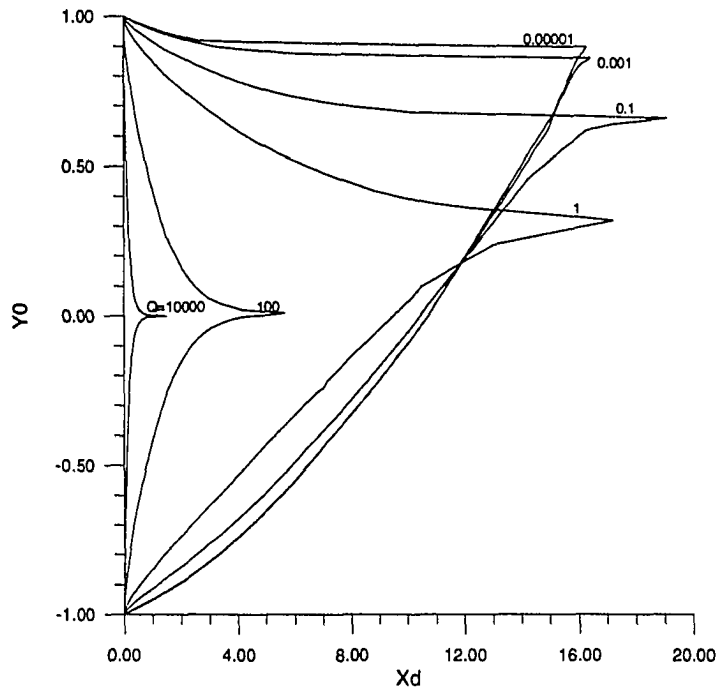

Figure 5.2.1 Particle Deposition Distance in a Convergent Channel at S=100, G=1 and θ =2.5°

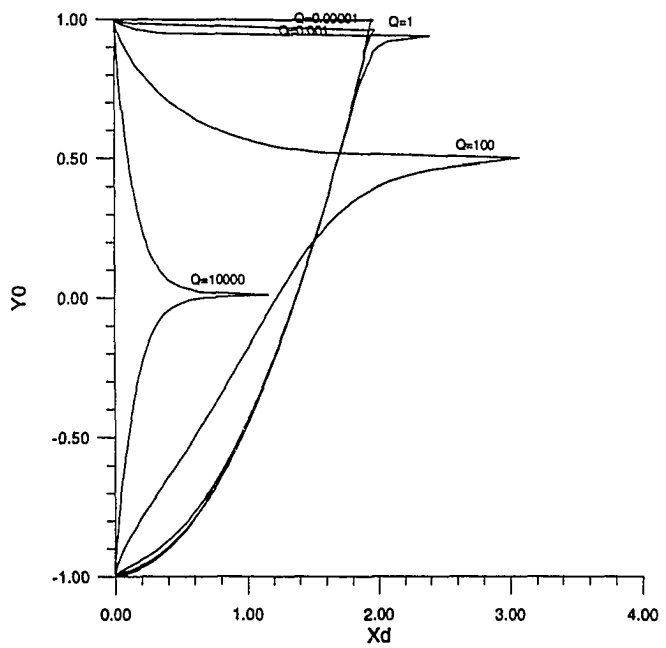

Figure 5.2.2 Particle Deposition Distance in a Convergent Channel at S=100, G=100 and θ =2.5°

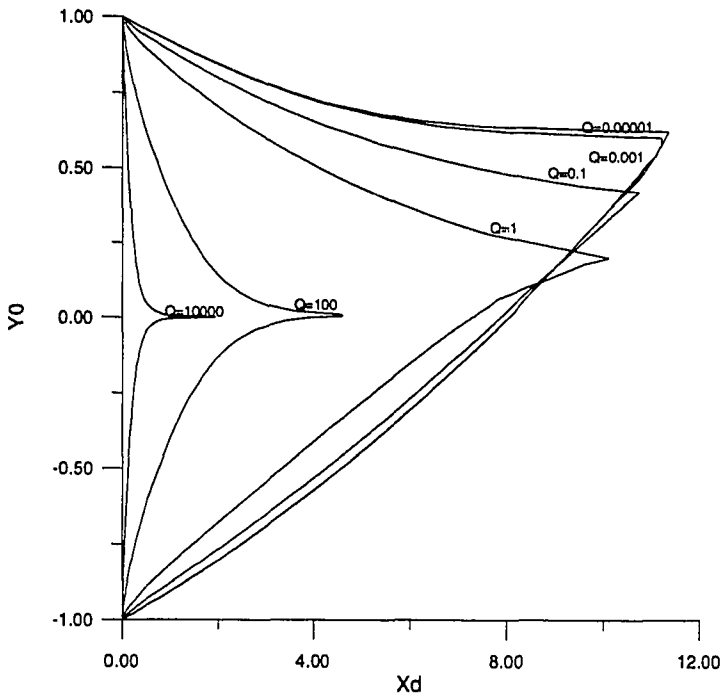

Figure 5.2.3 Particle Deposition Distance in a Convergent Channel at S=100, G=1 and θ =5.0°

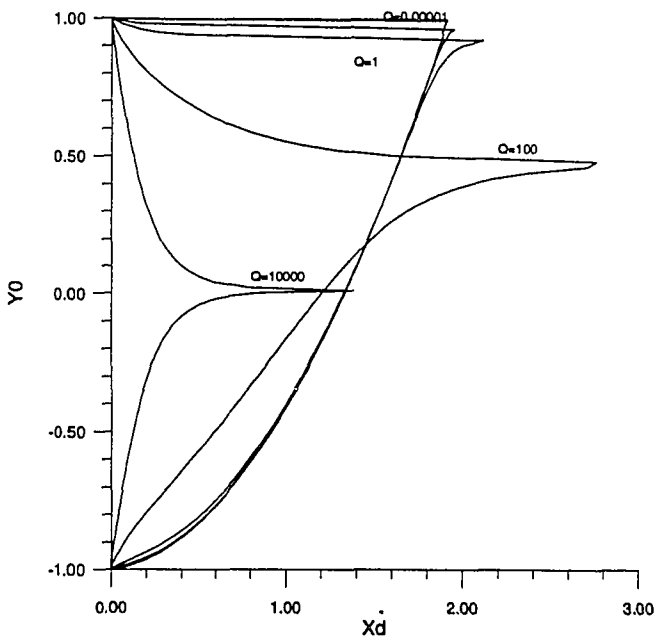

Figure 5.2.4 Particle Deposition Distance in a Convergent Channel at S=100, G=100 and θ =5.0°

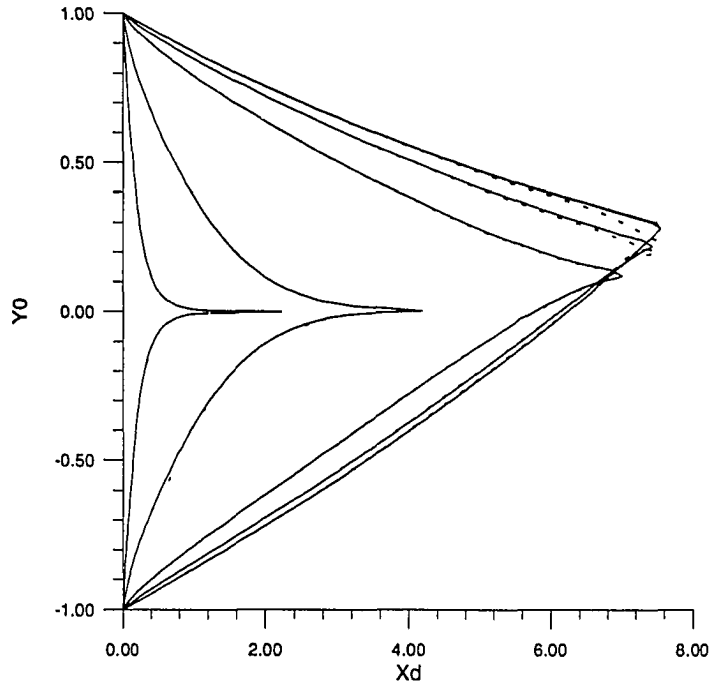

Figure 5.2.5 Particle Deposition Distance in a Convergent Channel at S=100, G=1 and $\theta = 7.5^{\circ}$

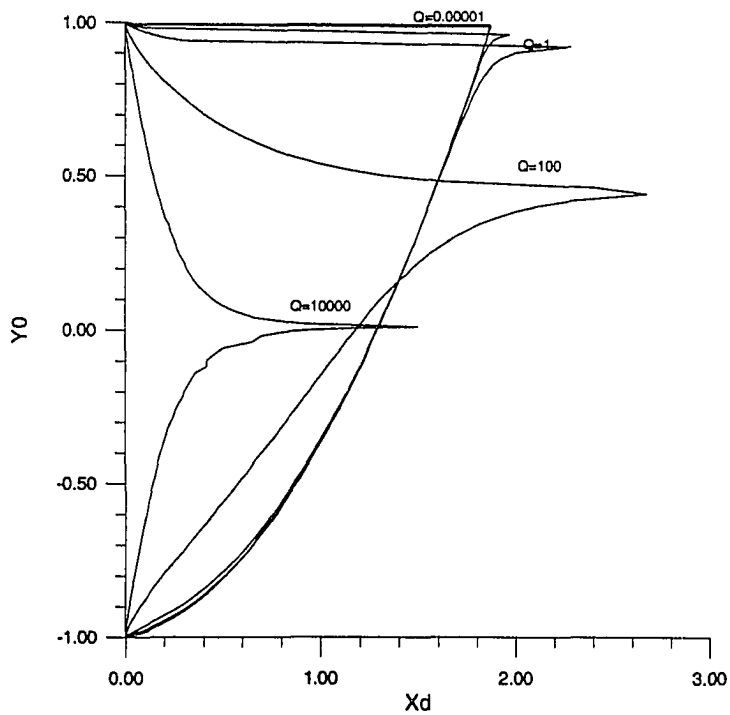

Figure 5.2.6 Particle Deposition Distance in a Convergent Channel at S=100, G=100 and $\theta = 7.5^{\circ}$

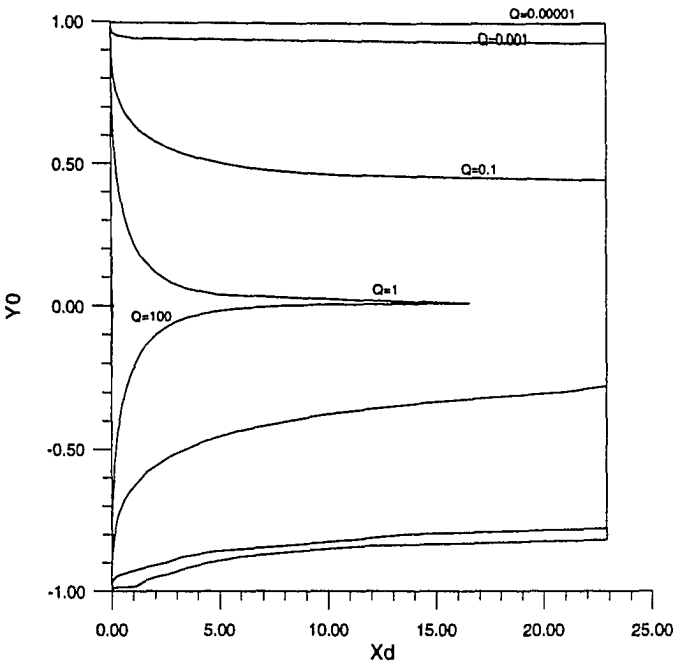

Figure 5.2.7 Particle Deposition Distance in a Divergent Channel at S=0.01, G=0.01 and $\theta = 5.0^{\circ}$

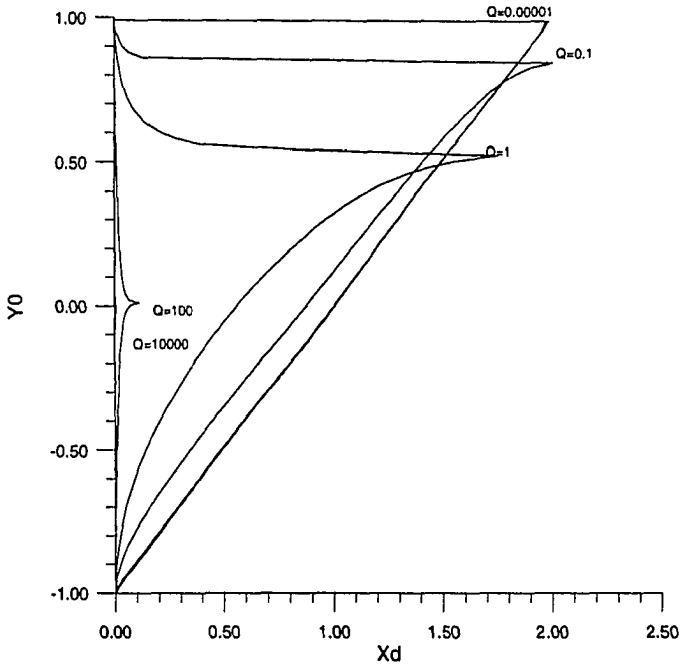

Figure 5.2.8 Particle Deposition Distance in a Divergent Channel at S=0.01, G=1 and $\theta = 5.0^{\circ}$

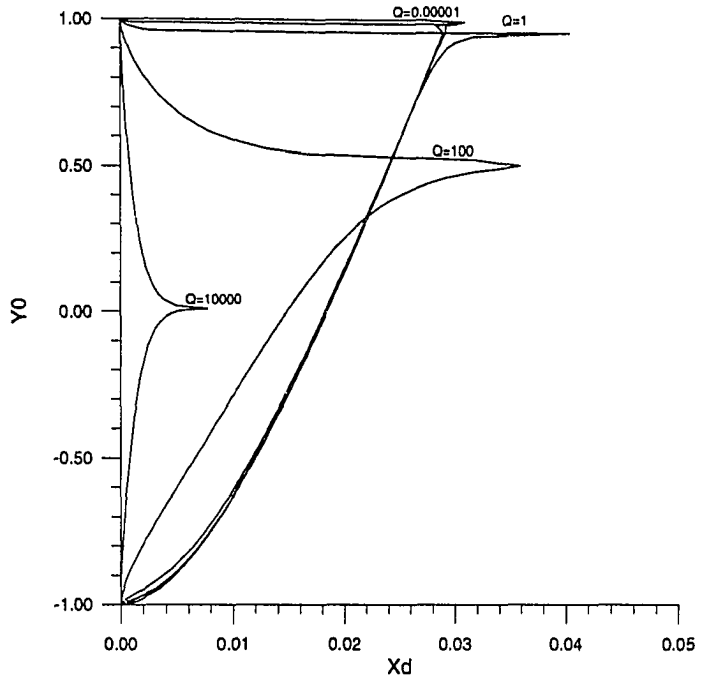

Figure 5.2.9 Particle Deposition Distance in a Divergent Channel at S=0.01, G=100 and $\theta = 5.0^{\circ}$

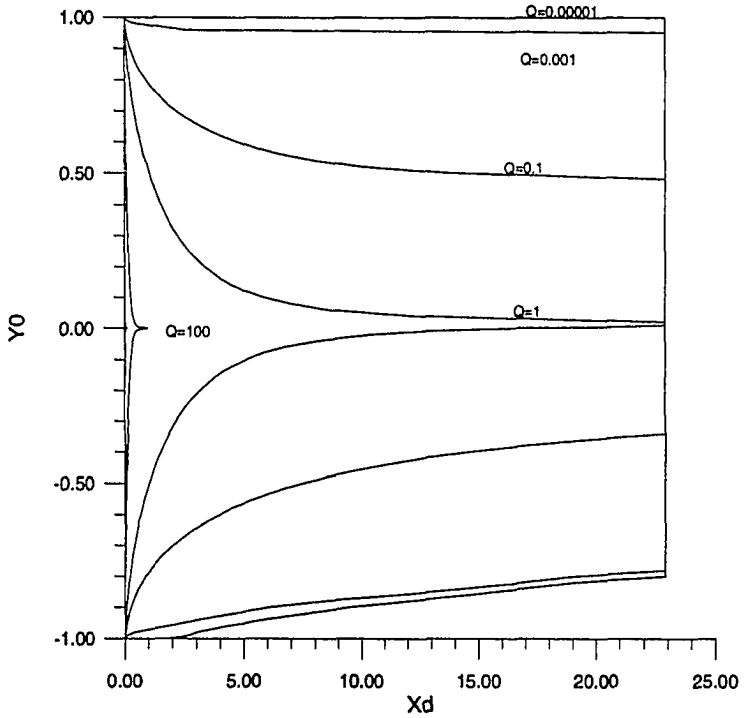

Figure 5.2.10 Particle Deposition Distance in a Divergent Channel at S=1, G=0.01 and $\theta = 5.0^{\circ}$

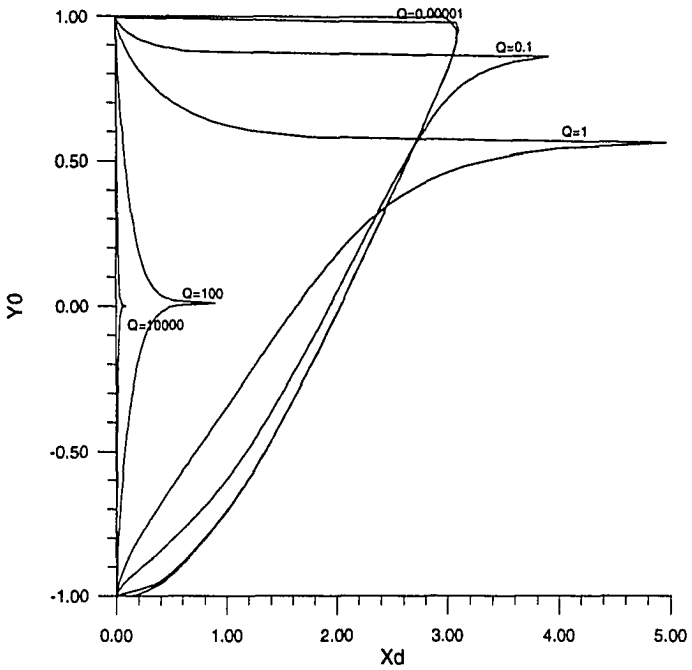

Figure 5.2.11 Particle Deposition Distance in a Divergent Channel at S=1, G=1 and $\theta = 5.0^{\circ}$

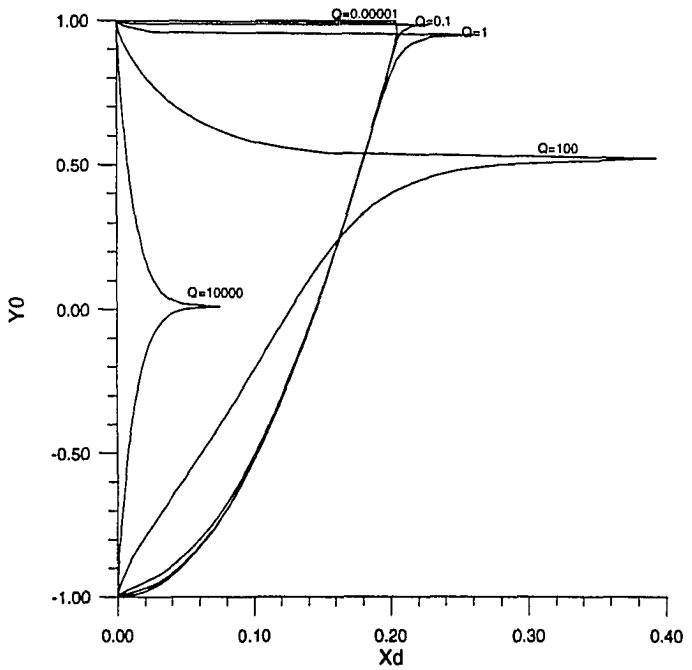

Figure 5.2.12 Particle Deposition Distance in a Divergent Channel at S=1, G=100and $\theta = 5.0^{\circ}$

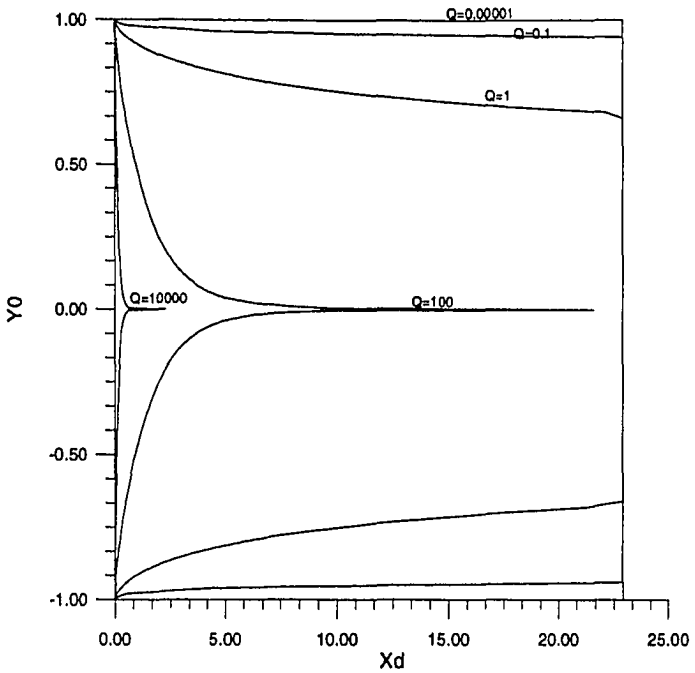

Figure 5.2.13 Particle Deposition Distance in a Divergent Channel at S=100, G=0.01 and $\theta = 5.0^{\circ}$

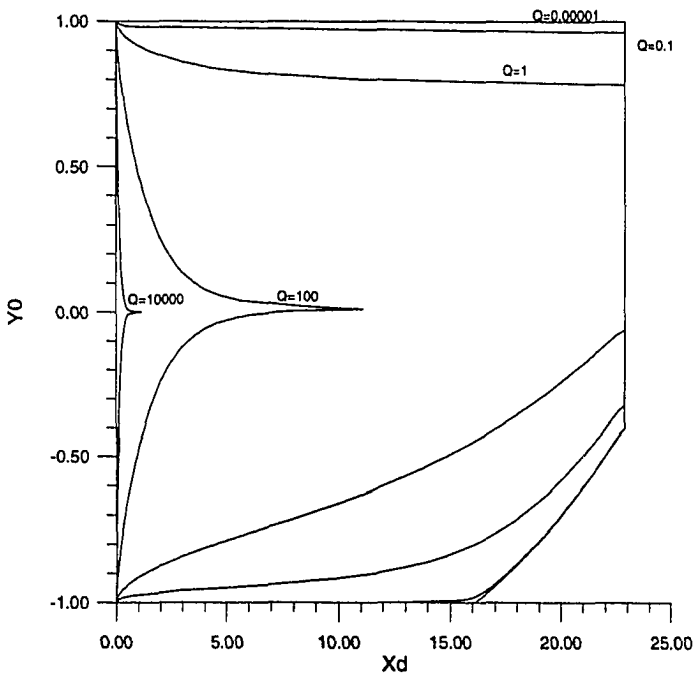

Figure 5.2.14 Particle Deposition Distance in a Divergent Channel at S=100, G=1 and $\theta = 5.0^{\circ}$

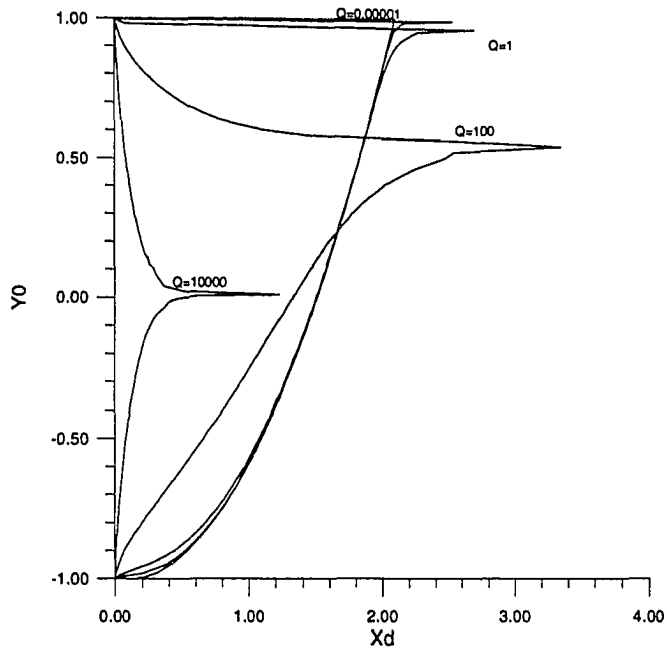

Figure 5.2.15 Particle Deposition Distance in a Divergent Channel at S=100, G=100 and $\theta = 5.0^{\circ}$

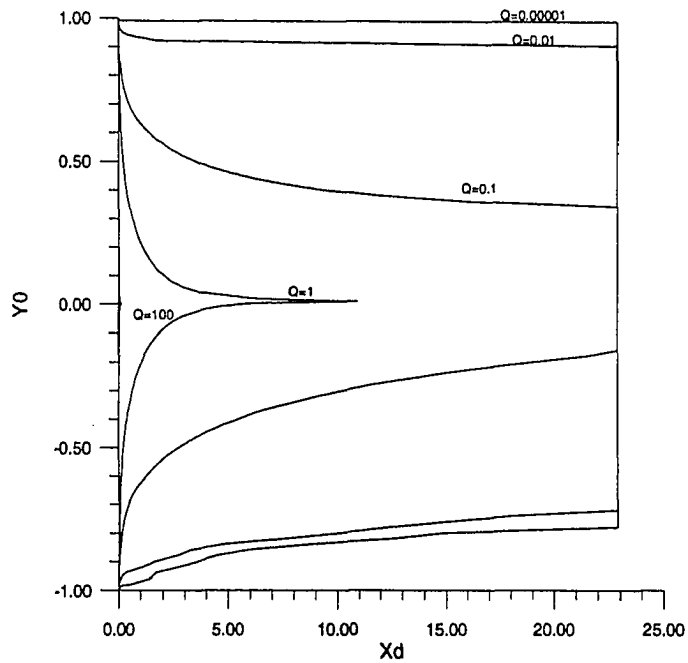

Figure 5.2.16 Particle Deposition Distance in a Divergent Channel at S=0.01, G=0.01 and $\theta = 2.5^{\circ}$

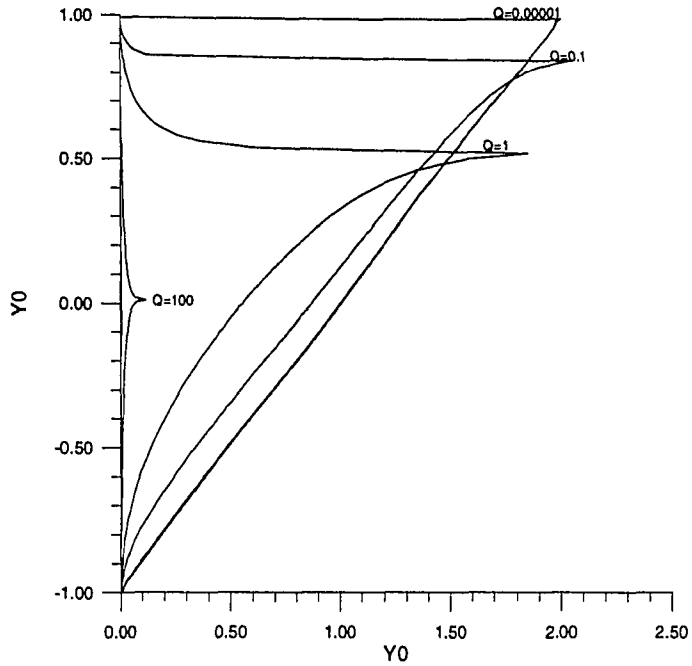

Figure 5.2.17 Particle Deposition Distance in a Divergent Channel at S=0.01, G=1 and $\theta = 2.5^{o}$

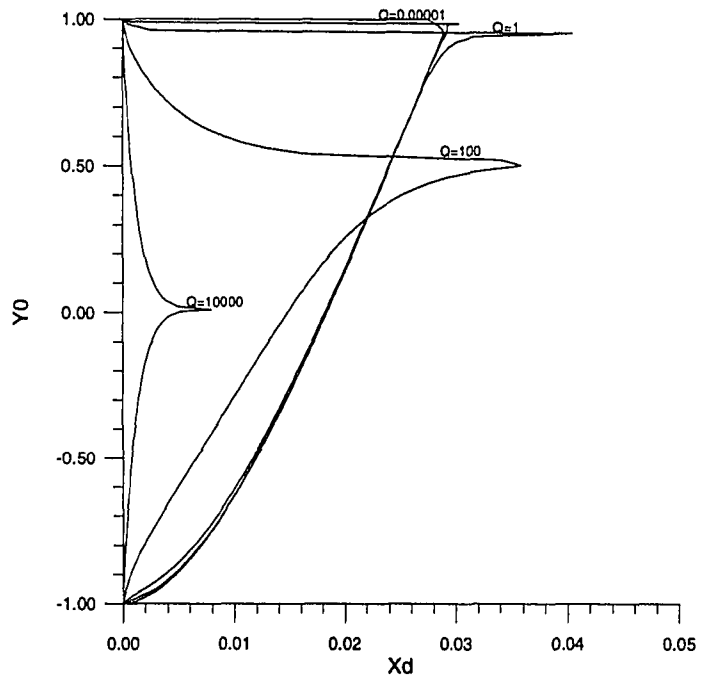

Figure 5.2.18 Particle Deposition Distance in a Divergent Channel at S=0.01, G=100 and $\theta = 2.5^{o}$

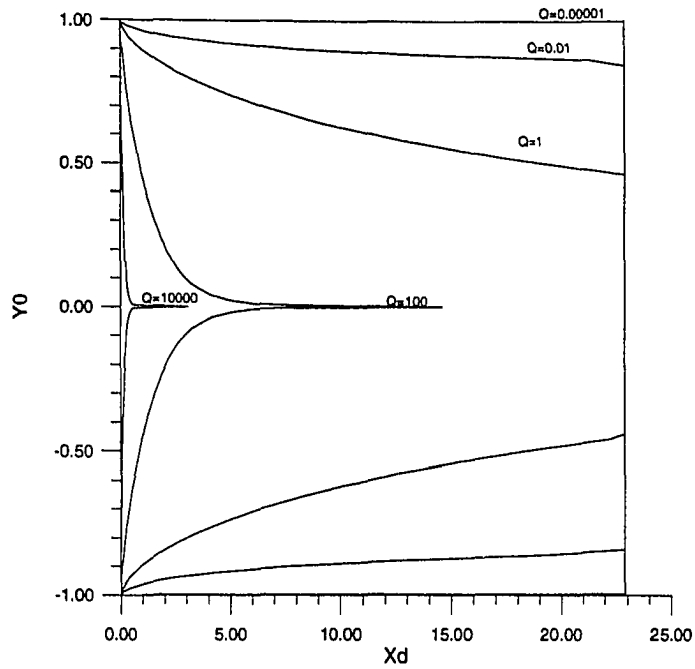

Figure 5.2.19 Particle Deposition Distance in a Divergent Channel at S=100, G=0.01 and $\theta = 2.5^{o}$

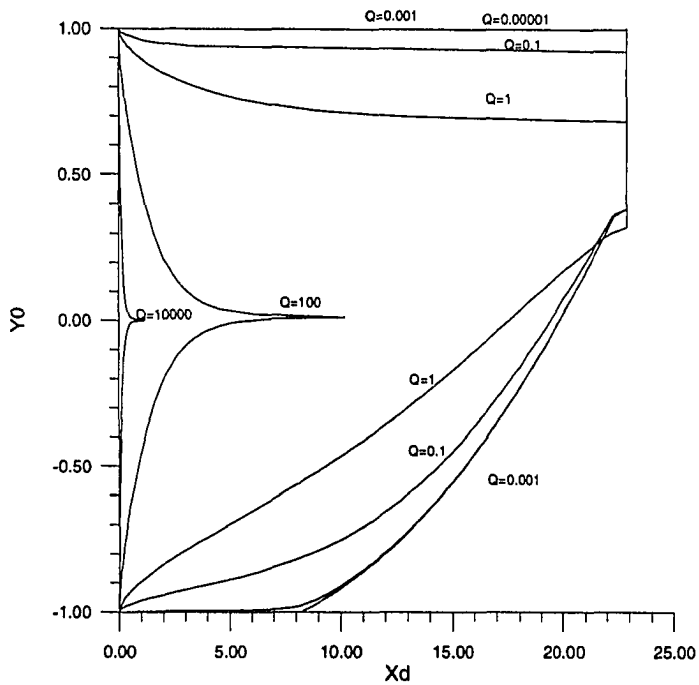

Figure 5.2.20 Particle Deposition Distance in a Divergent Channel at S=100, G=1 and $\theta = 2.5^{o}$

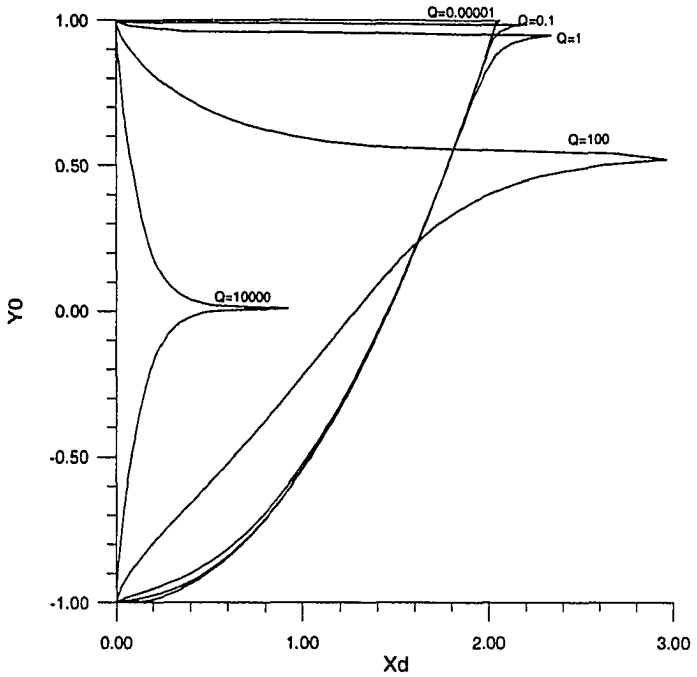

Figure 5.2.21 Particle Deposition Distance in a Divergent Channel at S=100, G=100 and $\theta = 2.5^{\circ}$

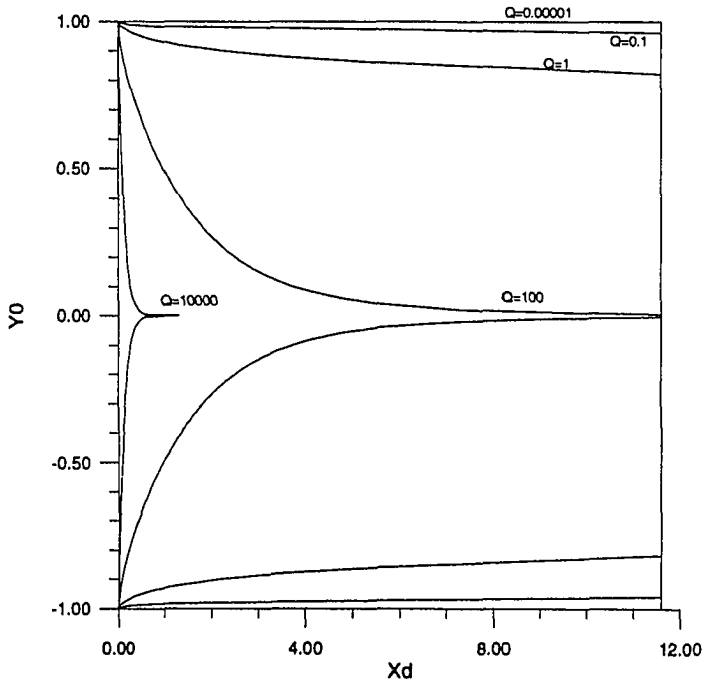

Figure 5.2.22 Particle Deposition Distance in a Divergent Channel at S=100, G=0.01 and $\theta = 7.5^{\circ}$

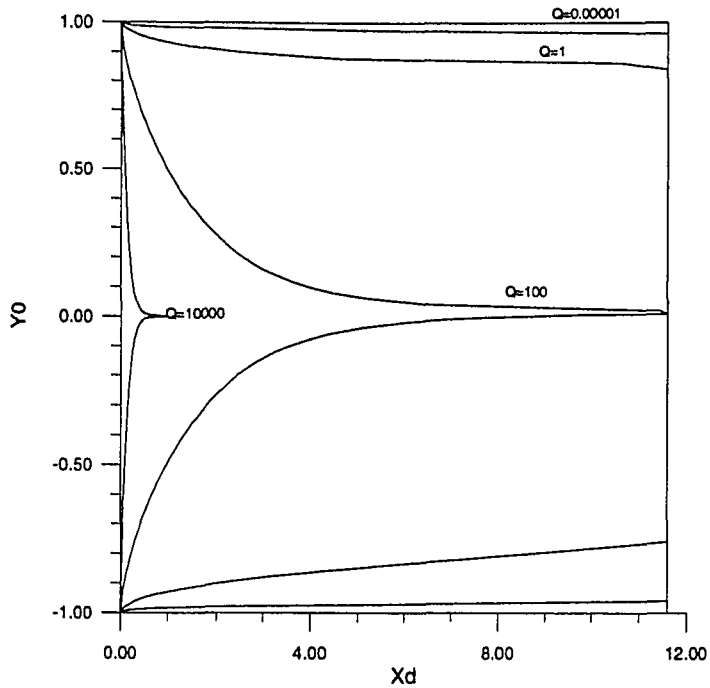

Figure 5.2.23 Particle Deposition Distance in a Divergent Channel at S=100, G=1 and $\theta = 7.5^{\circ}$

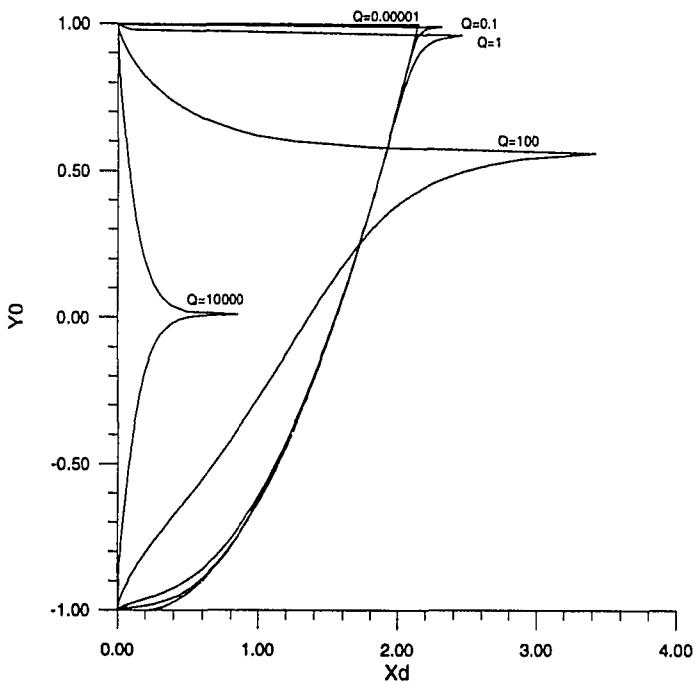

Figure 5.2.24 Particle Deposition Distance in a Divergent Channel at S=100, G=100 and $\theta = 7.5^{\circ}$

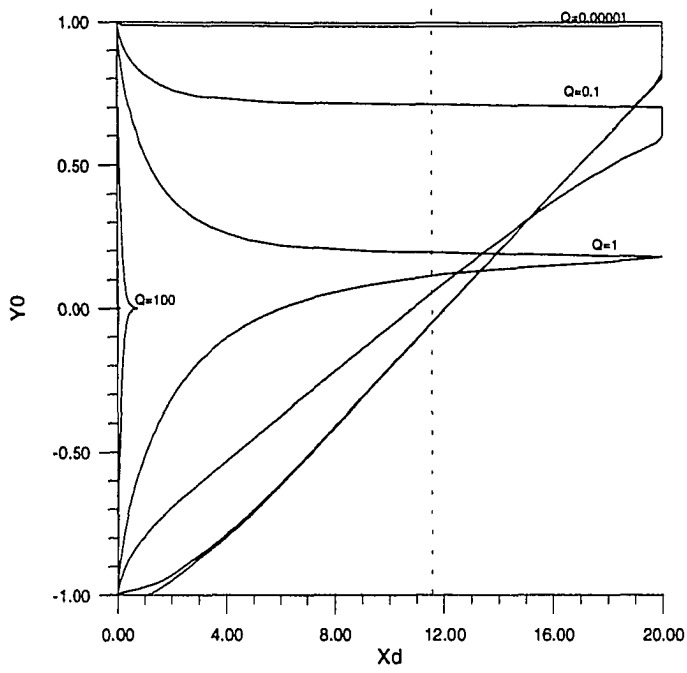

Figure 5.2.25 Particle Deposition Distance in a Divergent Channel at S=1, G=0.1 and $\theta = 7.5^{\circ}$

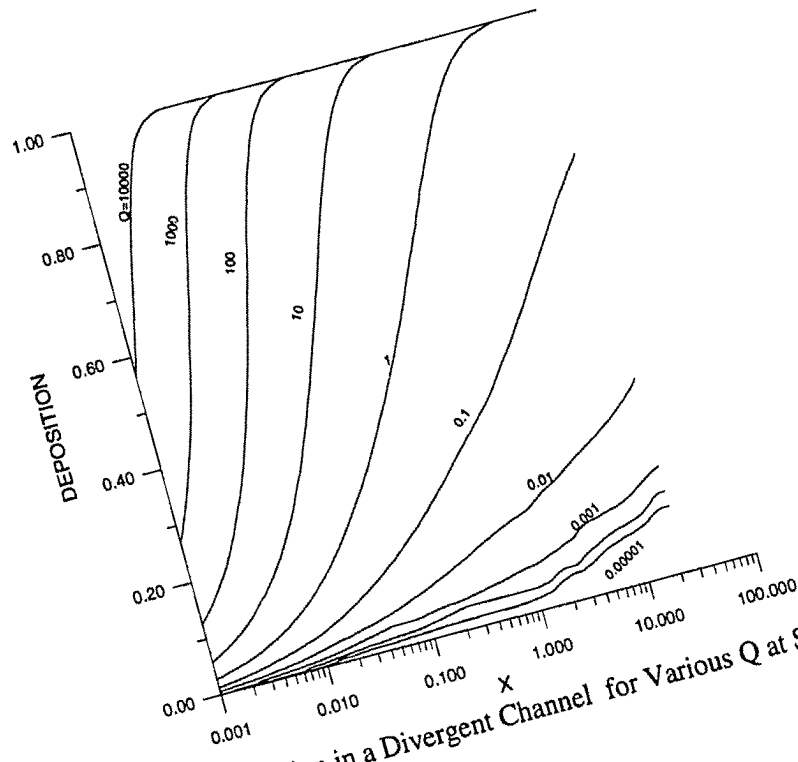

Figure 5.3.1 Deposition in a Divergent Channel for Various Q at S=0.01, G=0.01 and $\theta = 2.5^{\circ}$

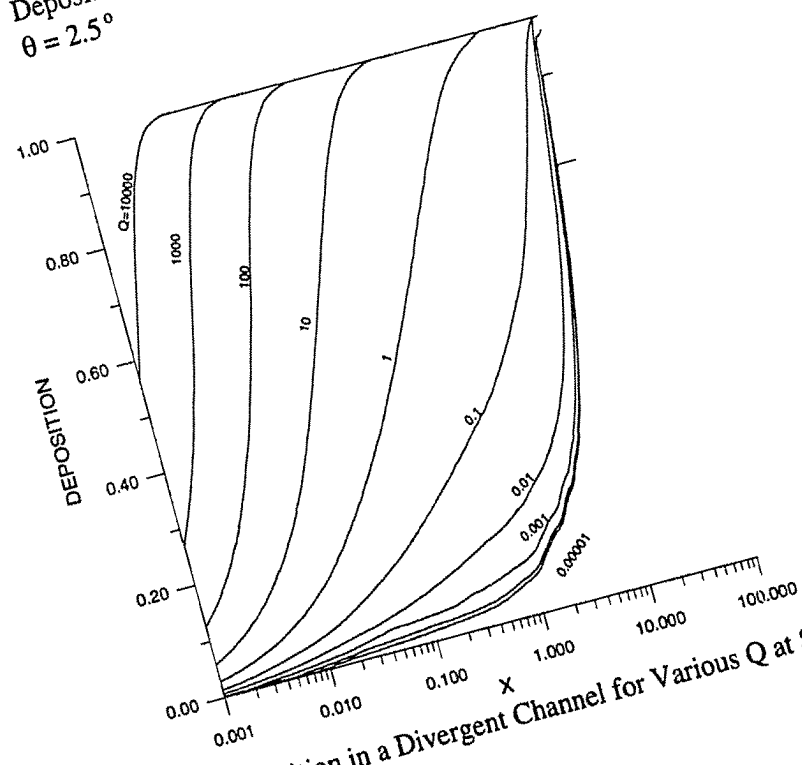

Figure 5.3.2 Deposition in a Divergent Channel for Various Q at S=0.01, G=0.1 and $\theta = 2.5^{\circ}$

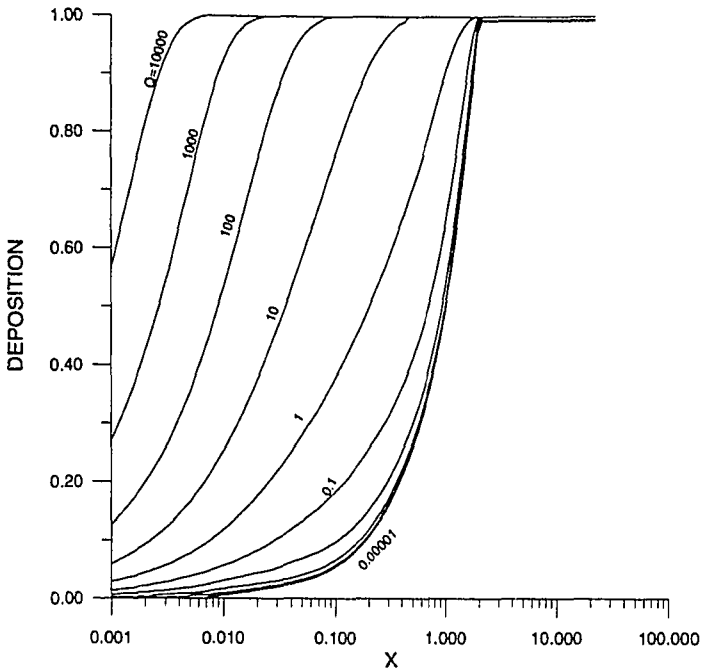

Figure 5.3.3 Deposition in a Divergent Channel for Various Q at S=0.01, G=1 and $\theta = 2.5°$

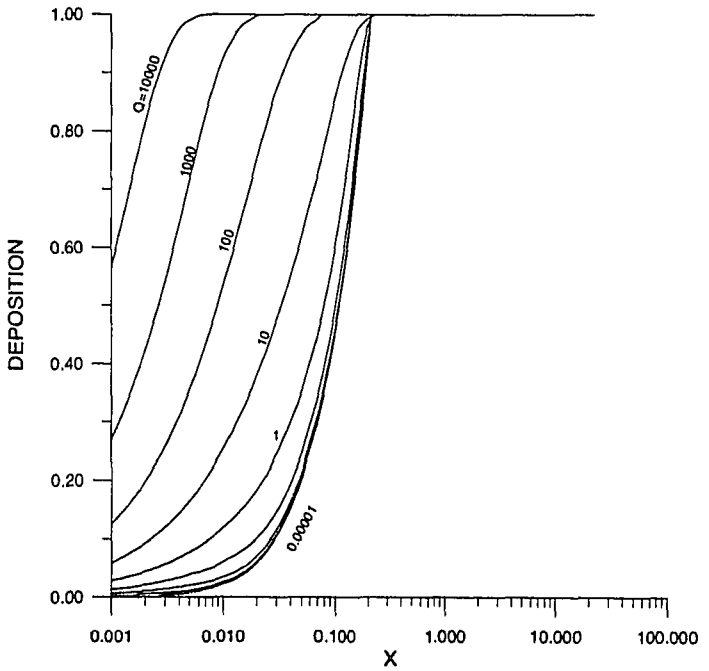

Figure 5.3.4 Deposition in a Divergent Channel for Various Q at S=0.01, G=10 and $\theta = 2.5°$

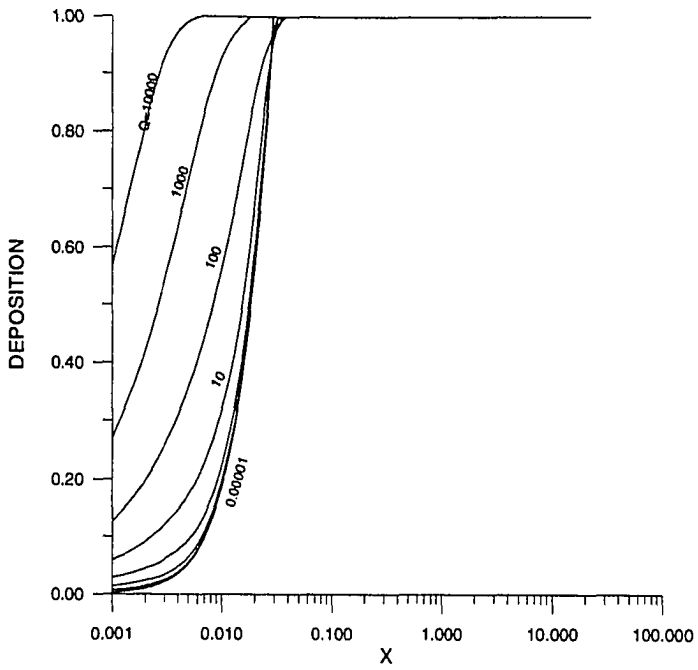

Figure 5.3.5 Deposition in a Divergent Channel for Various Q at S=0.01, G=100 and $\theta = 2.5°$

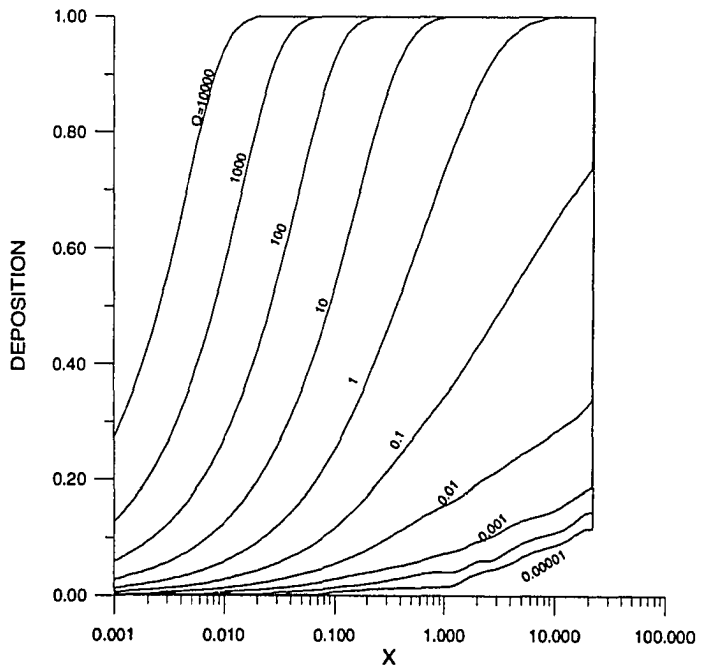

Figure 5.3.6 Deposition in a Divergent Channel for Various Q at S=0.1, G=0.01 and $\theta = 2.5°$

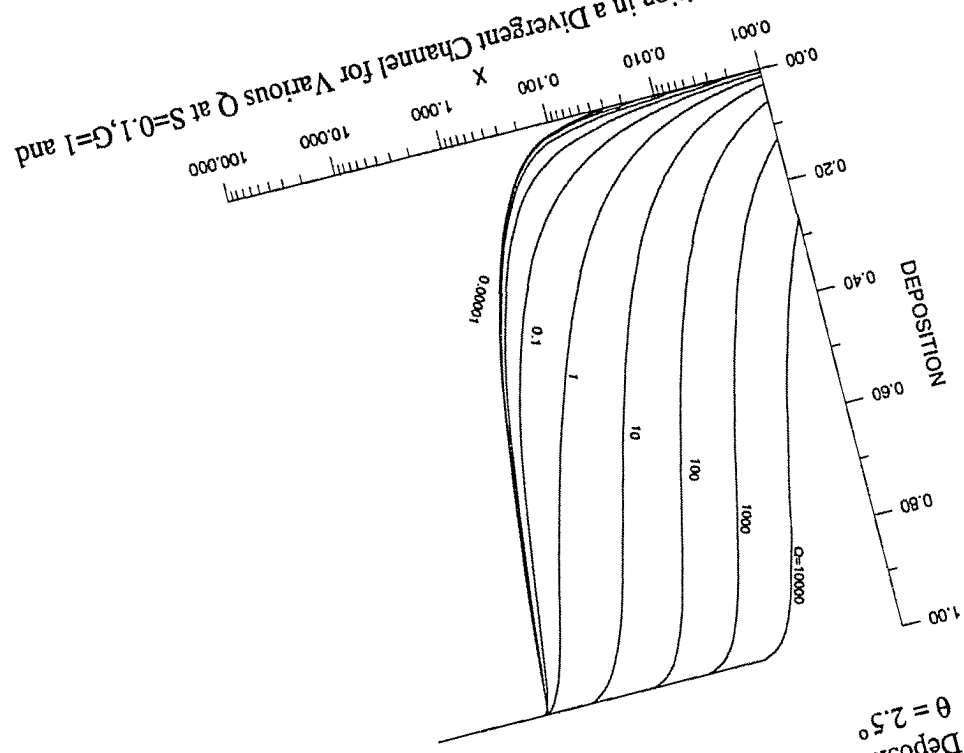

Figure 5.3.8 Deposition in a Divergent Channel for Various Q at S=0.1,G=1 and $\theta = 25^{o}$

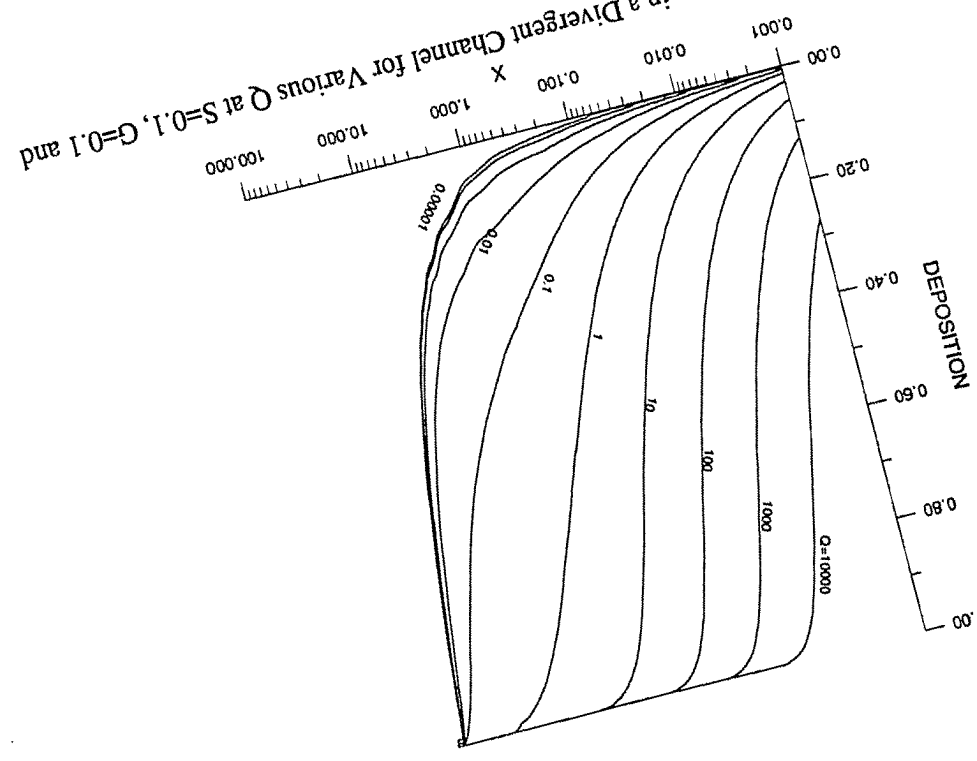

Figure 5.3.7 Deposition in a Divergent Channel for Various Q at S=0.1, G=0.1 and $\theta = 2.5^{o}$

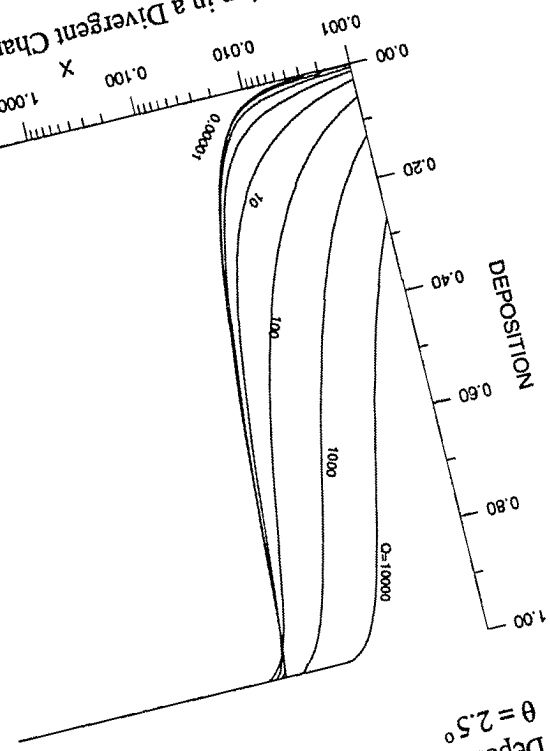

Figure 5.3.10 Deposition in a Divergent Channel for Various Q at S=0.1, G=100 and $\theta = 2.5^{o}$

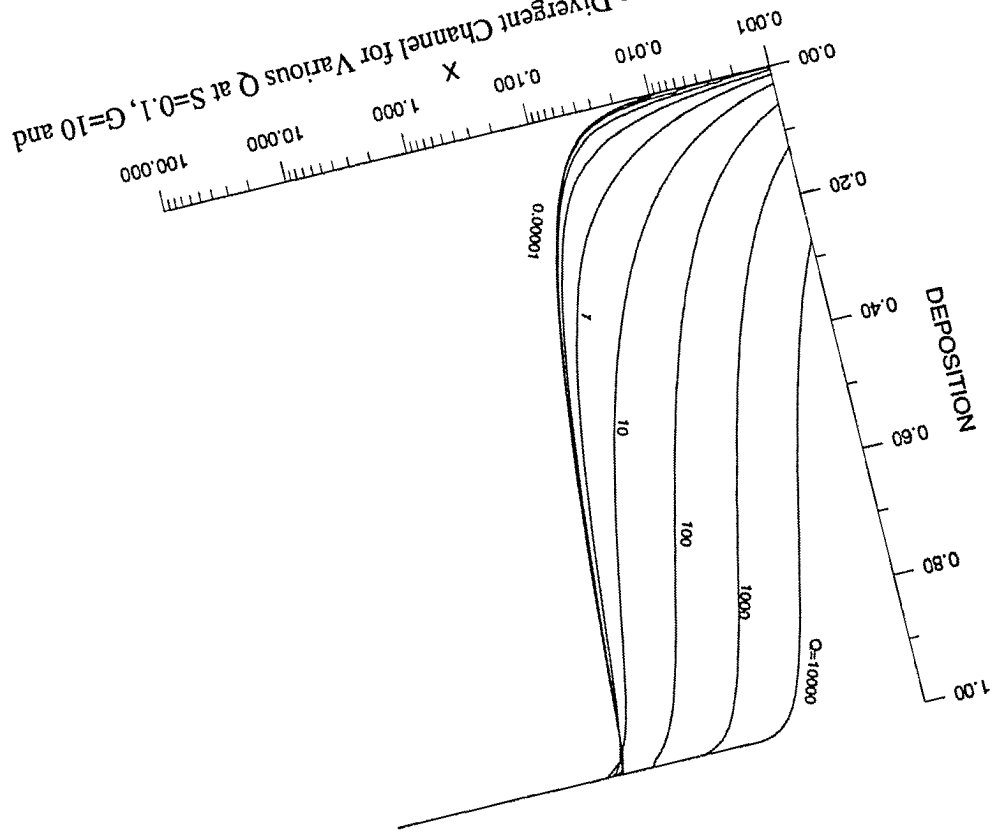

Figure 5.3.9 Deposition in a Divergent Channel for Various Q at S=0.1, G=10 and $\theta = 2.5^{o}$

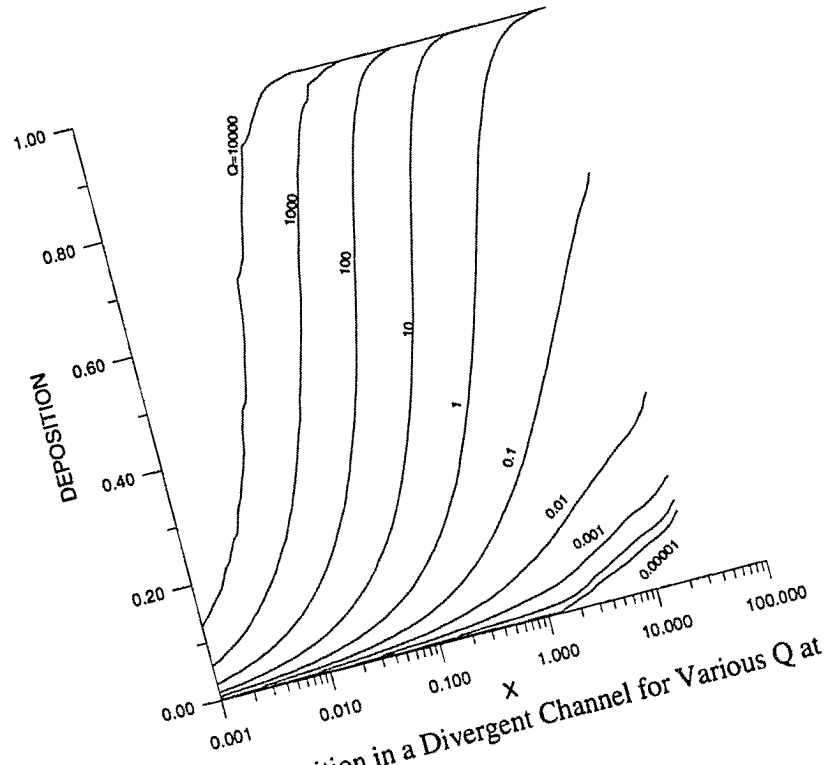

Figure 5. 3. 11 Deposition in a Divergent Channel for Various Q at S=1, G=0.01 and $\theta = 2.5^{\circ}$

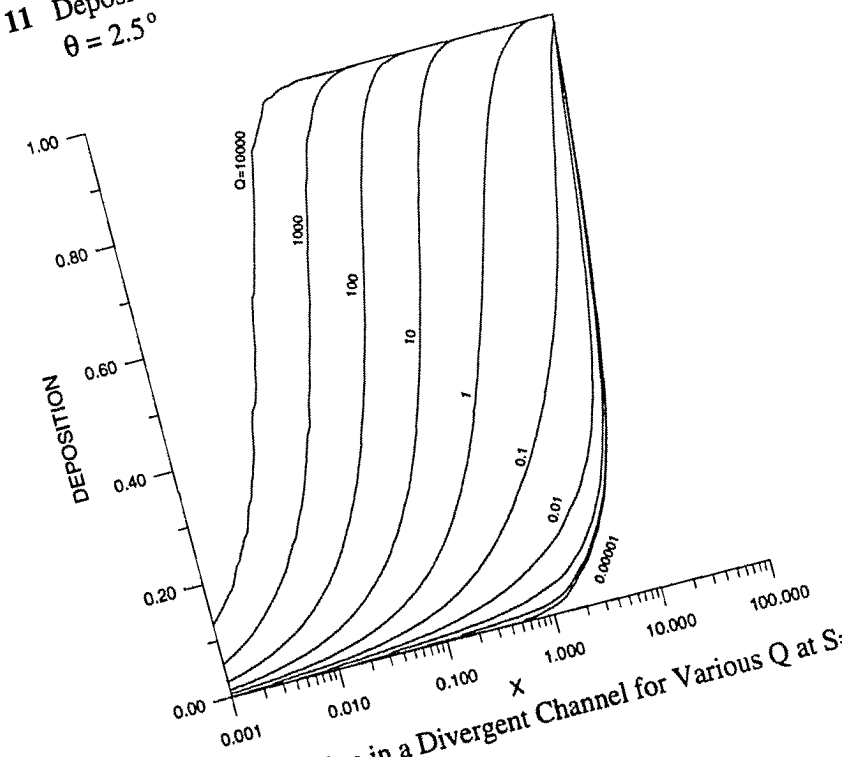

Figure 5.3.12 Deposition in a Divergent Channel for Various Q at S=1, G=0.1 and $\theta = 2.5^{\circ}$

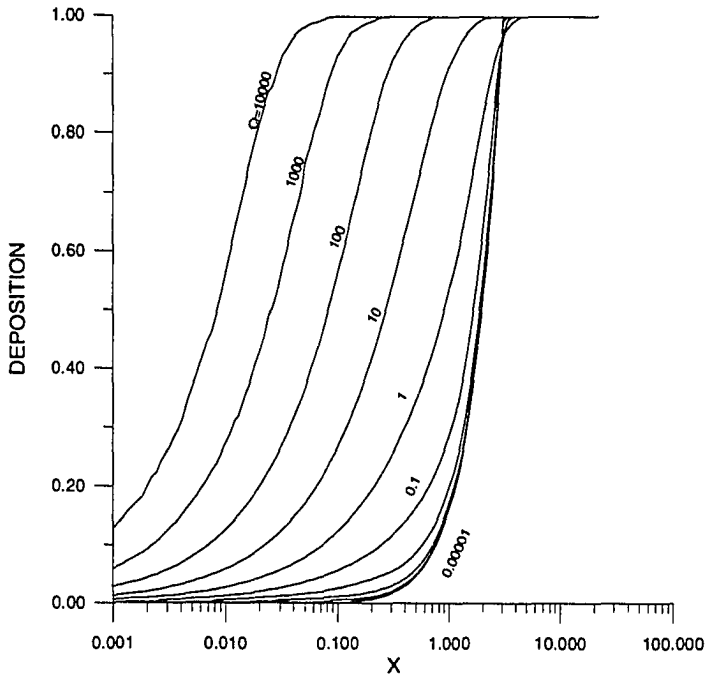

Figure 5.3.13 Deposition in a Divergent Channel for Various Q at S=1, G=0.1 and $\theta = 2.5^{\circ}$

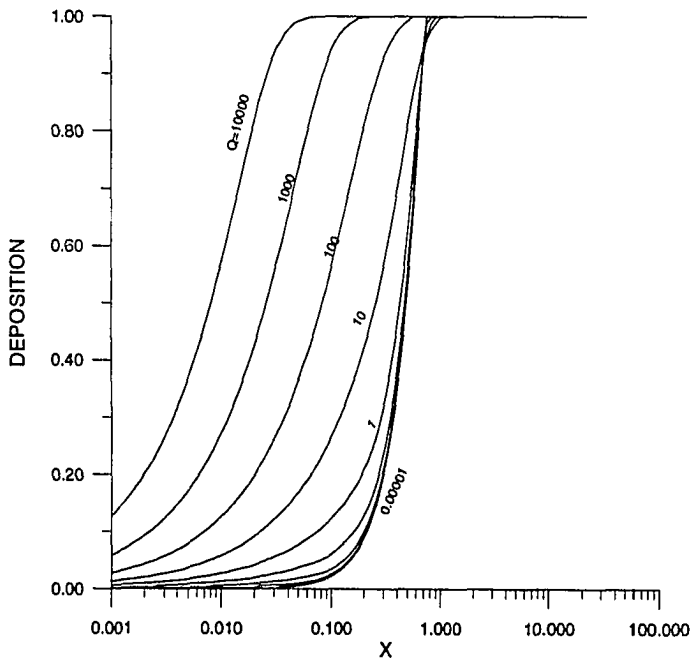

Figure 5.3.14 Deposition in a Divergent Channel for Various Q at S=1, G=10 and $\theta = 2.5^{\circ}$

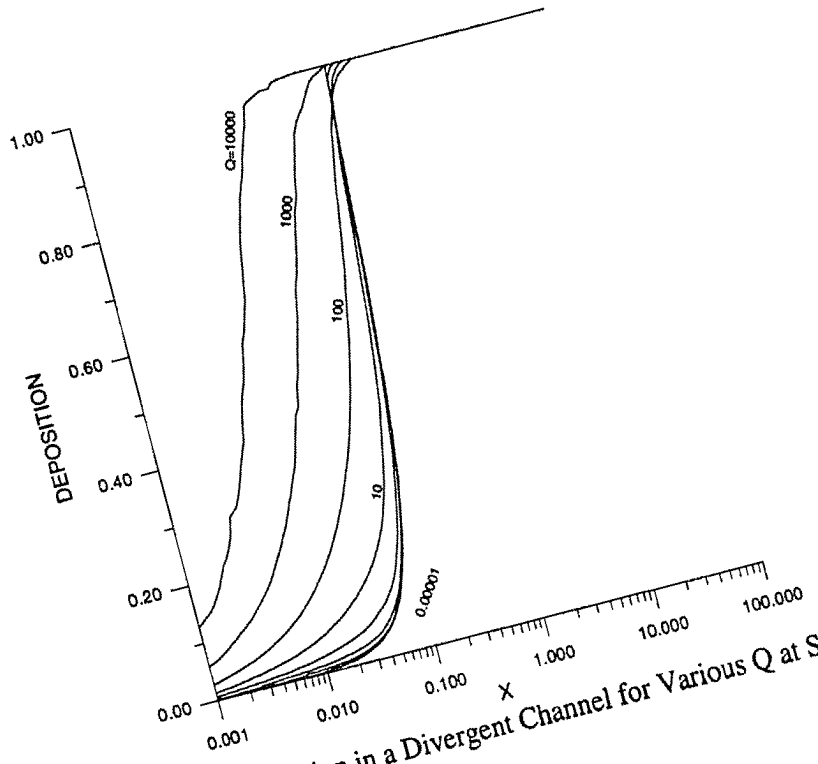

Figure 5.3.15 Deposition in a Divergent Channel for Various Q at S=1, G=100 and $\theta = 2.5^{\circ}$

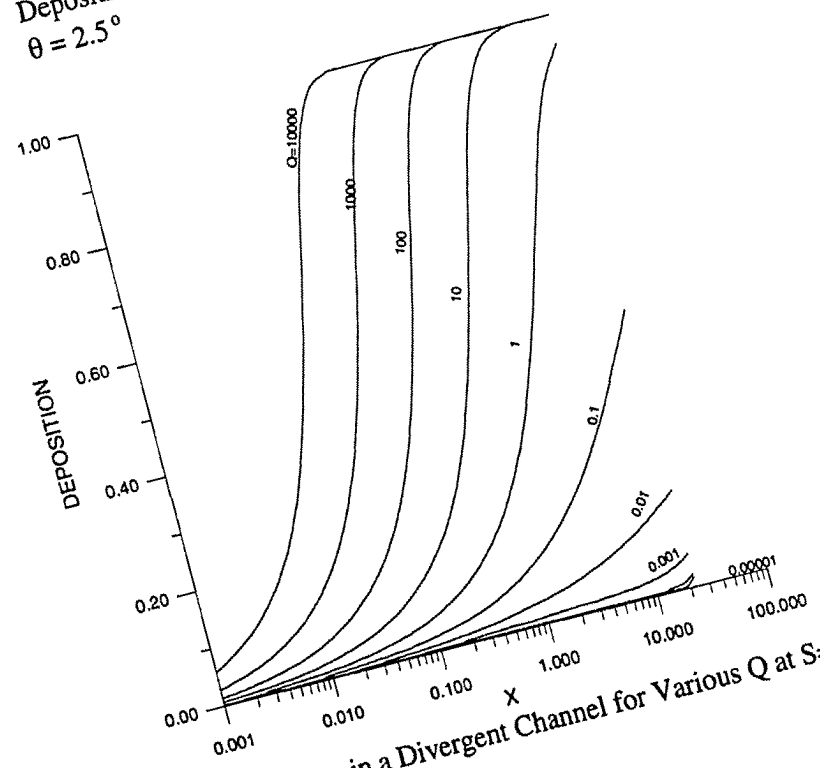

Figure 5.3.16 Deposition in a Divergent Channel for Various Q at S=10, G=0.01 and $\theta = 2.5^{\circ}$

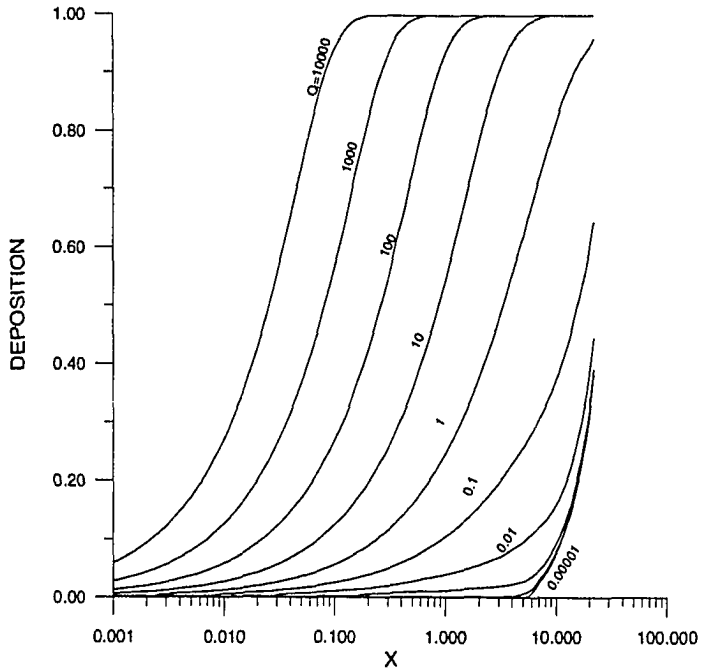

Figure 5.3.17 Deposition in a Divergent Channel for Various Q at S=10, G=0.1 and $\theta = 2.5°$

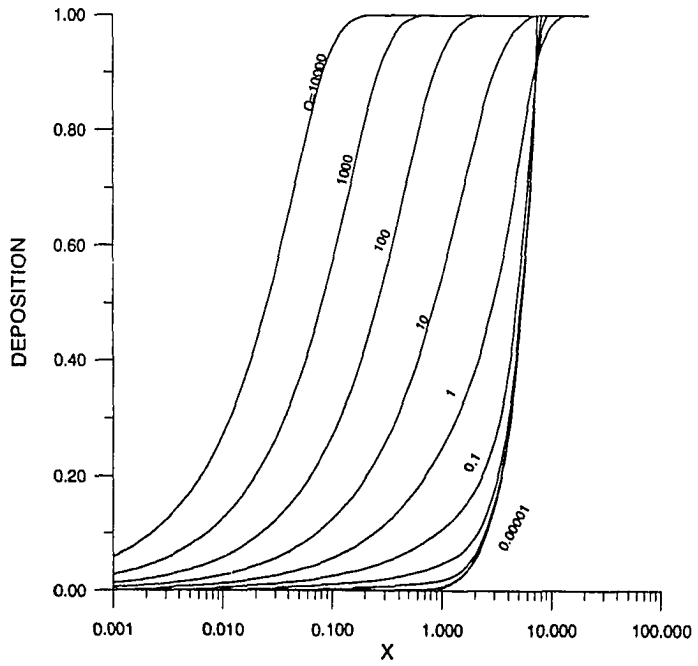

Figure 5.3.18 Deposition in a Divergent Channel for Various Q at S=10, G=1 and $\theta = 2.5°$

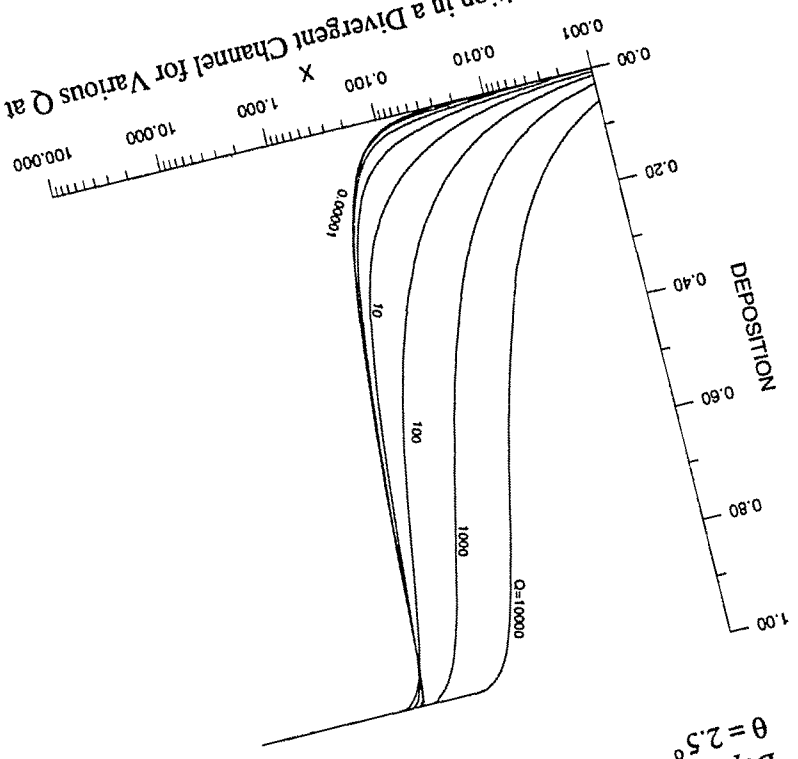

Figure 5.3.19 Deposition in a Divergent Channel for Various Q at S=10, G=10 and $\theta = 2.5^{o}$

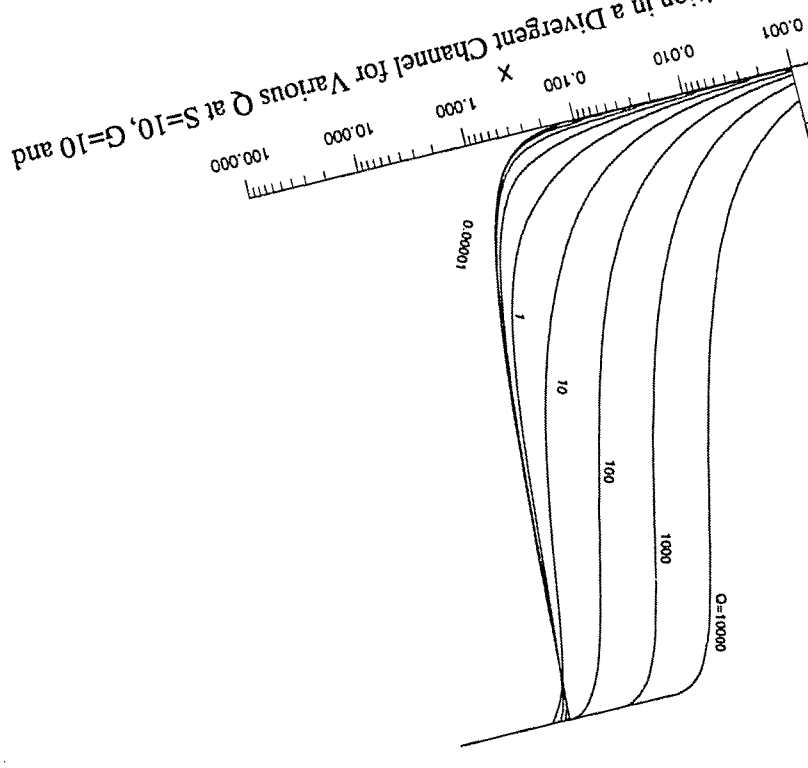

Figure 5.3.20 Deposition in a Divergent Channel for Various Q at S=10, G=100 and $\theta = 2.5^{o}$

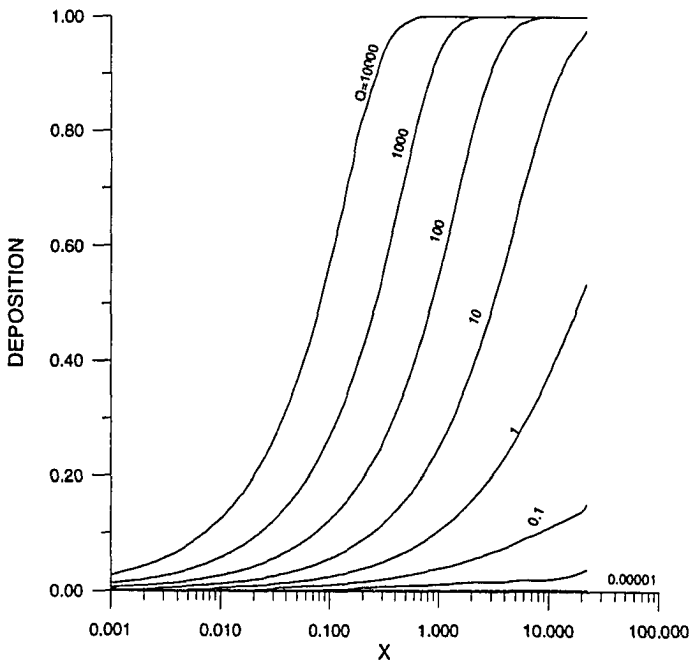

Figure 5.3.21 Deposition in a Divergent Channel for Various Q at S=100, G=0.01 and $\theta = 2.5°$

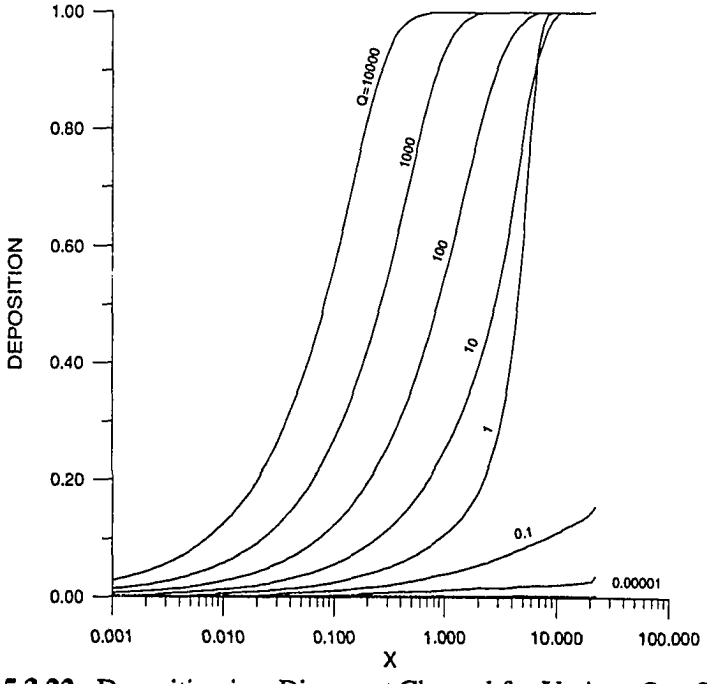

Figure 5.3.22 Deposition in a Divergent Channel for Various Q at S=100, G=0.1 and $\theta = 2.5°$

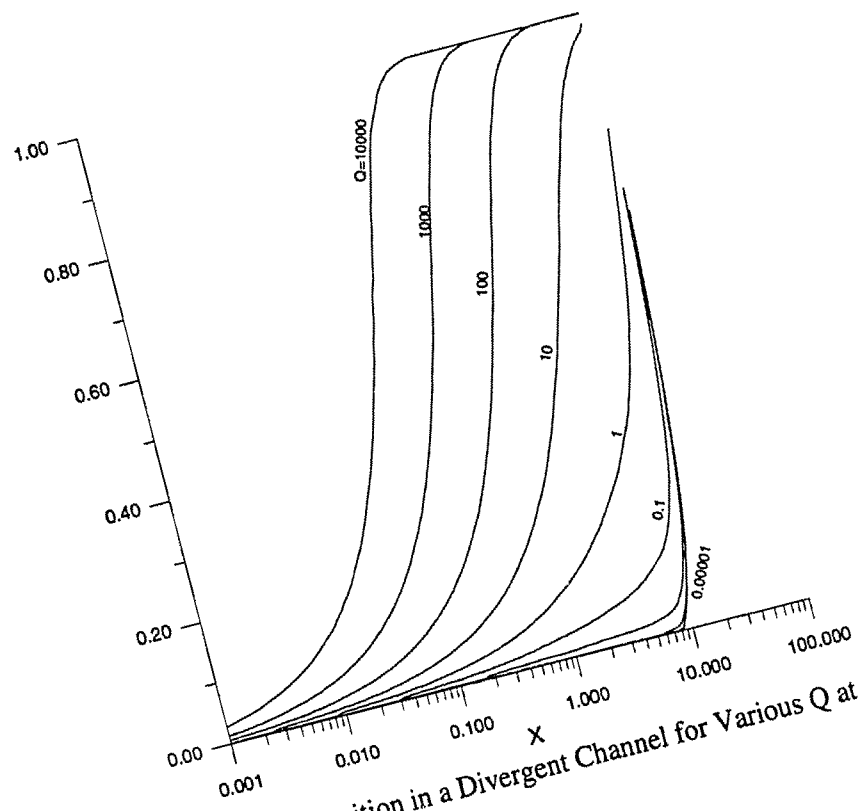

Figure 5.3.23 Deposition in a Divergent Channel for Various Q at S=100, G=1 and $\theta = 2.5^{\circ}$

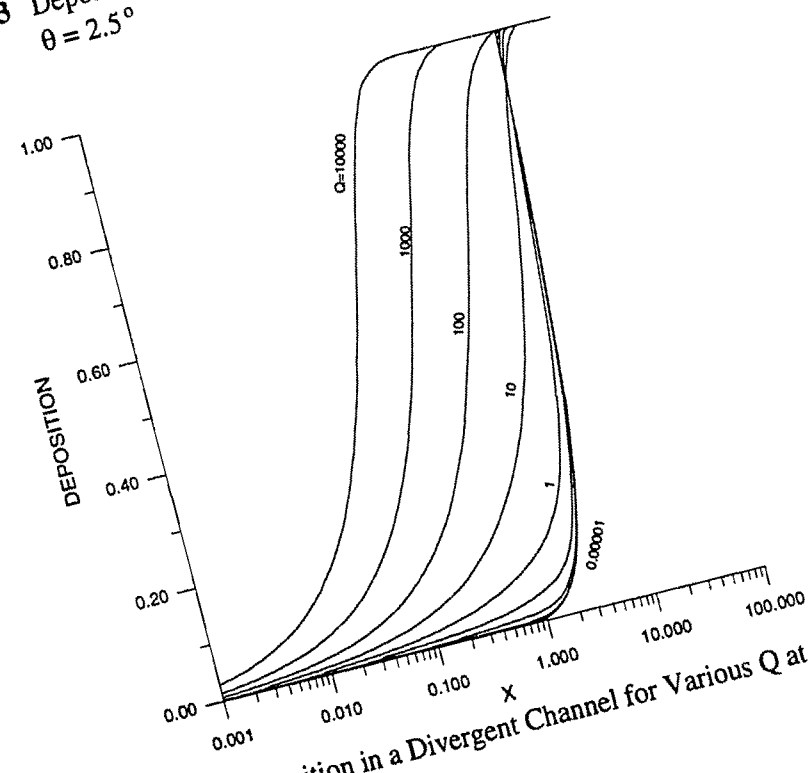

Figure 5.3.24 Deposition in a Divergent Channel for Various Q at S=100, G=10 and $\theta = 2.5^{\circ}$

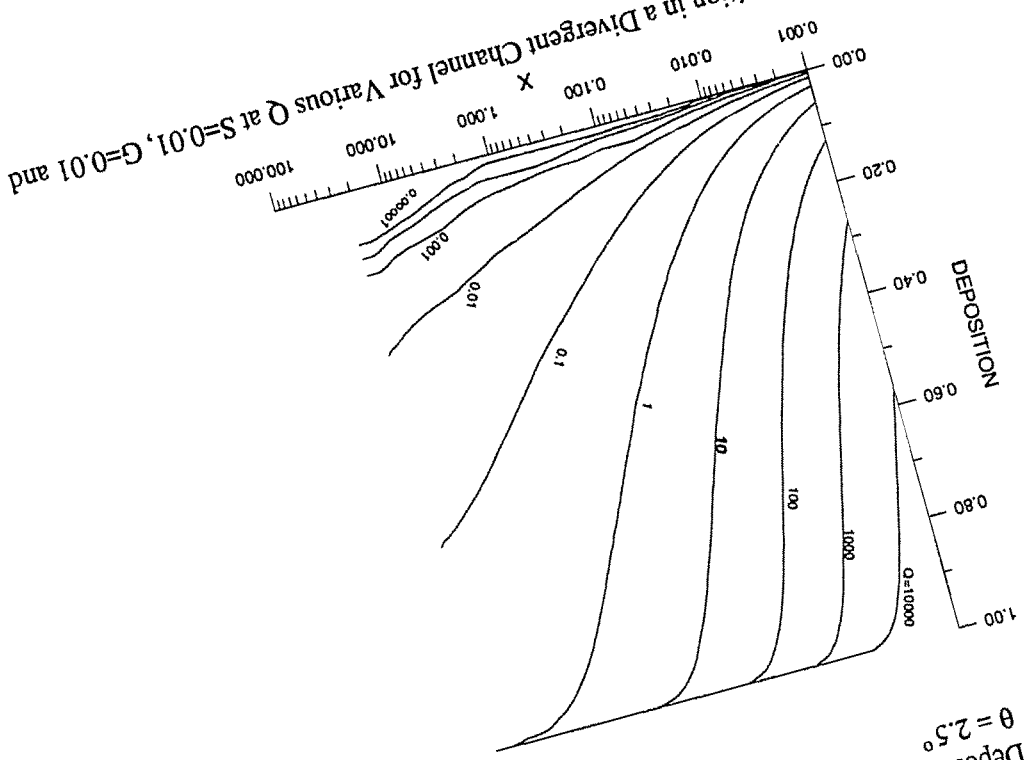

Figure 5.3.26 Deposition in a Divergent Channel for Various Q at S=0.01, G=0.01 and $\theta = 5.0^{o}$

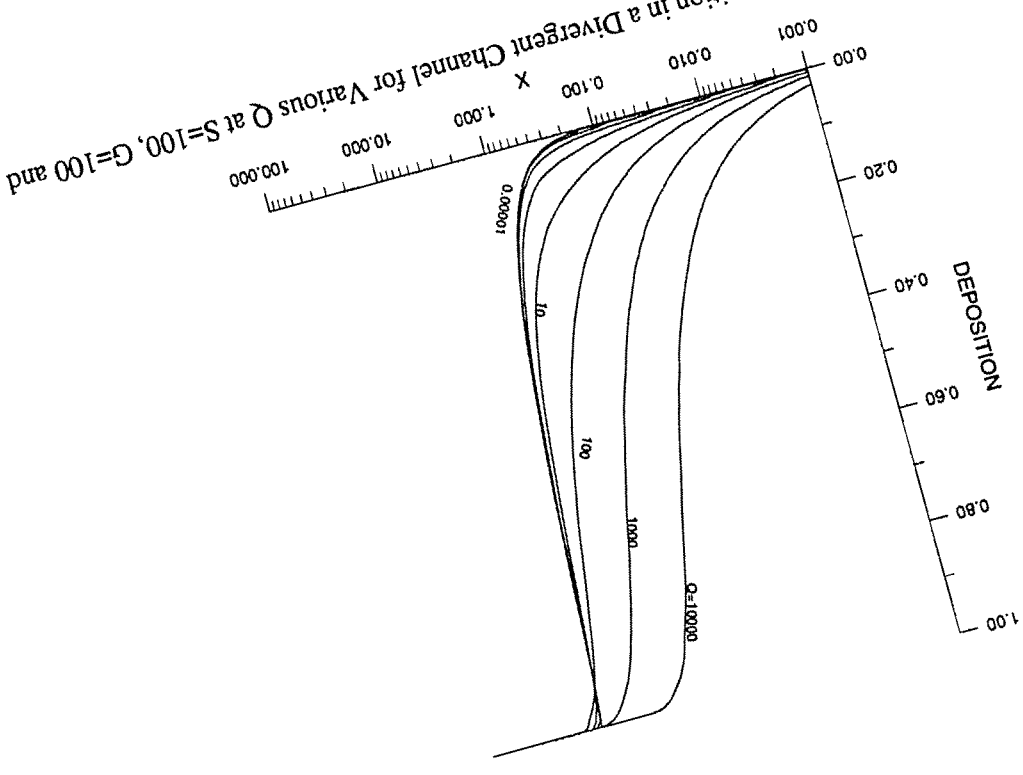

Figure 5.3.25 Deposition in a Divergent Channel for Various Q at S=100, G=100 and $\theta = 2.5^{o}$

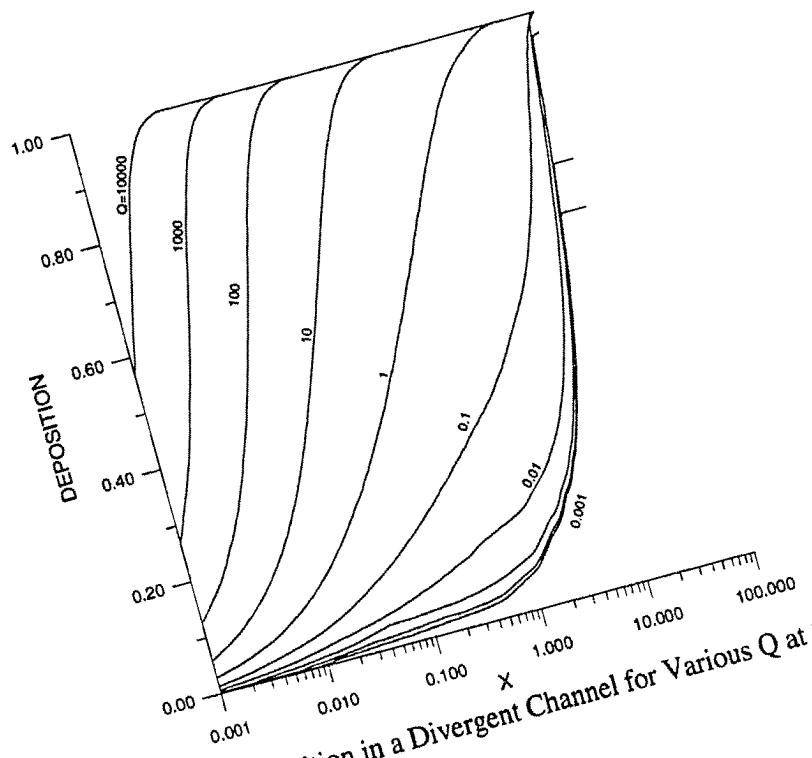

Figure 5.3.27 Deposition in a Divergent Channel for Various Q at S=0.01, G=0.1 and $\theta = 5.0^{\circ}$

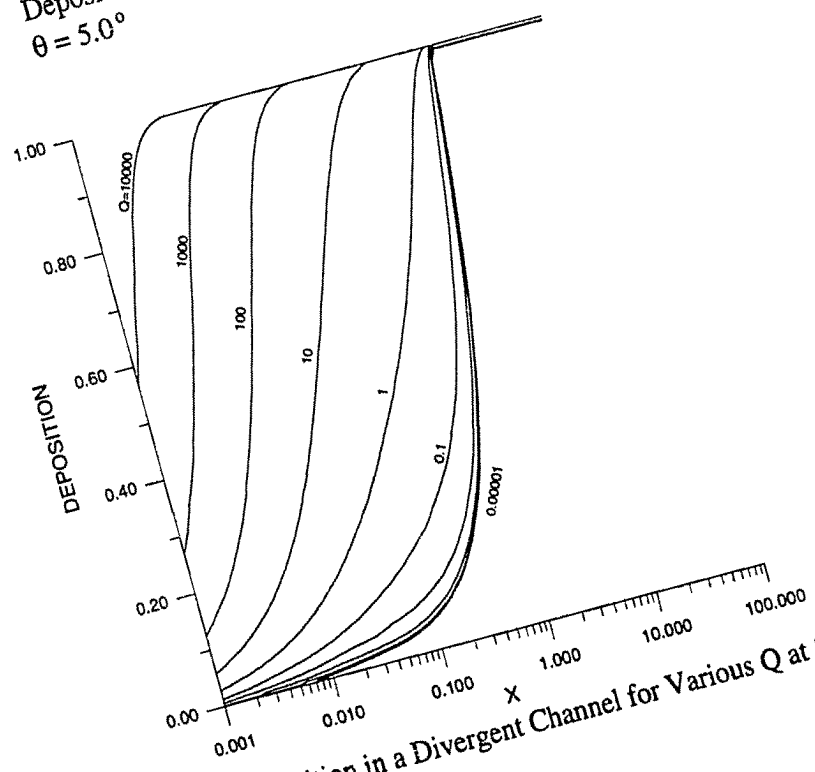

Figure 5.3.28 Deposition in a Divergent Channel for Various Q at S=0.01, G=1 and $\theta = 5.0^{\circ}$

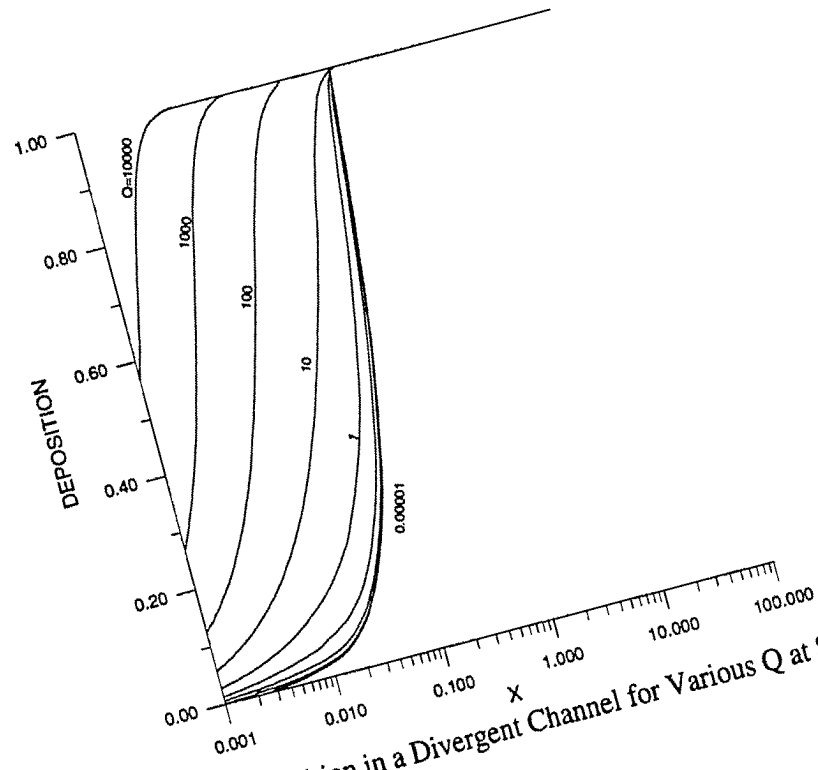

Figure 5.3.29 Deposition in a Divergent Channel for Various Q at S=0.01, G=10 and $\theta = 5.0^{\circ}$

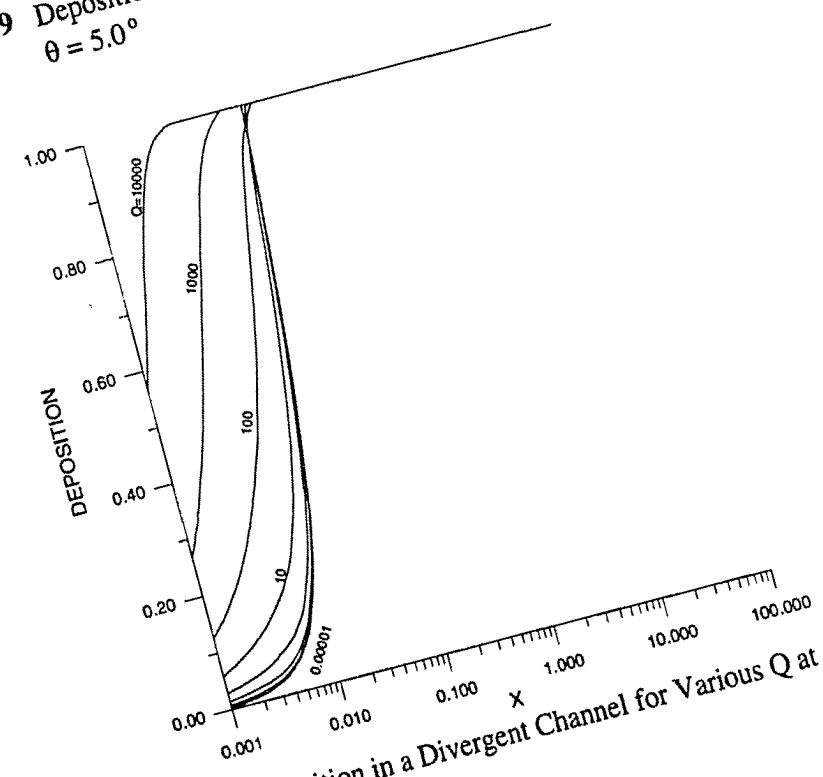

Figure 5.3.30 Deposition in a Divergent Channel for Various Q at S=0.01,G=100 and $\theta = 5.0^{\circ}$

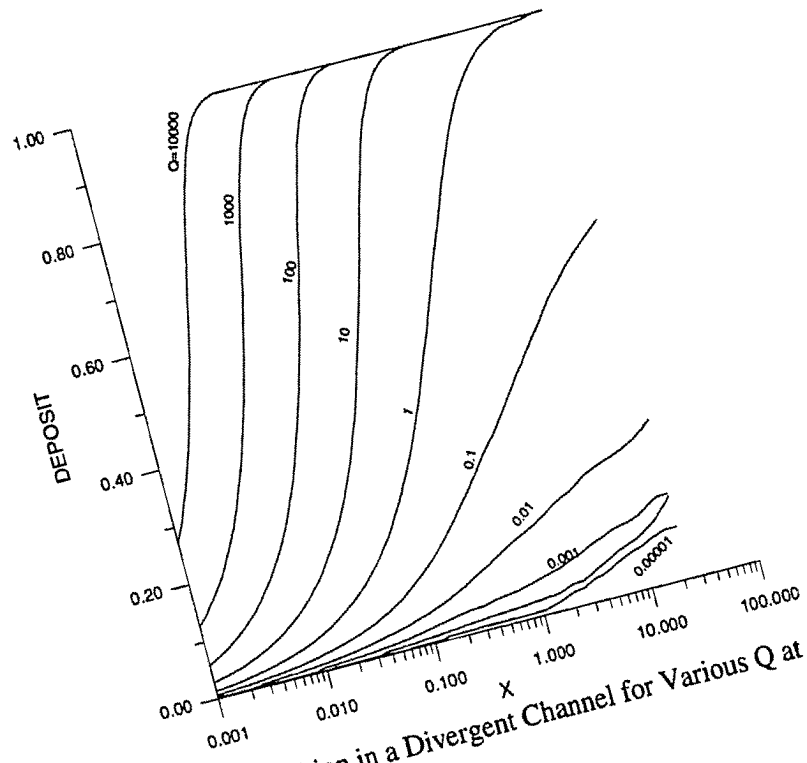

Figure 5.3.31 Deposition in a Divergent Channel for Various Q at S=0.1, G=0.01 and $\theta = 5.0^{\circ}$

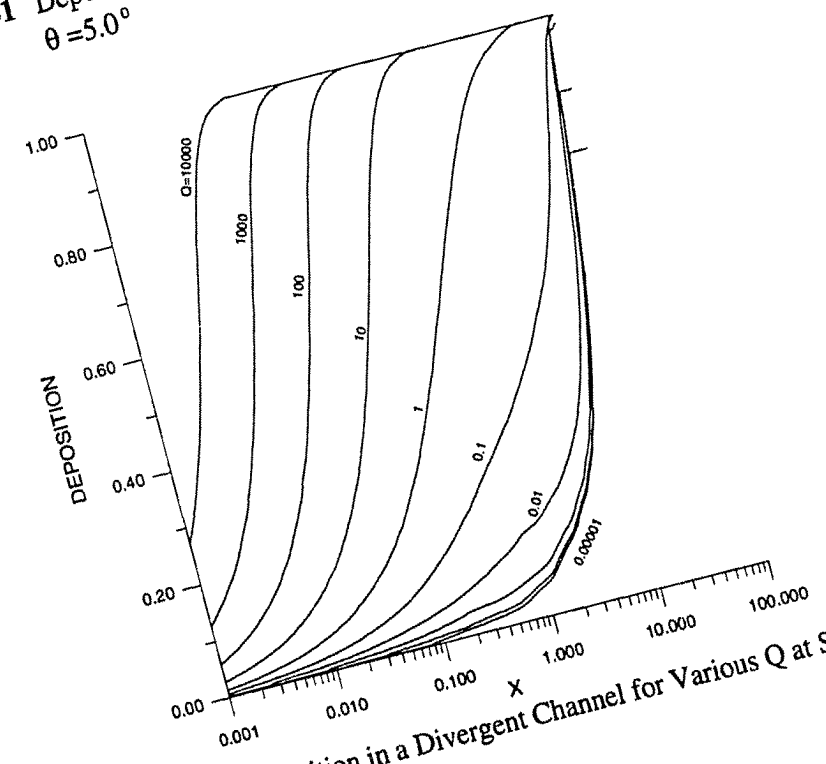

Figure 5.3.32 Deposition in a Divergent Channel for Various Q at S=10, G=0.1 and $\theta = 5.0^{\circ}$

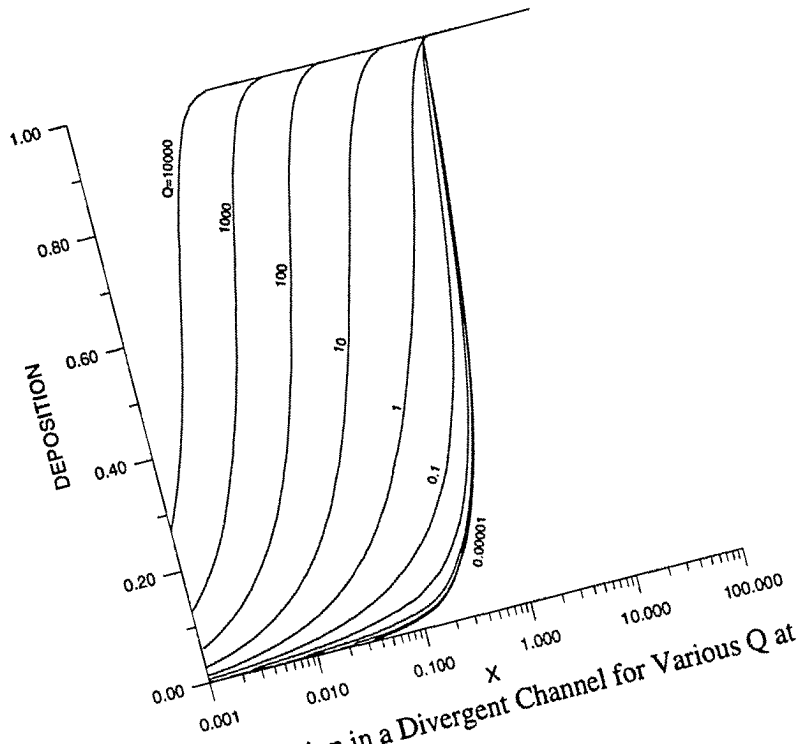

Figure 5.3.33 Deposition in a Divergent Channel for Various Q at S=0.1, G=1 and $\theta = 5.0^{\circ}$

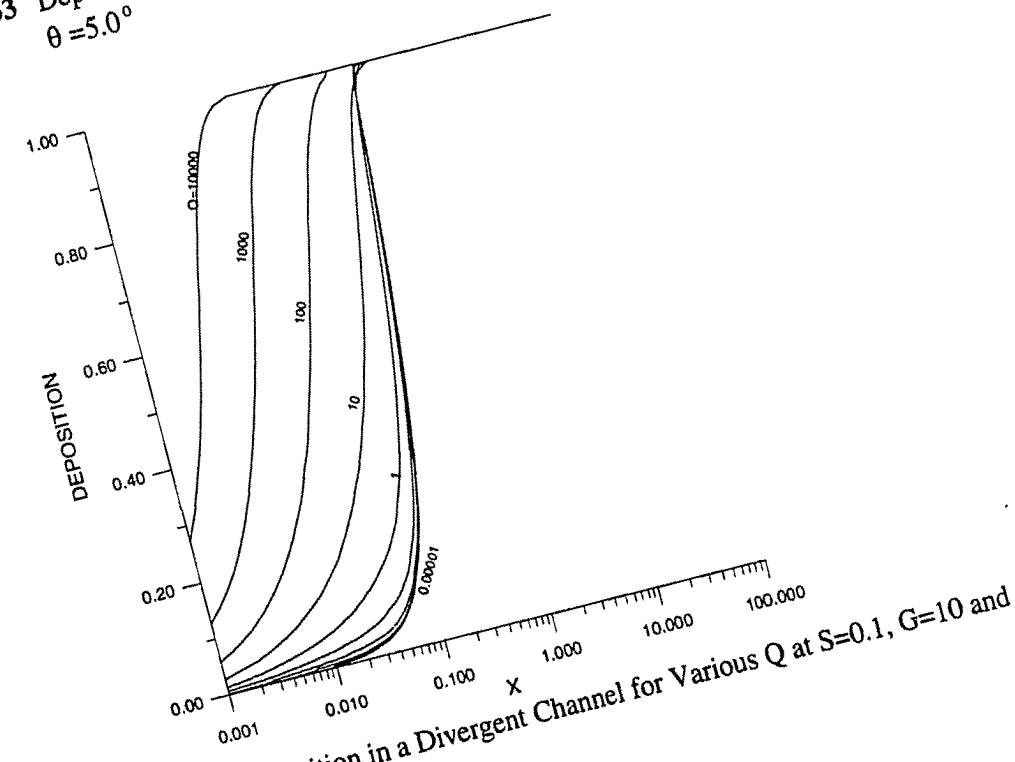

Figure 5.3.34 Deposition in a Divergent Channel for Various Q at S=0.1, G=10 and $\theta = 5.0^{\circ}$

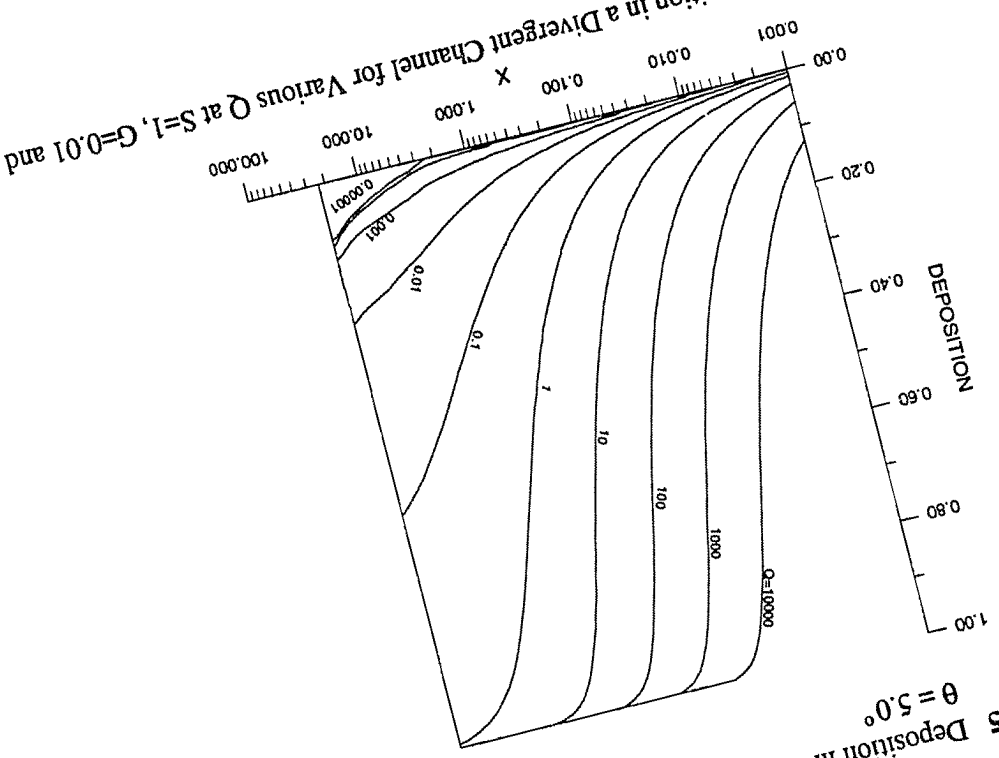

Figure 5.3.35 Deposition in a Divergent Channel for Various Q at S=0.1, G=100 and $\theta = 5.0^{o}$

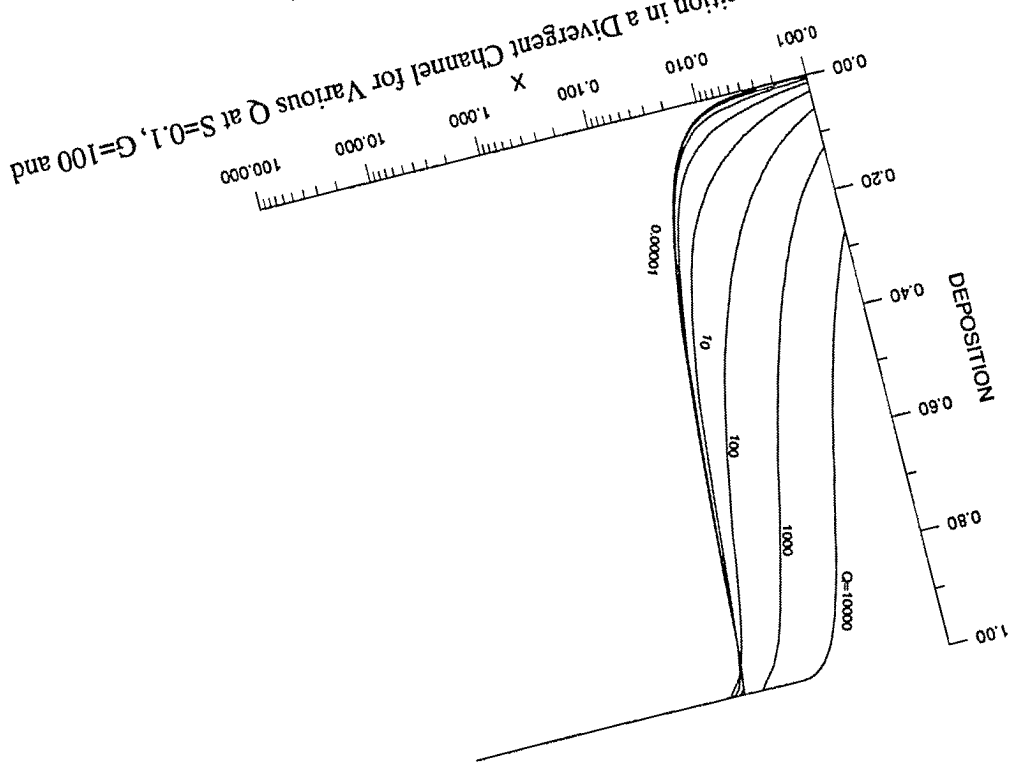

Figure 5.3.36 Deposition in a Divergent Channel for Various Q at S=1, G=0.01 and $\theta = 5.0^{o}$

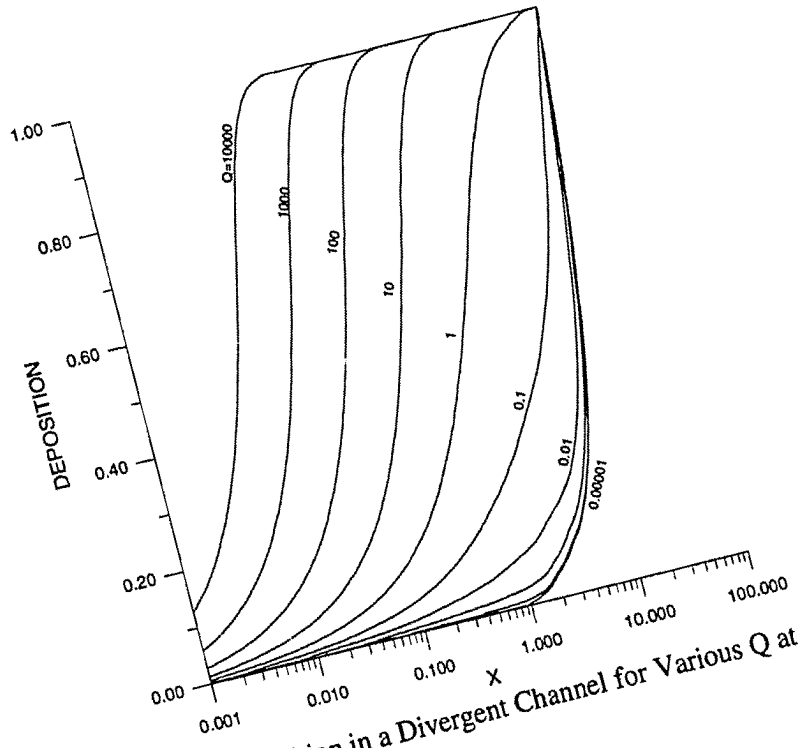

Figure 5.3.37 Deposition in a Divergent Channel for Various Q at S=1, G=0.1 and $\theta = 5.0°$

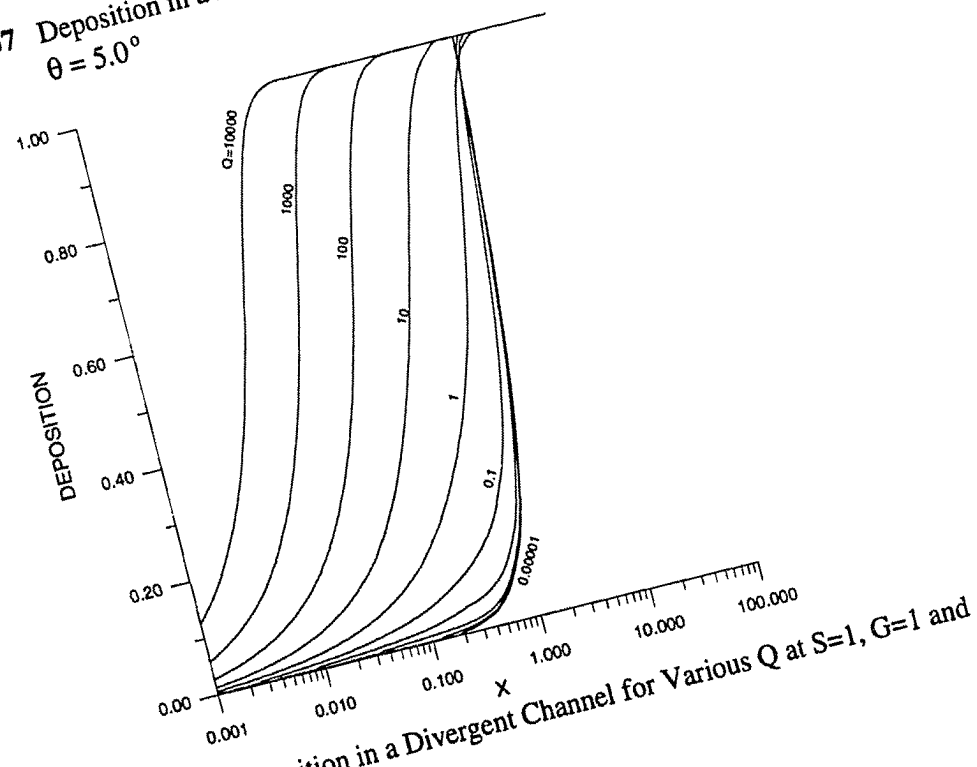

Figure 5.3.38 Deposition in a Divergent Channel for Various Q at S=1, G=1 and $\theta = 5.0°$

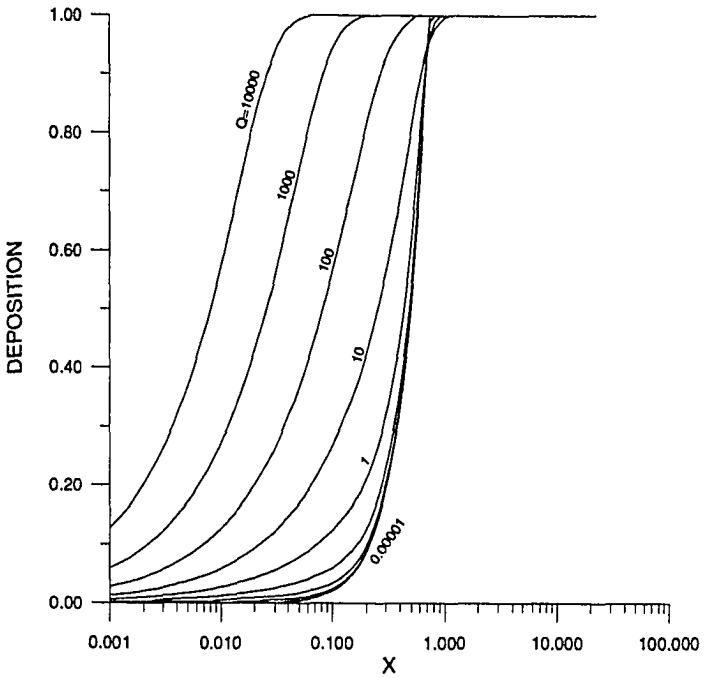

Figure 5.3.39 Deposition in a Divergent Channel for Various Q at S=1, G=10 and $\theta = 5.0^{\circ}$

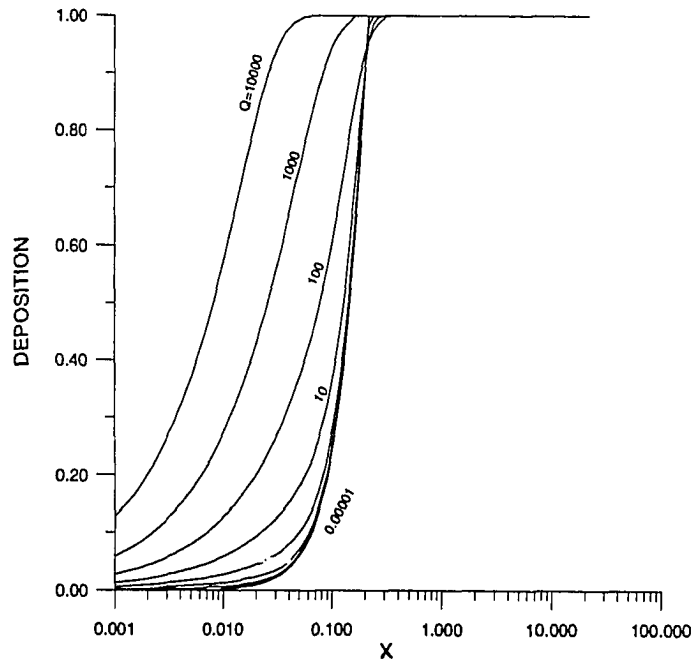

Figure 5.3.40 Deposition in a Divergent Channel for Various Q at S=1, G=100 and $\theta = 5.0^{\circ}$

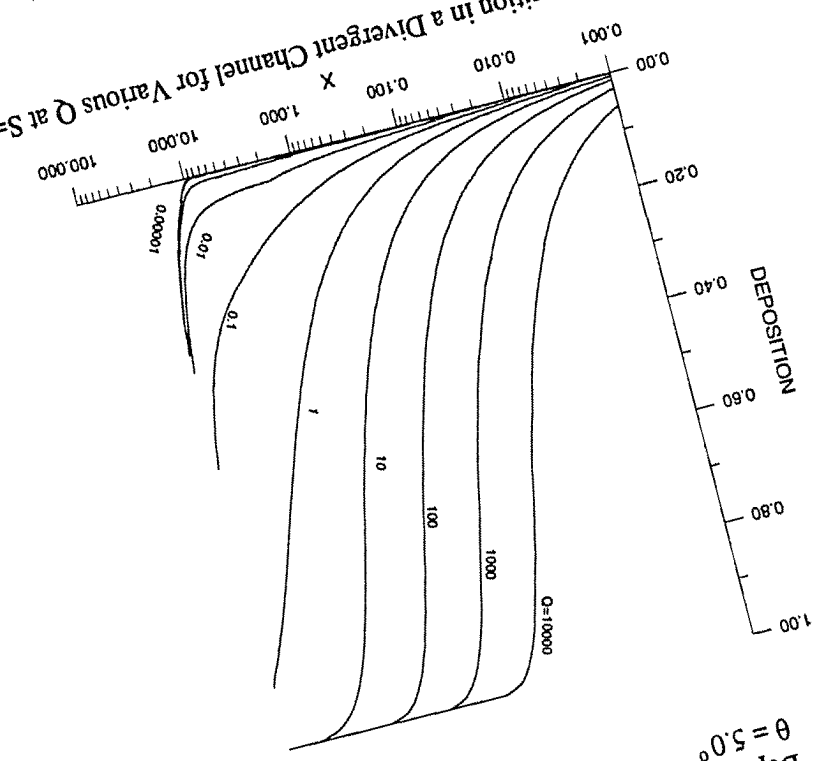

Figure 5.3.42 Deposition in a Divergent Channel for Various Q at S=10, G=0.1 and $\theta = 5.0^{o}$

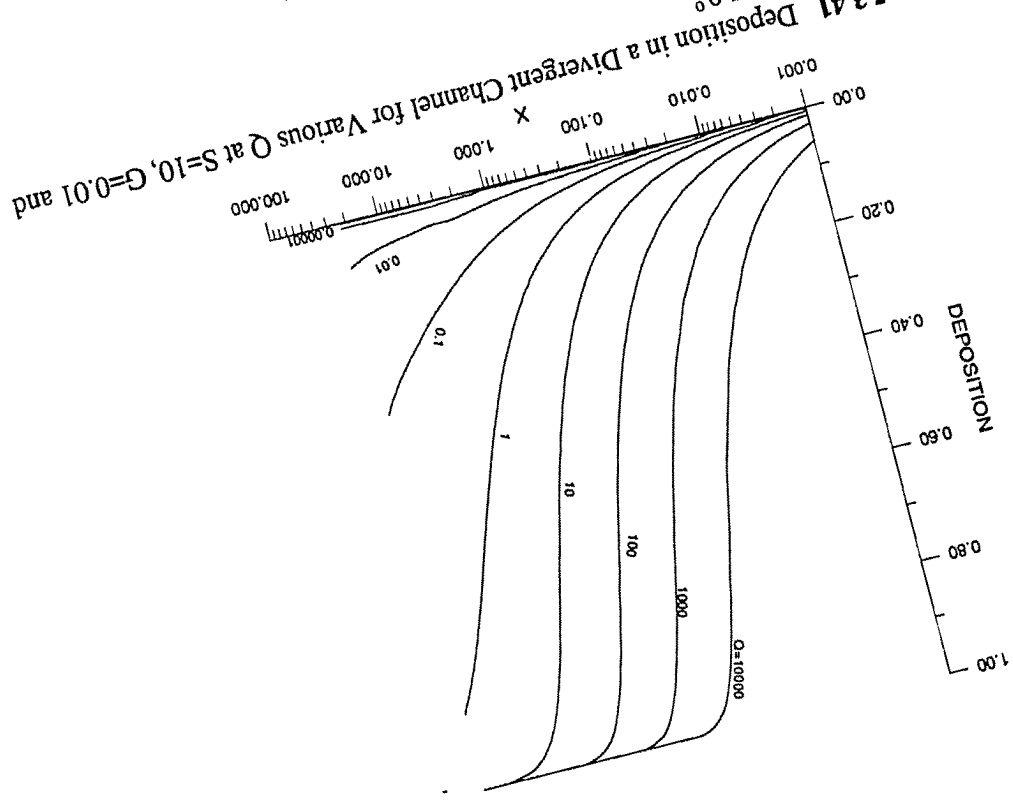

Figure 5.3.41 Deposition in a Divergent Channel for Various Q at S=10, G=0.01 and $\theta = 5.0^{o}$

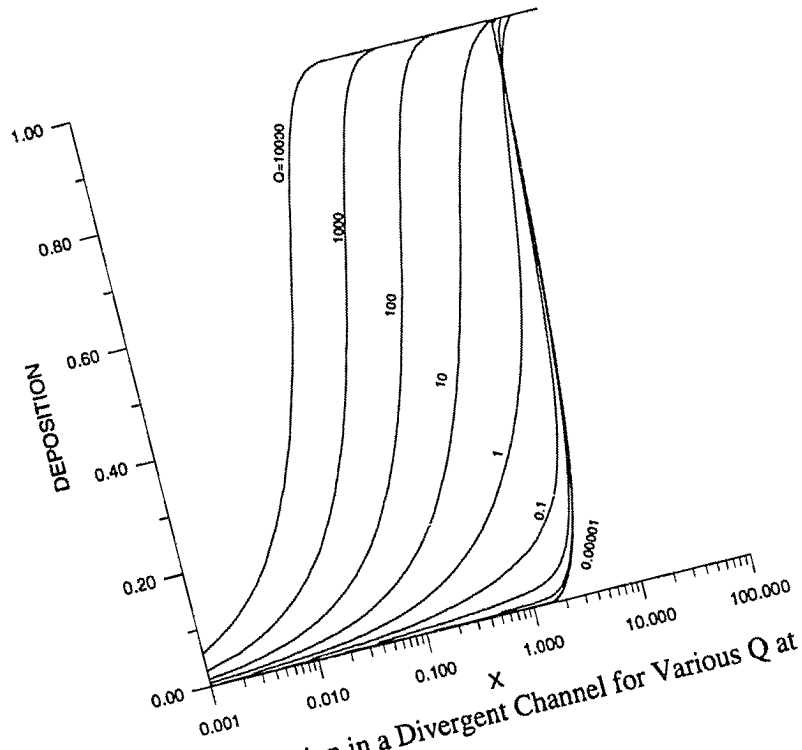

Figure 5.3.43 Deposition in a Divergent Channel for Various Q at S=10, G=1 and $\theta = 5.0^{\circ}$

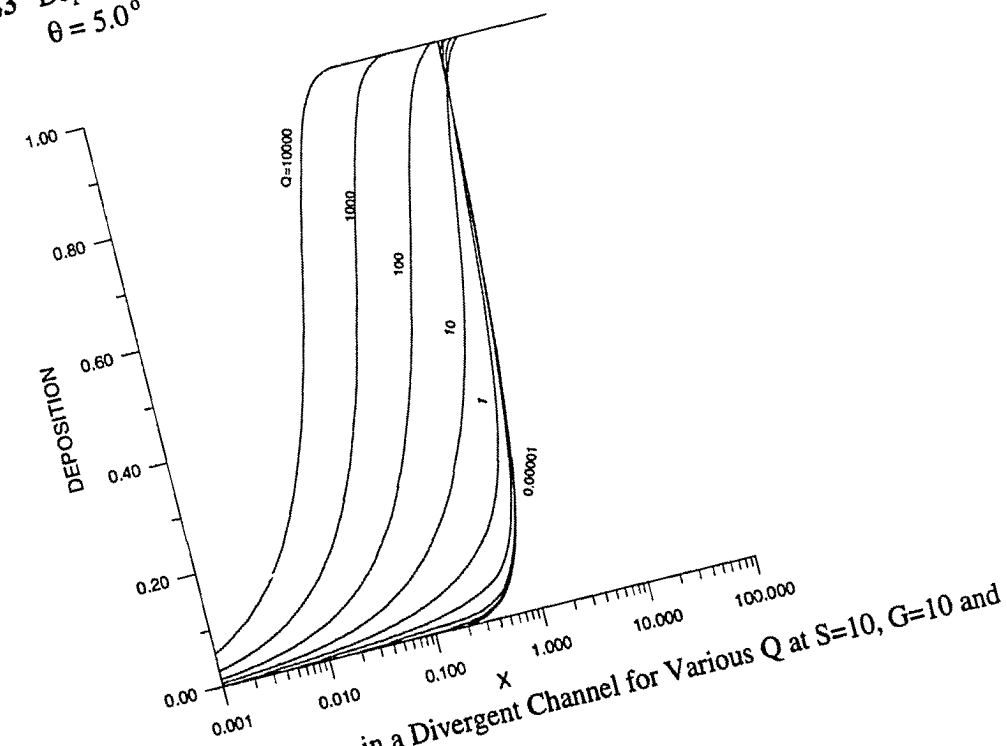

Figure 5.3.44 Deposition in a Divergent Channel for Various Q at S=10, G=10 and $\theta = 5.0^{\circ}$

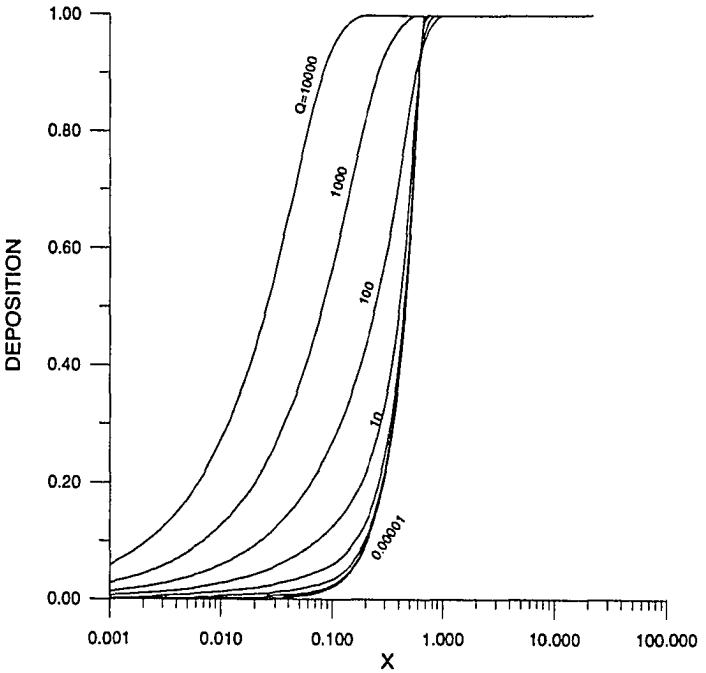

Figure 5.3.45 Deposition in a Divergent Channel for Various Q at S=10, G=100 and $\theta = 5.0°$

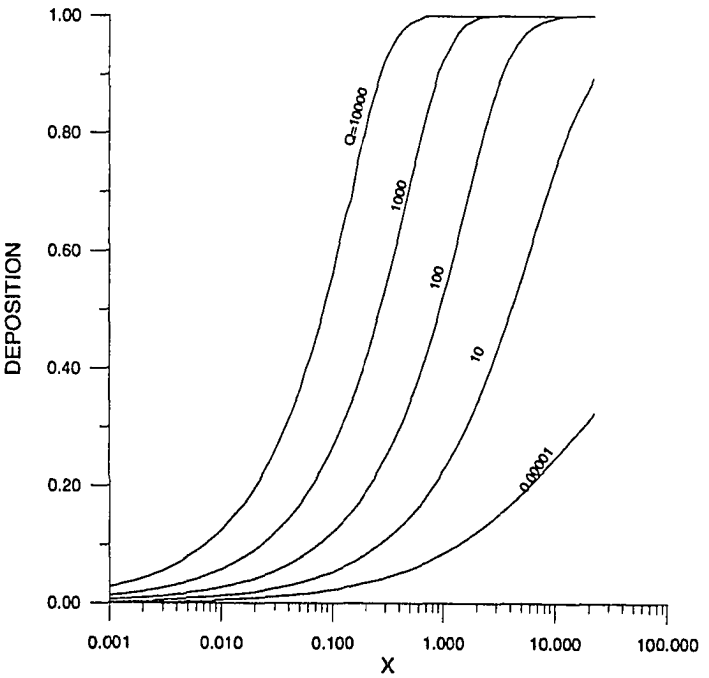

Figure 5.3.46 Deposition in a Divergent Channel for Various Q at S=100,G=0.01 and $\theta = 5.0°$

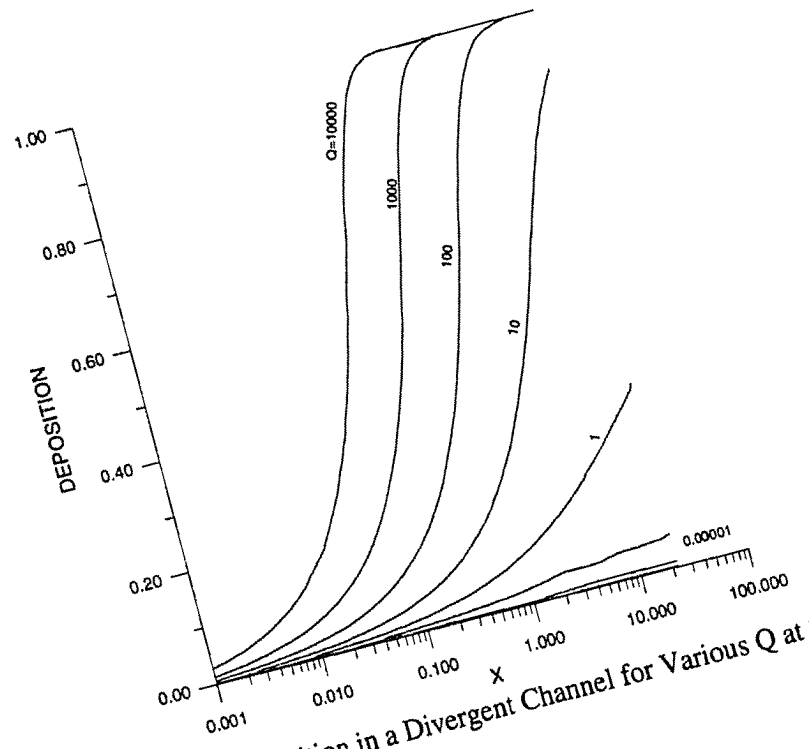

Figure 5.3.47 Deposition in a Divergent Channel for Various Q at S=100, G=0.1 and $\theta = 5.0^{o}$

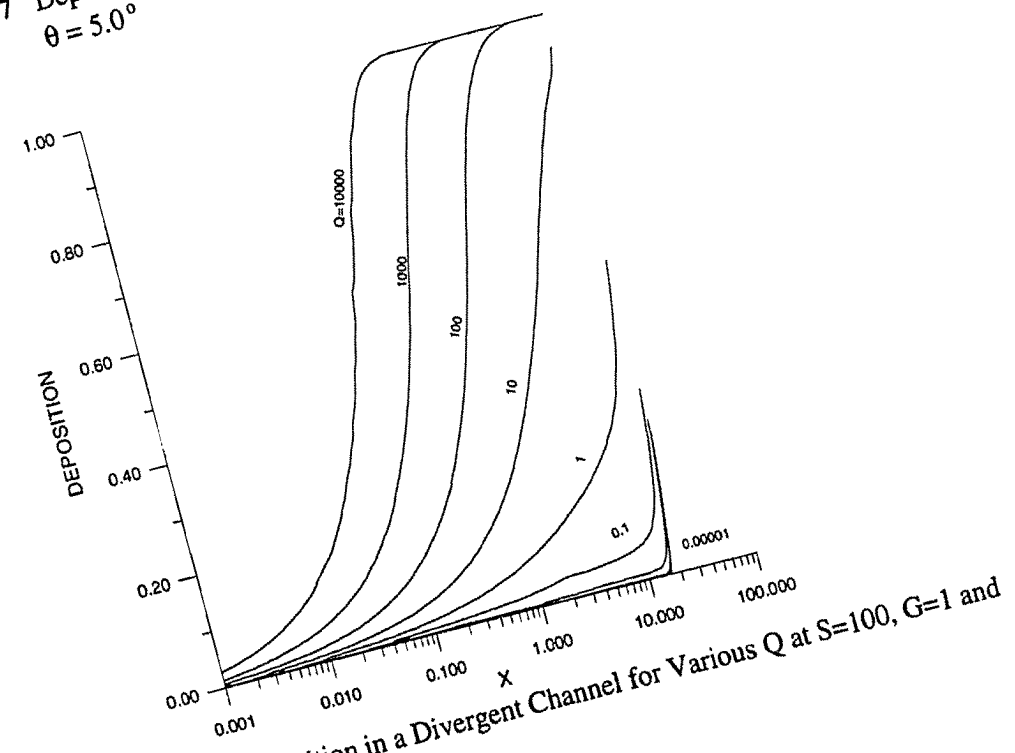

Figure 5.3.48 Deposition in a Divergent Channel for Various Q at S=100, G=1 and $\theta = 5.0^{o}$

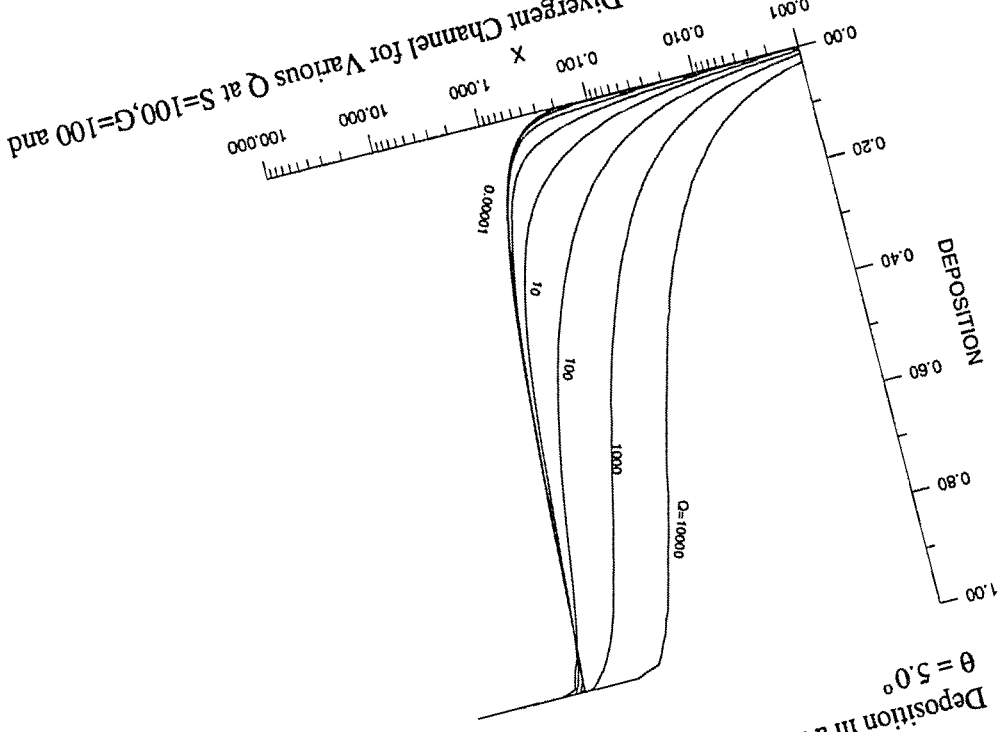

Figure 5.3.50 Deposition in a Divergent Channel for Various Q at S=100,G=100 and $\theta = 5.0^{o}$

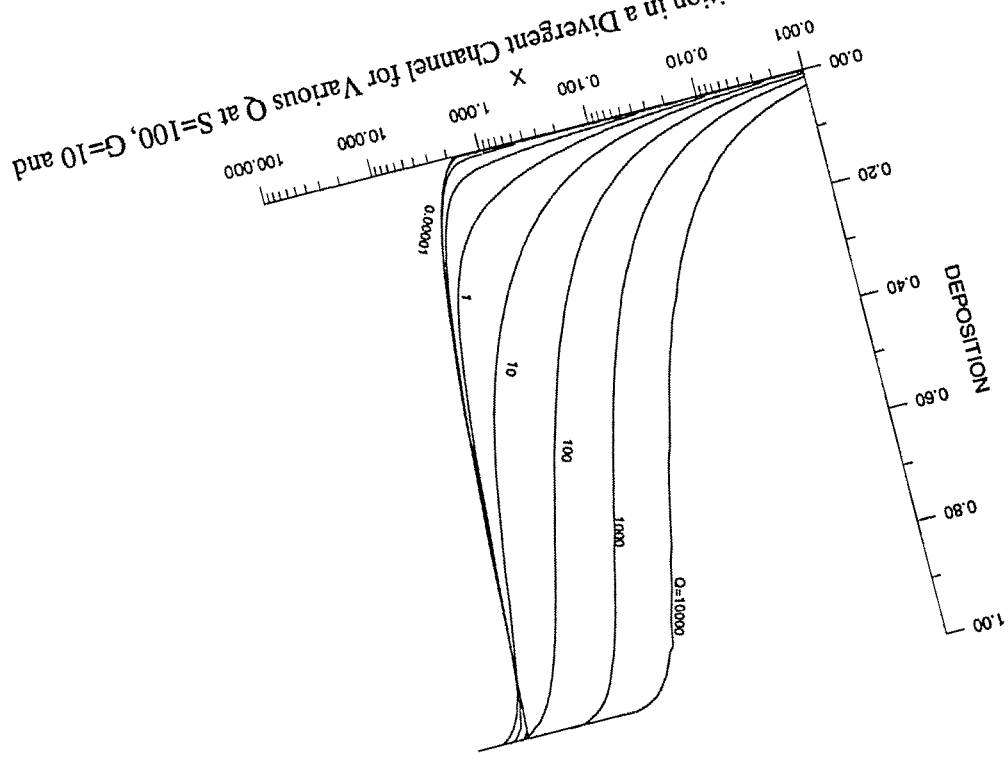

Figure 5.3.49 Deposition in a Divergent Channel for Various Q at S=100, G=10 and $\theta = 5.0^{o}$

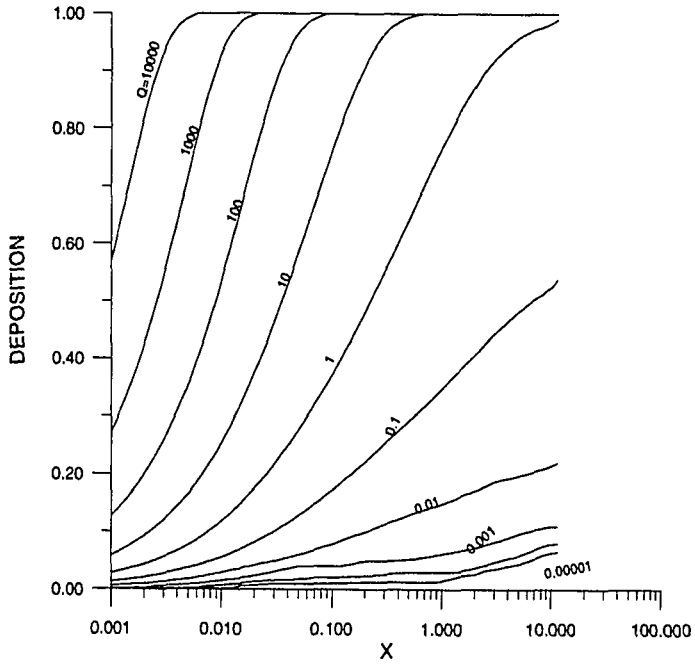

Figure 5.3.51 Deposition in a Divergent Channel for Various Q at S=0.01, G=0.01 and $\theta = 7.5°$

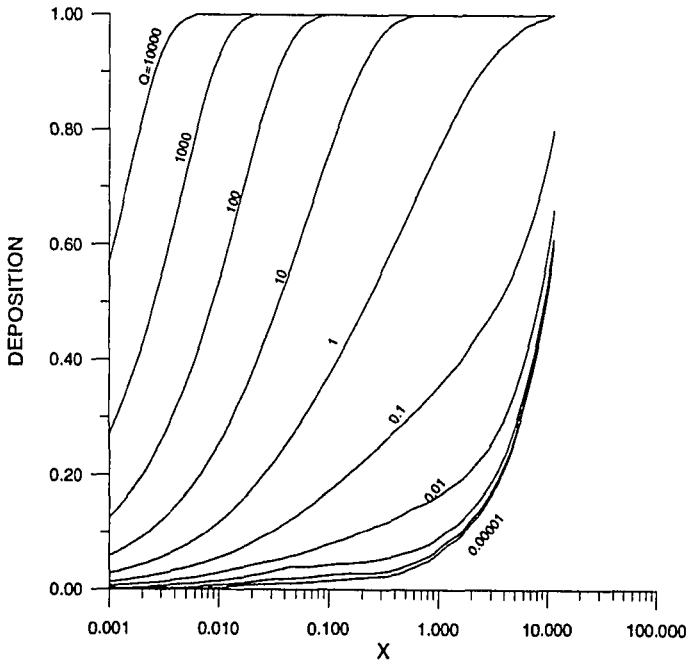

Figure 5.3.52 Deposition in a Divergent Channel for Various Q at S=0.01, G=0.1 and $\theta = 7.5°$

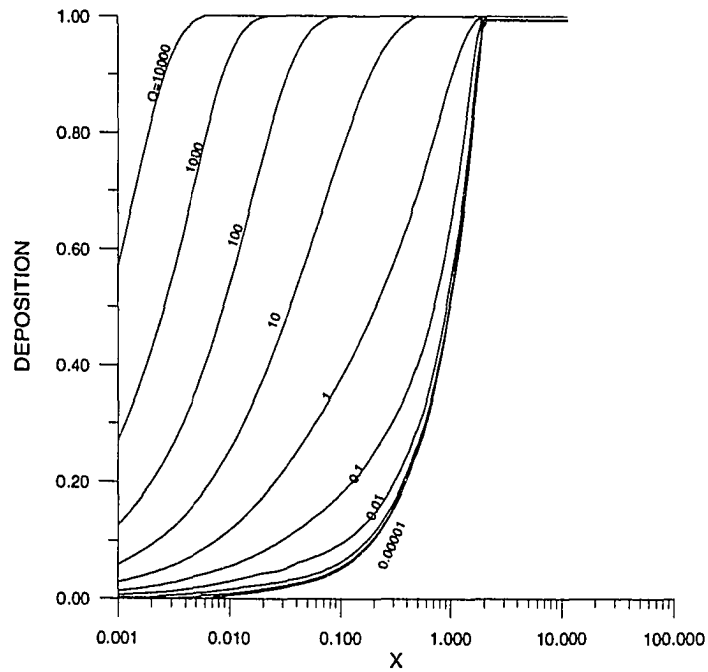

Figure 5.3.53 Deposition in a Divergent Channel for Various Q at S=0.01, G=1 and $\theta = 7.5°$

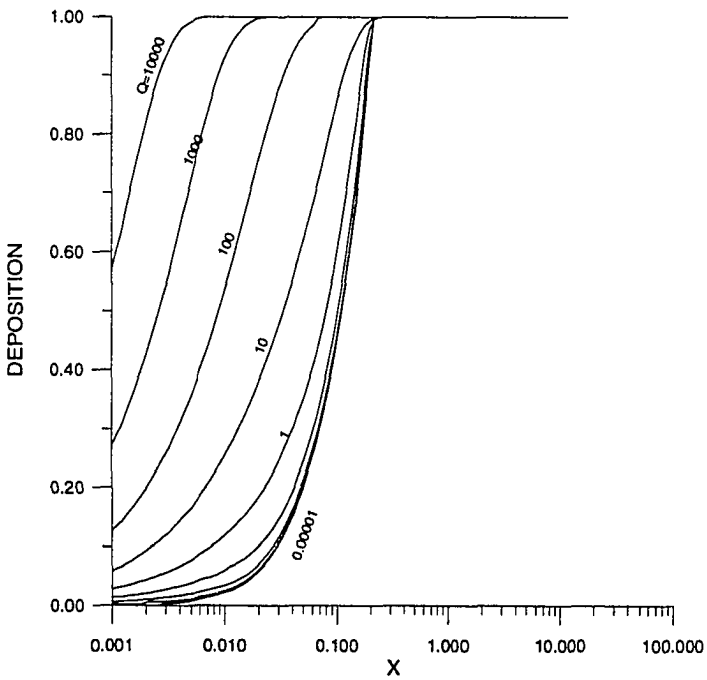

Figure 5.3.54 Deposition in a Divergent Channel for Various Q at S=0.01, G =1 and $\theta = 7.5°$

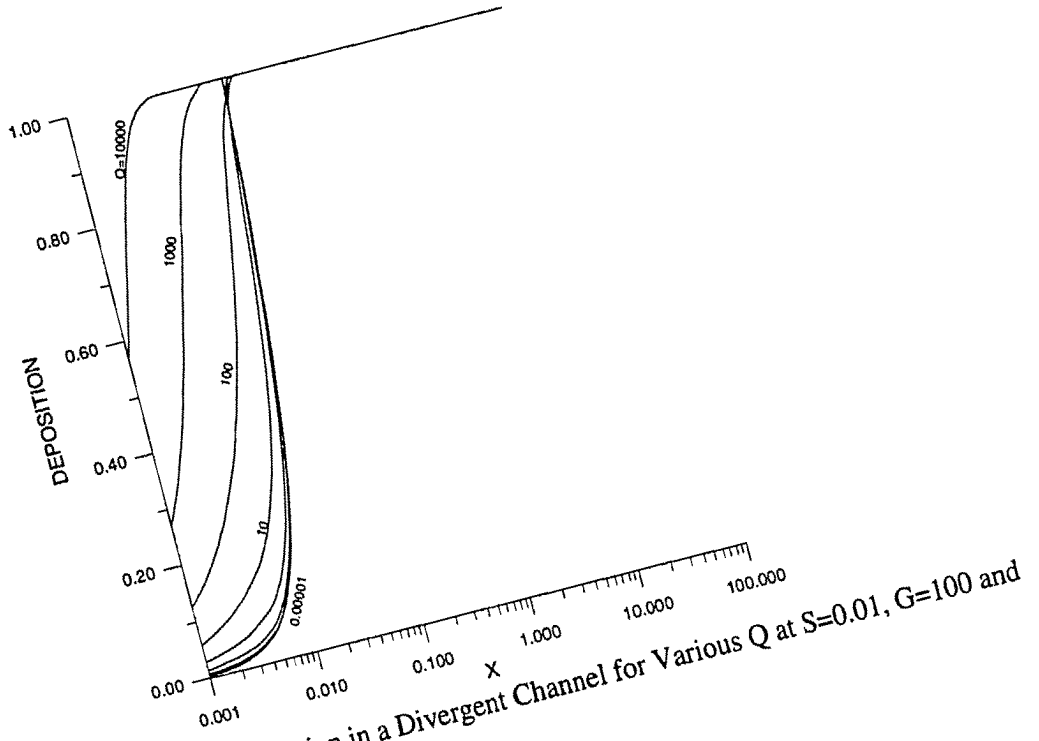

Figure 5.3.55 Deposition in a Divergent Channel for Various Q at S=0.01, G=100 and $\theta = 7.5°$

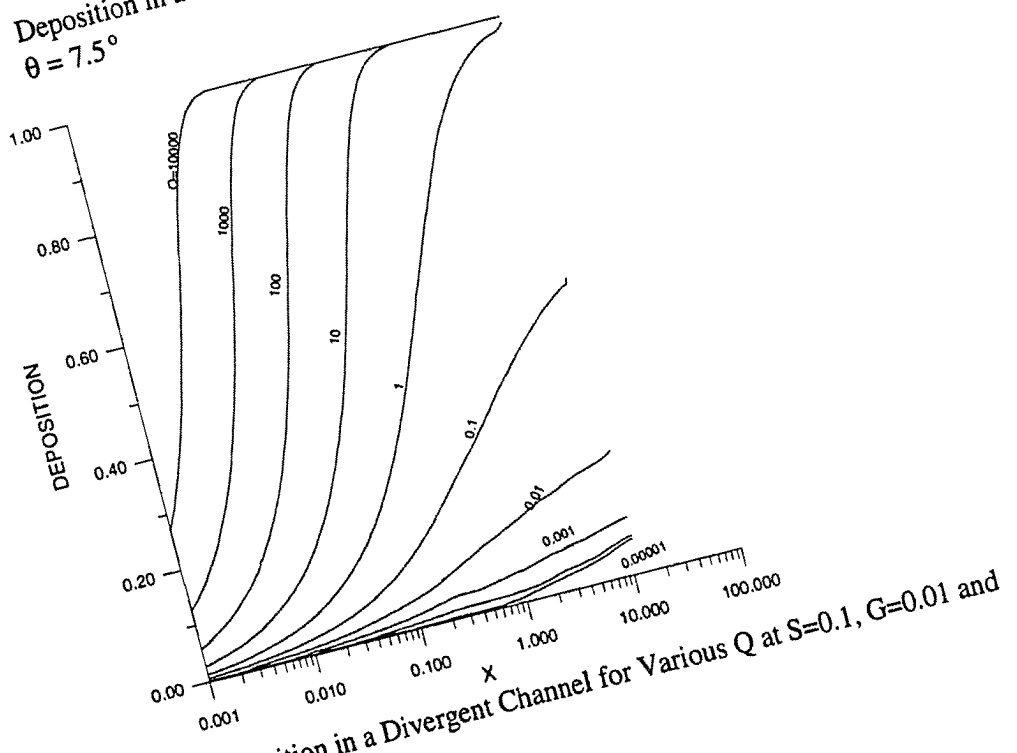

Figure 5.3.56 Deposition in a Divergent Channel for Various Q at S=0.1, G=0.01 and $\theta = 7.5°$

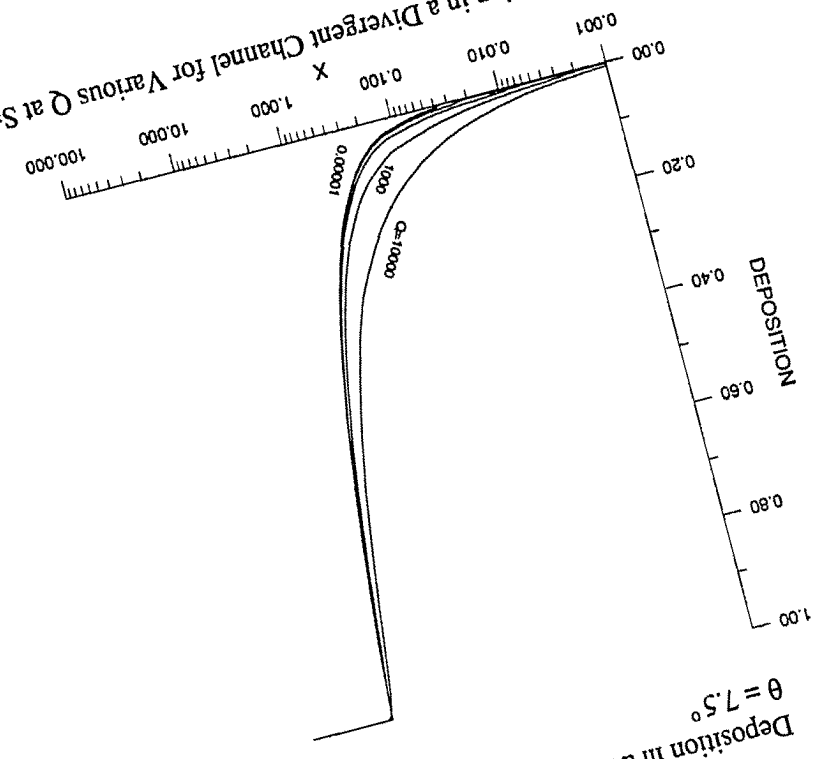

Figure 5.3.57 Deposition in a Divergent Channel for Various Q at S=0.1, G=0.1 and $\theta = 7.5^{o}$

Figure 5.3.58 Deposition in a Divergent Channel for Various Q at S=0.1, G=1 and $\theta = 7.5^{o}$

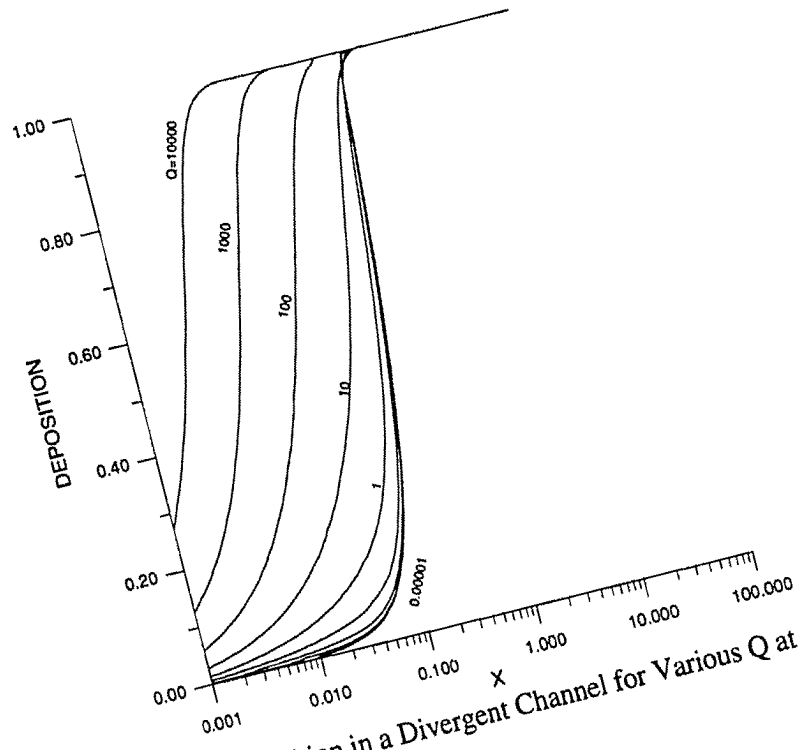

Figure 5.3.59 Deposition in a Divergent Channel for Various Q at S=0.1, G=10 and $\theta = 7.5°$

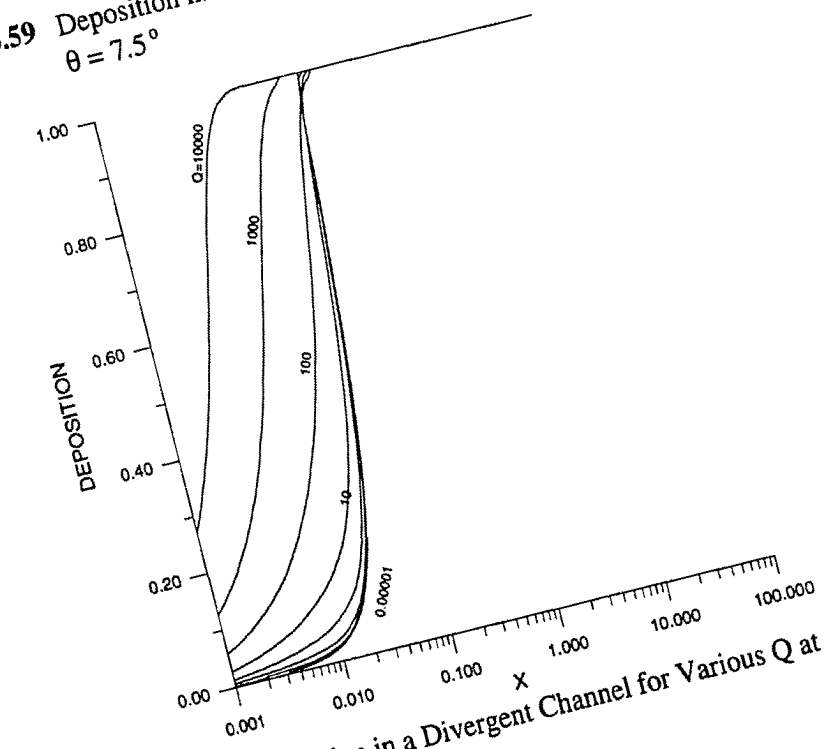

Figure 5.3.60 Deposition in a Divergent Channel for Various Q at S=0.1, G=100 and $\theta = 7.5°$

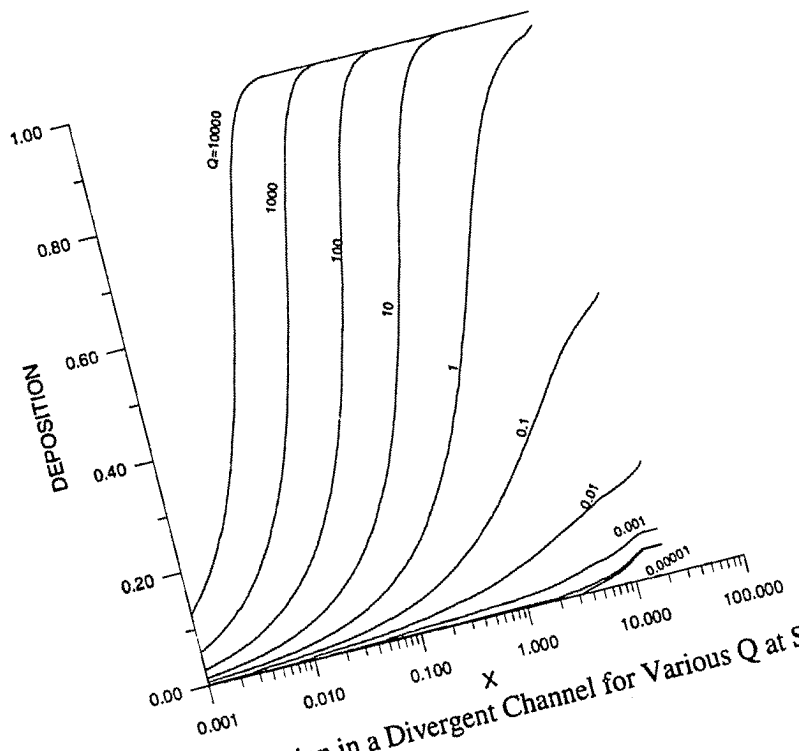

Figure 5.3.61 Deposition in a Divergent Channel for Various Q at S=1, G=0.01 and $\theta = 7.5^{\circ}$

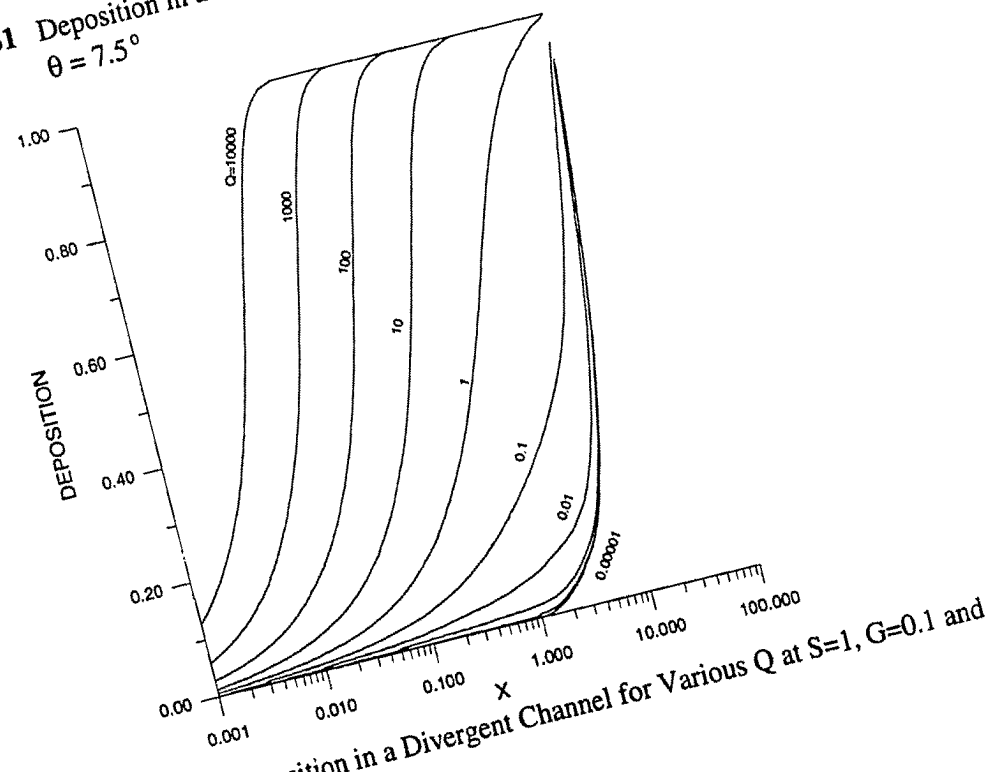

Figure 5.3.62 Deposition in a Divergent Channel for Various Q at S=1, G=0.1 and $\theta = 7.5^{\circ}$

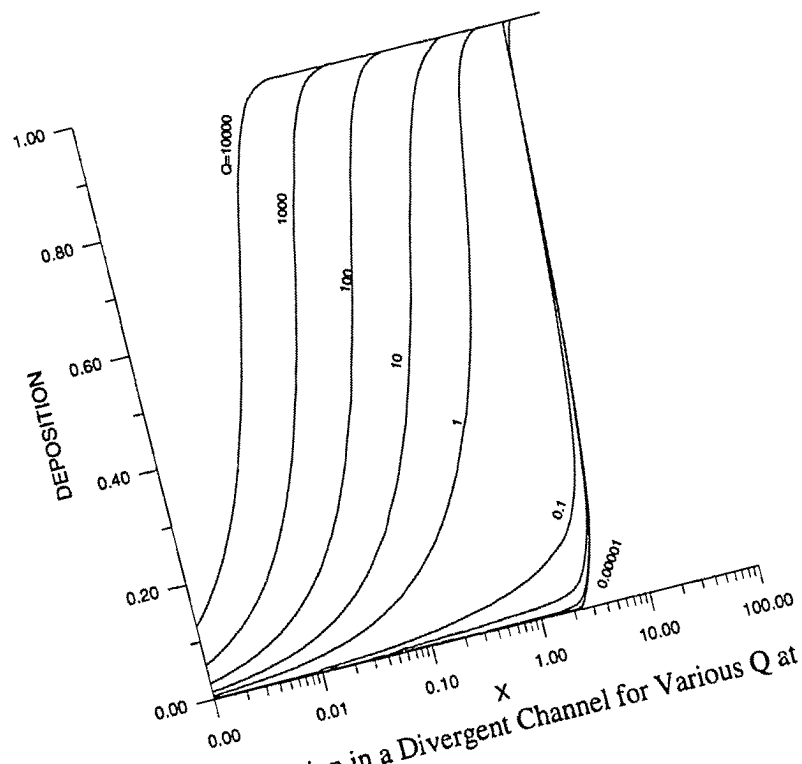

Figure 5.3.63 Deposition in a Divergent Channel for Various Q at S=1, G=1 and $\theta = 7.5°$

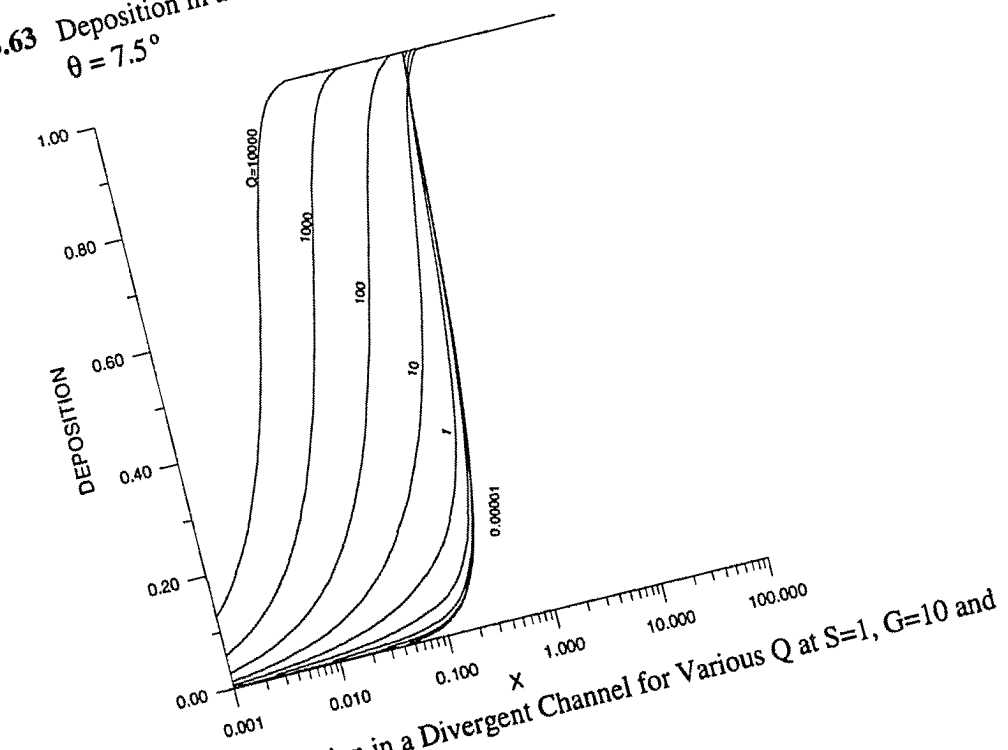

Figure 5.3.64 Deposition in a Divergent Channel for Various Q at S=1, G=10 and $\theta = 7.5°$

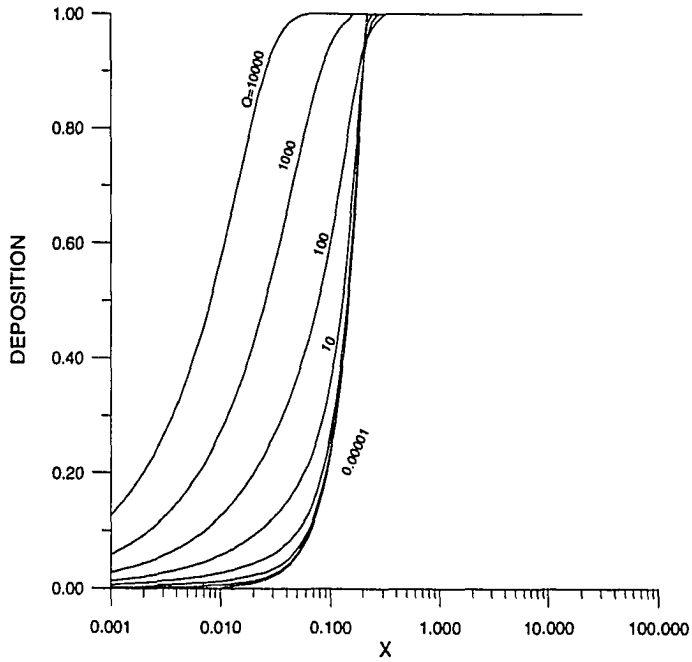

Figure 5.3.65 Deposition in a Divergent Channel for Various Q at S=1, G=100 and $\theta = 7.5°$

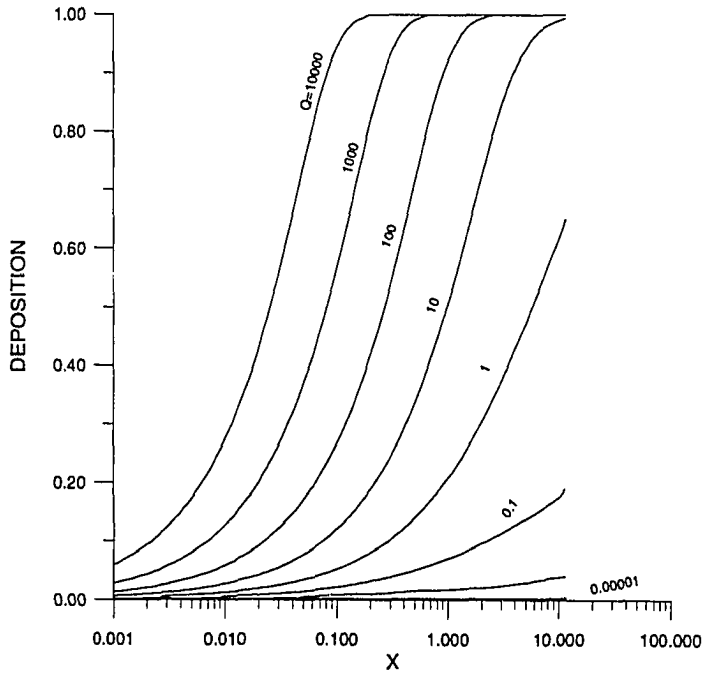

Figure 5.3.66 Deposition in a Divergent Channel for Various Q at S=10, G=0.01 and $\theta = 7.5°$

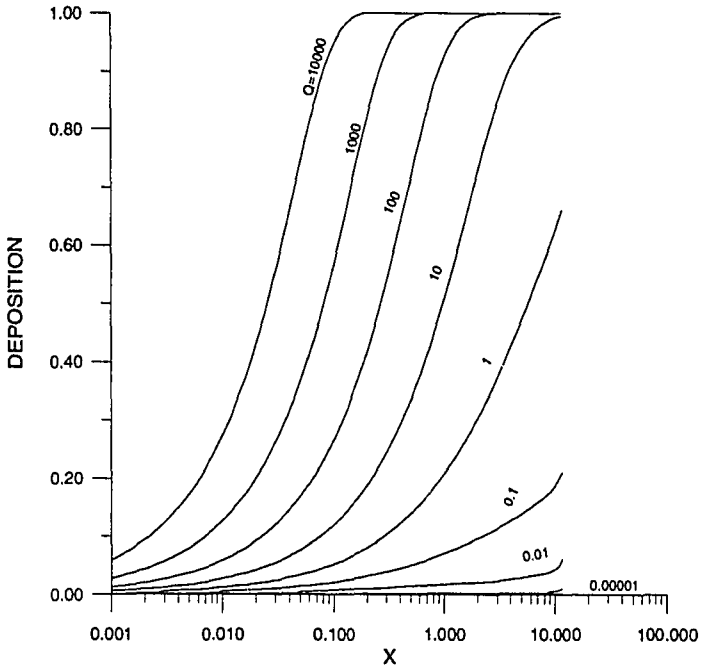

Figure 5.3.67 Deposition in a Divergent Channel for Various Q at S=10, G=0.1 and $\theta = 7.5°$

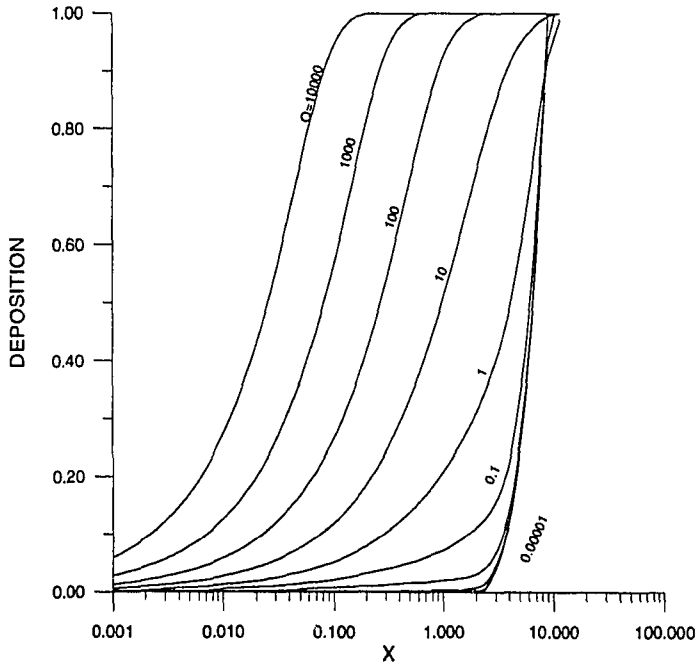

Figure 5.3.68 Deposition in a Divergent Channel for Various Q at S=10, G=1 and $\theta = 7.5°$

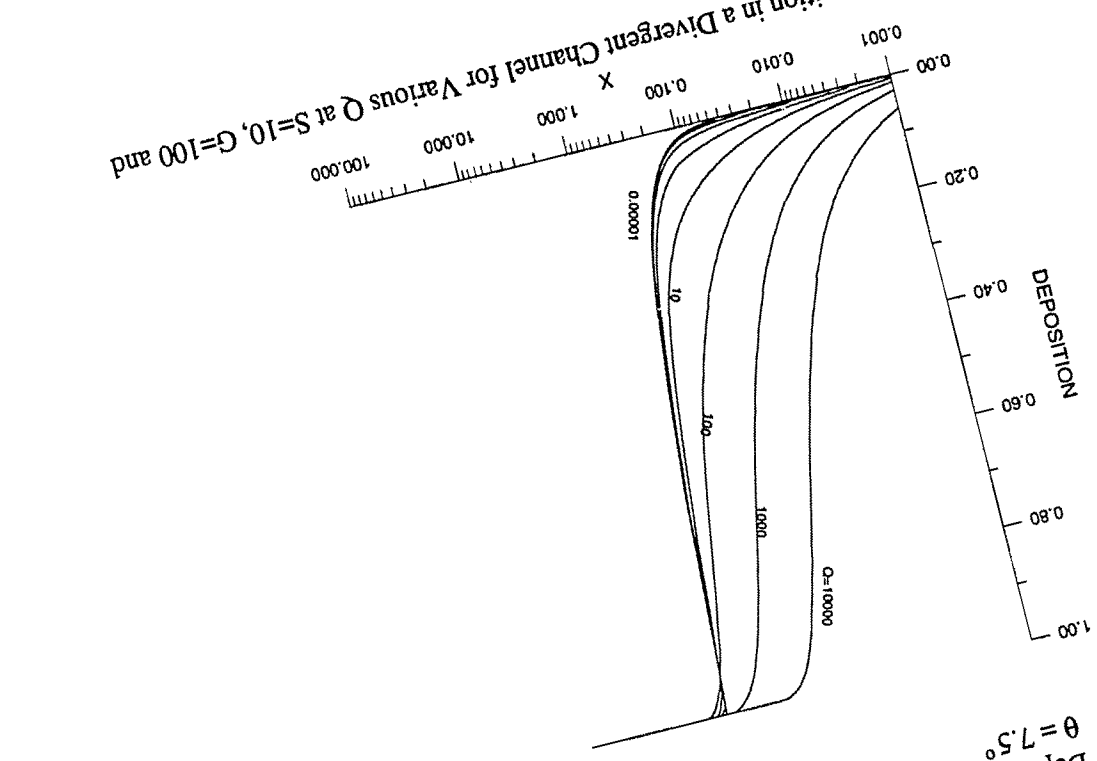

Figure 5.3.70 Deposition in a Divergent Channel for Various Q at S=10, G=100 and $\theta = 7.5^{o}$

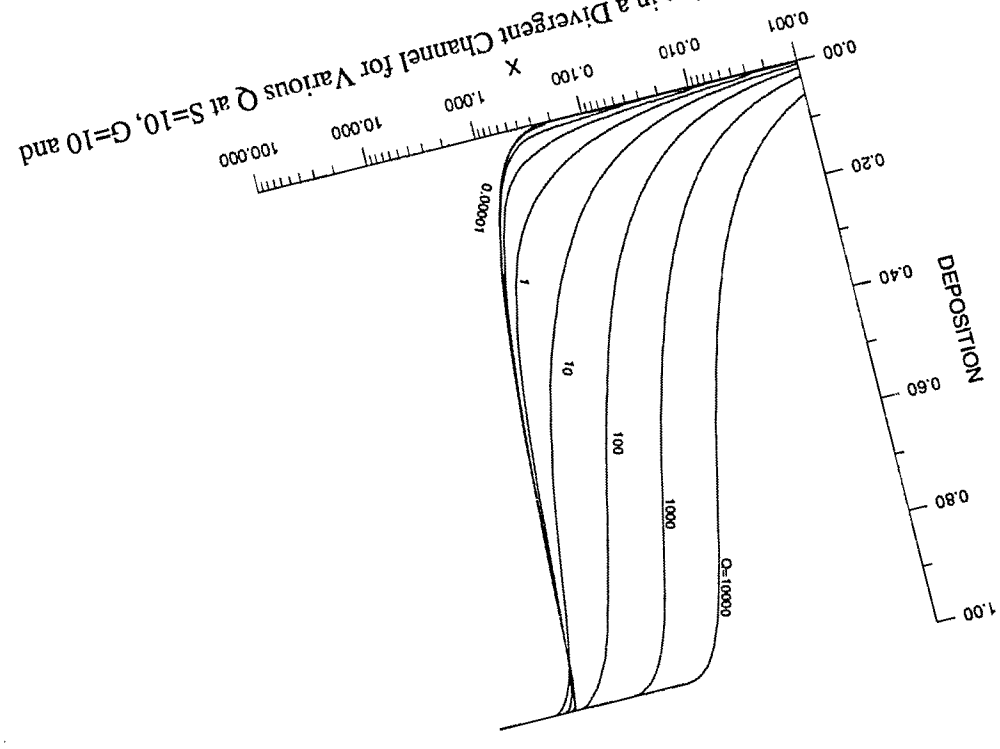

Figure 5.3.69 Deposition in a Divergent Channel for Various Q at S=10, G=10 and $\theta = 7.5^{o}$

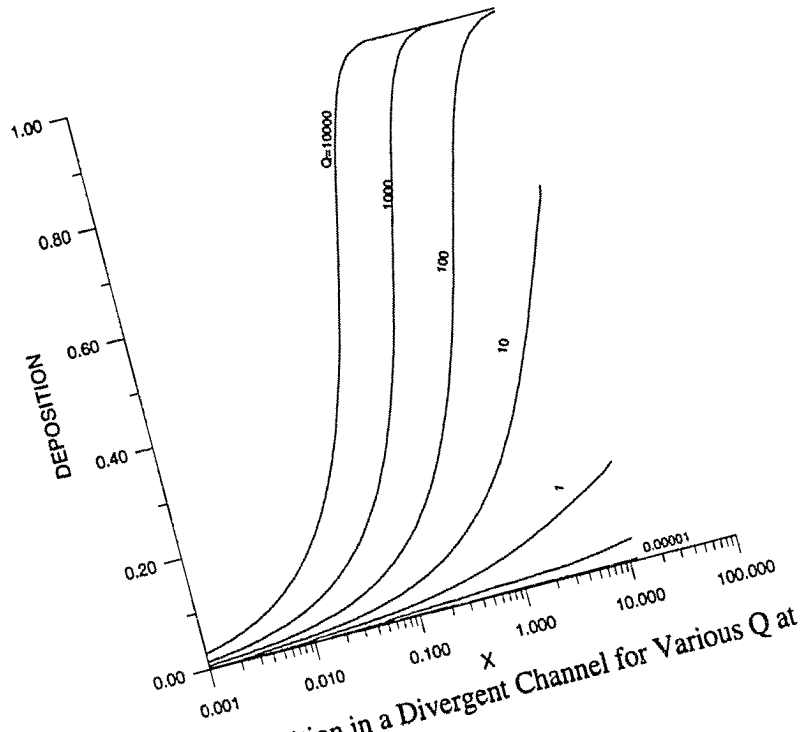

Figure 5.3.71 Deposition in a Divergent Channel for Various Q at S=100, G=0.01 and $\theta = 7.5°$

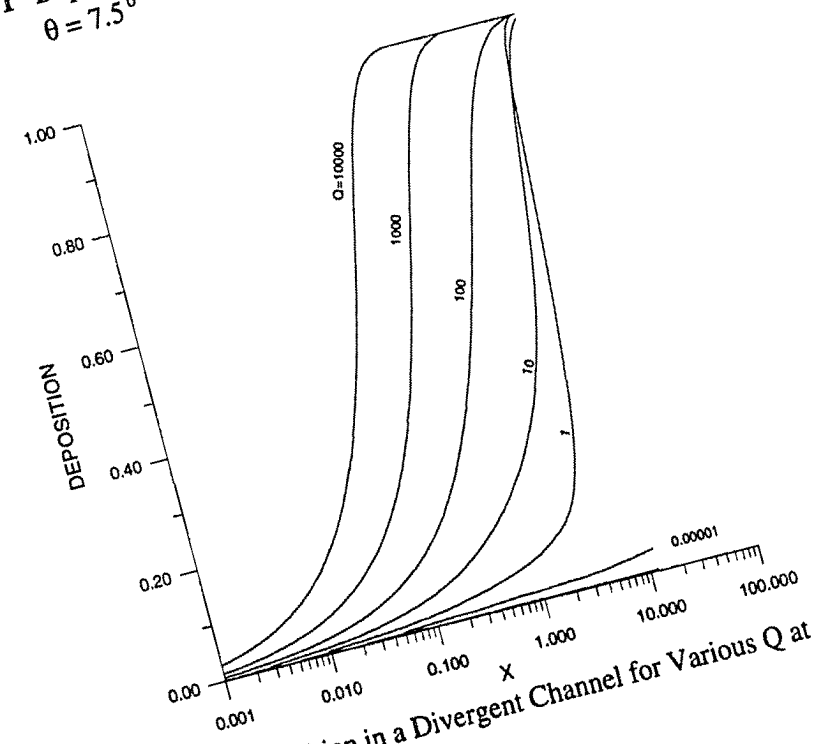

Figure 5.3.72 Deposition in a Divergent Channel for Various Q at S=100, G=0.1 and $\theta = 7.5°$

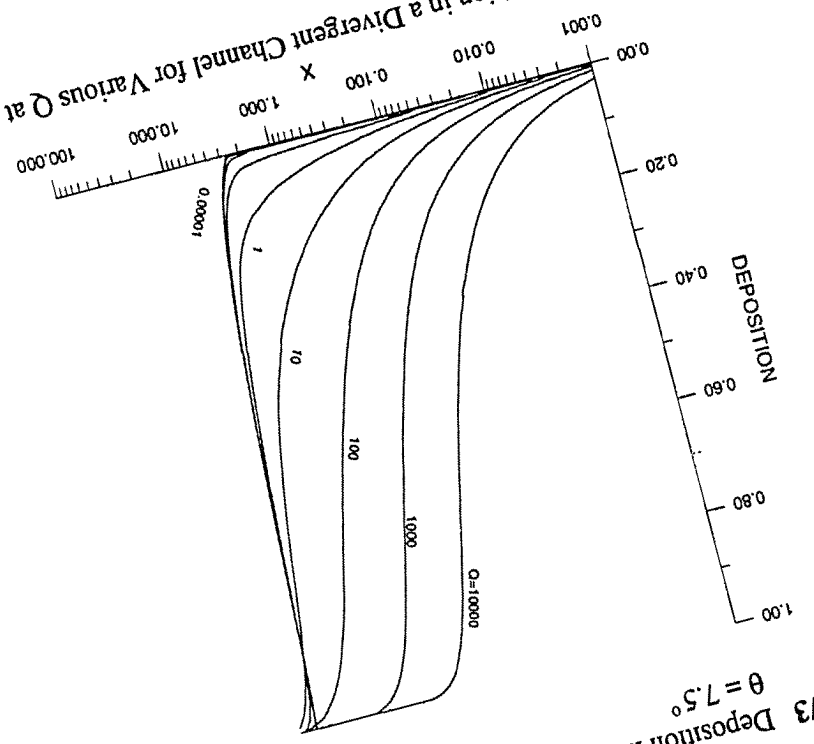

Figure 5.3.74 Deposition in a Divergent Channel for Various Q at S=100, G=10 and $\theta = 7.5^{o}$

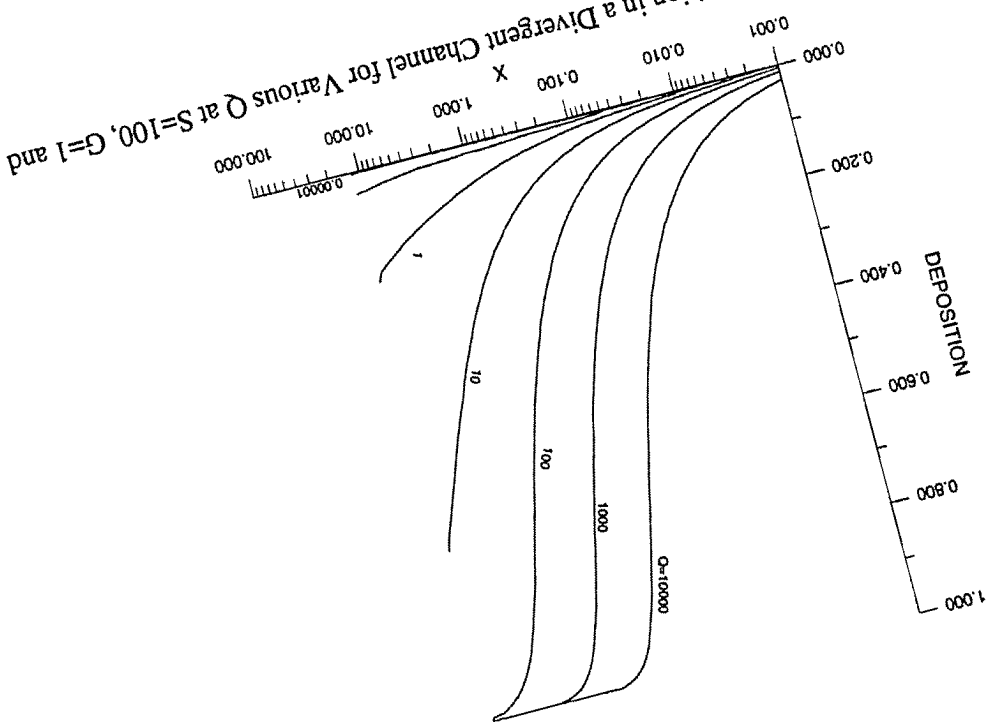

Figure 5.3.73 Deposition in a Divergent Channel for Various Q at S=100, G=1 and $\theta = 7.5^{o}$

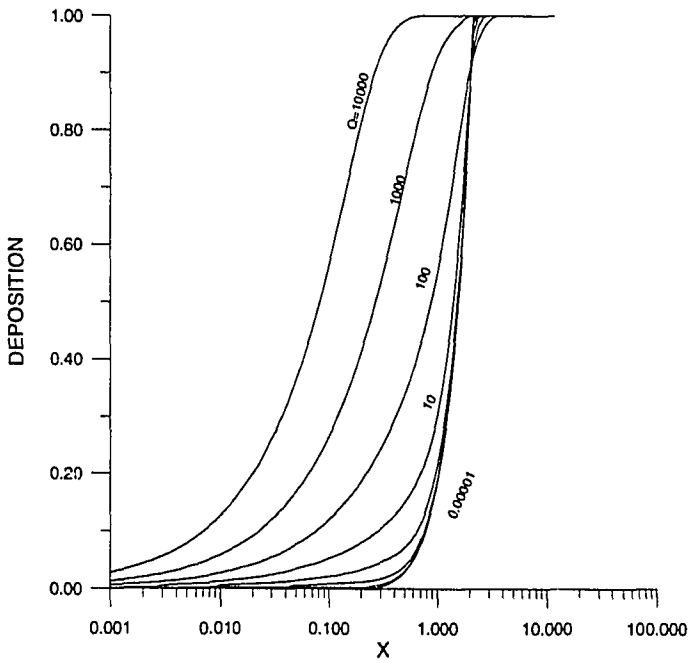

Figure 5.3.75 Deposition in a Divergent Channel for Various Q at S=100, G=100 and $\theta = 7.5°$

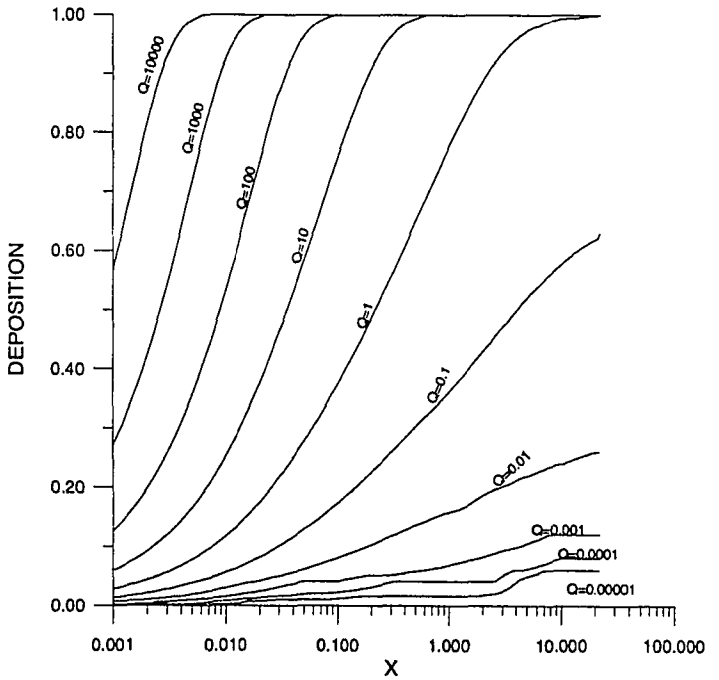

Figure 5.3.76 Deposition in a Divergent Channel for Various Q at S=0.01, G=0 and $\theta = 5.0°$

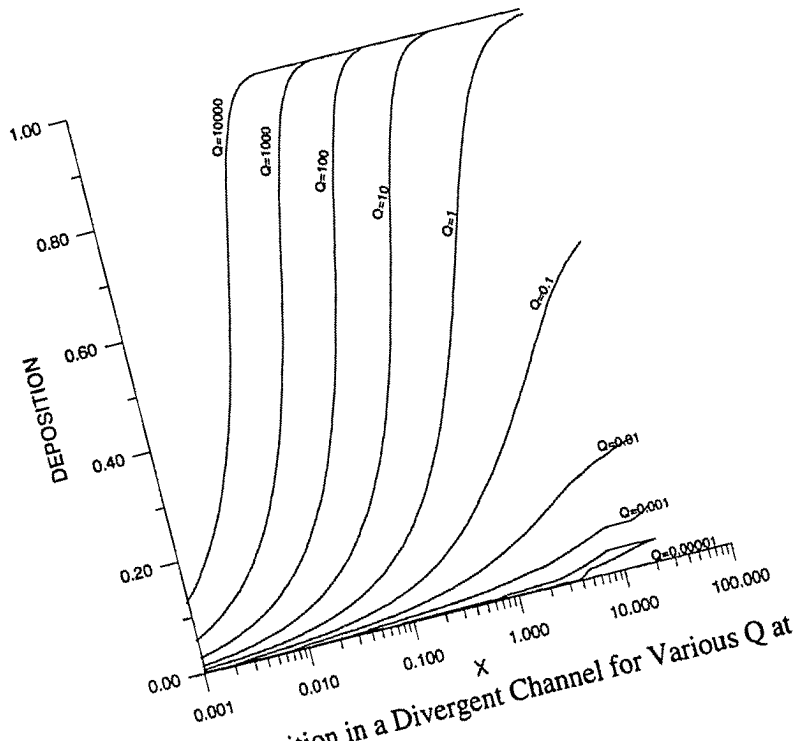

Figure 5.3.77 Deposition in a Divergent Channel for Various Q at S=1,G=0 and $\theta = 5.0^{\circ}$

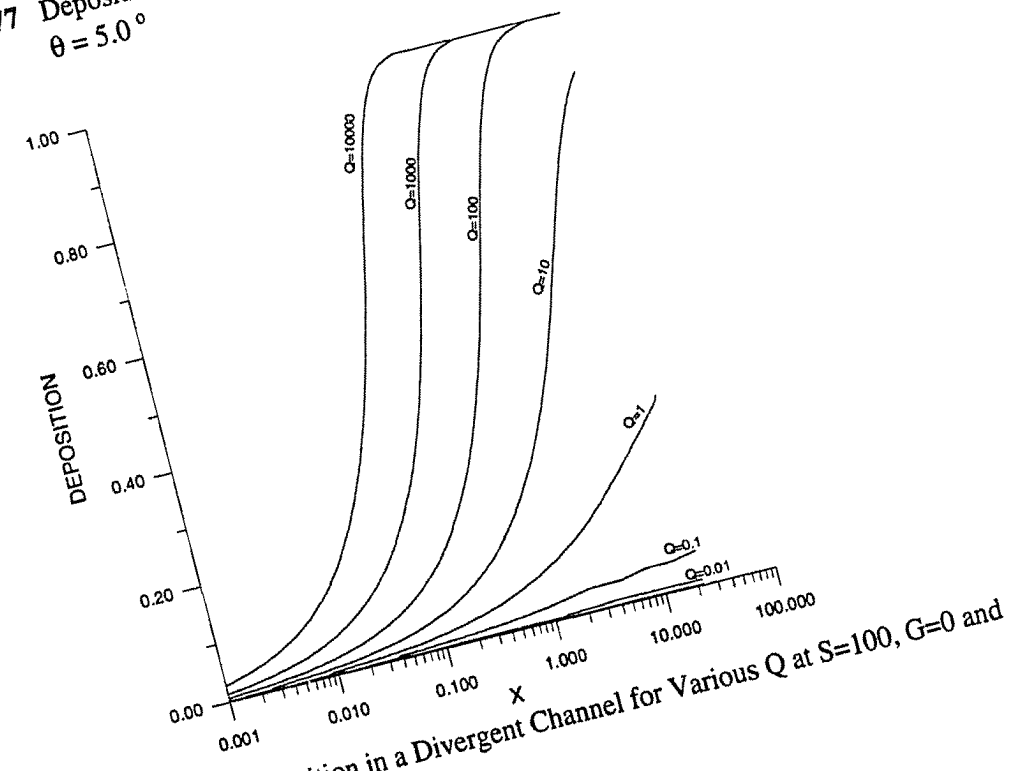

Figure 5.3.78 Deposition in a Divergent Channel for Various Q at S=100, G=0 and $\theta = 5.0^{\circ}$

REFERENCES

[1] Abuzeid, S., Busnaina, A. A. and Ahmadi, G., Wall Deposition of Aerosol Particles in a Turbulent Channel Flow, *J. of Aerosol Sci.* 1991 **22(1)** 43.

[2] Arastoopour, H., Pakdel, P. and Adewumi, M., Hydrodynamic Analysis of Dilute Gas-Solids Flow in a Vertical Pipe, *Powder Technology*, 1990 **62** 163

[3] Ayoub, A. M., and Kliuzing, G. E., Effect of Particle Size and Shape on Setting Using an Integral Approach, *Powder Technology*1983 **35** 63.

[4] Badekas, D., and Knight, D. D., Eddy Correlation for Laminar Axisymmetric Sudden Expansion Flows, *J. of Fluids Engineering*, ASME 1992 **114**.

[5] Bailey, A. G., Electrostatic Phenomena During Powder Handling, *Powder Technology* 1984 **37** 226.

[6] Baron, T., et al., Electrostatic Effects on Entrainment from a Fluidized Bed, *Powder Technology*, 1988 **57** 78.

[7] Biswas, P., Tian, Yi and Pratsinis, Sotiris E., Receptor Modeling of Microcontamination in Clean Rooms, *J. of Aerosol Sci.* 1989 **20(8)** 1361.

[8] Bush, P. V., and Snyder, T. R., Implications of Particulate Properties on Electrostatic Precipitator and Fabric Filter Performance, *Powder Technology* 1992 **72** 188.

[9] Burden, R. L., and Faires, J. D., *Numerical Analysis*, 3nd ed., PWS Publishers, New York, 1985.

[10] Chen, W. C., "Deposition of Particles in Tubes Due to Gravity and Electrostatic Charges", Doctoral Dissertation, New Jersey Institute of Technology, Newark, N.J. 1986.

[11] Chen, R. Y., Deposition of Aerosol Particles in a Channel due to Diffusion and Electric Charge, *J. of Aerosol Sci.* 1978 **9** 253.

[12] Chen, R. Y., Chiou, H. C., and Sun, D., Deposition of Particles in a Convergent Channel, *Powder Technology*, 1995.

[13] Chen, R. Y., and Gelber, M. W., Deposition of Particles in a Parallel Plate Channel due to Electrostatic Charge, Diffusion and Gravitational Effects, *Powder Tech.*, Vol.28 1981 **128** 43.

[14] Chen, R.Y., Pawel, H. E., and Chen, W. C., Inertia Effect on Deposition of Charged Particles in a Parallel-Plate Channel, *Powder Tech.* 1983 **38(2)** 249.

[15] Chen, R. Y., Hui, K. W., and Lu, C. H., A Theoretical Study of Deposition of Charged Particles in a Convergent Channel Due to Image Forces, *Powder Tech.* 1990 **61** 225.

[16] Chen, R. Y., et al, Deposition of Charged Particle in a Channel, *Powder Technology* 1993 **72** 121.

[17] Chow, C. Y., *An Introduction to Computational Fluid Mechanics*, John Wiley & Sons, Inc., New York 1979.

[18] Chung, T. J., *Finite Element Analysis in Fluid Dynamics*, McGraw Hill New York, 1978.

[19] Cooper, D. W., Particulate Contamination and Microelectronics Manufacturing: An Introduction, *Aero Sci. Technol.* 1986 **5** 287.

[20] Cooper, D. W., Peters, M. H., and Miller, R. J., Predicted Deposition of Submicron Particles due to Diffusion and Electrostatics in Viscous Axisymmetric Stagnation-point Flow, *Aero Sci. Technol.* 1989 **11** 55.

[21] Corn, M. The Adhesion of Solid Particles to Solid Surfaces, *J. Air Pollution Control Assoc.* 1961 11(1) 523 and 1961 **11(12)** 566.

[22] Crooke, P. S., and Walsh, R. A., The Flow of a Dusty Gas through an Infinitely Long Pipe, *Powder Technology* 1974 **9**.

[23] Crowley, J. M., *Fundamentals of Applied Electrostatics*, A Wiley-Interscience Publication John Wiley & Sons, New York 1986.

[24] Douglas, P. L., and S. Ilias, S., On the Deposition of Aerosol Particles on Cylinders in Turbulent Cross Flow, *J. of Aerosol Sci.* 1988 **19(3)** 451.

[25] Dry, R. J., et al., Two-Phase Theory and Fine Powders, *Powder Technology* 1983 **34**.

[26] Eldighidy, S. M., Chen, R. Y., and Conparin, R. A., Deposition of Suspensions in the Entrance of a Channel, *J. of Fluids Engrg.*, Trans. ASME 1977 **99(6)** 365.

[27] Fan, B., McFarland, A. R., and Anand, N. K., Characterization of The Aerosol Particle Lift Force, *J. of Aerosol Sci.* 1992 **23(4)** 379.

[28] Fan, F., and Ahmadi, G., A Sublayer Model For Turbulent Deposition of Particles in Vertical Dusts with Smooth and Rough Surfaces, *J. of Aerosol Sci.* 1993 **24(1)** 45.

[29] Fichman, M., Gutfinger, C., and Pnueli, D., A Model for Turbulent Deposition of Aerosols, *J. of Aerosol Sci.* 1988 **19(1)** 123.

[30] Flemmer, R. L. C., and Banks, C. L., On the Drag Coefficient of a Sphere, *Powder Technology* 1986 **48** 217.

[31] *FIDAP MANUAL*, REVISION5.0, Fluid Dynamics International, Inc. 1990.

[32] Friedlander, S. K., and Johnstone, H. F., Deposition of Suspended Particles from Turbulent Gas Streams, *Ind. and Eng. Chem.* 1957 **49(7)** 1151.

[33] Fuchs, N., The *Mechanics of Aerosols*, MacMillan Co, New York 1964.

[34] Geldart, D., and Rhodes, M. J., Survey of Current World-Wide Research in Gas Fluidization(January 1989-December 1991), *Powder Technology* 1992 **71**.

[35] Geldart, D., Estimation of Basic Particle Properties for Use in Fluid-Particle Process Calculations, *Powder Technology* 1990 **60**.

[36] Haider, A., and Levenspiel, O., Drag Coefficient and Terminal Velocity of Spherical and Nonspherical Particles, *Powder Technology* 1989 **58** 63.

[37] Harnwell, G. P., *Principles of Electricity and Electromaguetism*, McGraw-Hill Book Company, Inc., New York 1949.

[38] Hidy, G. M., *Aerosols - An Industrial and Environmental Science*, Academic Press, Inc., Drlando, FL 1984.

[39] Hughwark, G. A., Solid Particle Deposition from a Turbulent Gas Stream, *A. I. Ch. E. Journal* 1979 **18(2)**.327

[40] Ingham, D. B., Deposition of Charged Particles Near the Entrances of a Cylindrical Tube, *J. of Aerosol Sci.* 1979 **11** 47.

[41] Kalinske, A. A., and Van Driest, E. R., *Proceedings of Fifth International Congress on Applied Mechanics*, Mechanics, Cambridge, Mass. 1938 **416**.

[42] Kemp, L. C., Oakley, D. E., and Bahu, R. E., Computational Fluid Dynamics Modeling of Vertical Pneumatic Conveying Dryers, *Powder Technology* 1991 **65**.

[43] George E. Klinzing, G. E., *Gas-Solid Transport*, McGraw-Hill Book Company, New York 1981.

[44] Li, A., and Ahmadi, G., Deposition of Aerosols on Surfaces in a Turbulent Channel Flow, *Int. J. Engng Sci.* 1993 **31(3)** 435.

[45] Loureno, L. M., Riethmuller, M. L., and Essers, J. A., A Kinetic Approach to Gas-Particle Suspensions, *Gas-Solid Flows*, Edited by J. T. Jurewicz, ASME 1983.

[46] Mathews, J. H., *Numerical Methods - For Computer Science, Engineering, and Mathematics*, Prentice-Hall, Inc. Englewood Cliffs,NJ 1987.

[47] McLaughlin, J. B., Aerosol Particle Deposition in Numerically Simulated Channel Flow, *Phys. Fluids A 1* 1989 **7** 1211.

[48] Peddieson, J. J., The Hydrodynamics of Dust Collection, *Proceedings of the Annual Technical Meeting of the Institute of Environmental Sciences* 1972.

[49] Peddieson, J. J., Dust Collection at Moderate Void Fractions, *Proceedings of the Annual Technical Meeting of the Institute of Environmental Sciences* 1973.

[50] Pich, J. J., Theory of Gravitational Deposition of Particles from Laminar Flows in Channel, *J. Aerosol Sci.* 1972 **3** 351.

[51] Proudman, I., and Pearson, R. A., *Fluid J., Mech.* 1957 **2** 237.

[52] Putnam, A., Integrable Form of Droplet Drag Coefficient, *ARs J.* 1961 **31**.

[53] Puri, I. K., and Libby, P. A., On the Force of Droplets in Poiseuille Flow, *Phys. Fluids A 2* 1990 **7** 1281.

[54] Radovanovic, M., *Fluidized-Bed Combustion*, Hemisphere Publishing Corporation 1986.

[55] Ramarao, B. V., and Tien, C., Aerosol Deposition in Two-Dimensional Laminar Stagnation Flow, *J. of Aerosol Sci.* 1989 **20** 775.

[56] Ramarao, B. V., and Tien, C., Role of Basset Force on Particle Deposition in Stagnation Flow, *J. of Aerosol Sci* 1990 **21 (5)** 56.

[57] Rudinger, G., *Fundamentals of Gas-Particle Flow*, Elsevier Scientific Publishing Company New York 1980.

[58] Schlichting, H., *Boundary Layer Theory*, McGraw-Hill, New York 1979.

[59] Scott, P., and Mirza, M., A Finite Element Analysis of Laminar Flows Through Planar and Axisymmetric Abrupt Expansions, *Computers and Fluids* 1986 **14**.

[60] Shchukin, E. R., et al., Deposition of Aerosol Particles in Plane-parallel Channels at Different Wall Temperature, *J. Aerosol Sci.* 1990, **21(2)** 127.

[61] Soo, S. L., Comparisons of Formulations of Multiphase Flow, *Powder Technology* 1991 **66** 1.

[62] Soo, S. L., *Fluid Dynamics of Multiphase Systems*, Blaisdell Publishing Company, Waltham, MA, 1967.

[63] Soo, S. L., and Rodgers, L. W., Further Studies on the Electro-Aerodynamic Precipitator, *Powder Technology* 1971 **5**.

[64] Soo, S. L., and Tung, S. K., Pipe Flow of Suspensions in Turbulent Fluid, Electrostatic and Gravity Effects, *Appl. Sci. Res.* 1971 **24** 83.

[65] Soo,S. L., and Tung, S. K., Deposition and Entrainment in Pipe Flow of a Suspensions, *Powder Technology* 1992 **6** 283.

[66] Stukel, J. J., and Soo, S. L., Turbulent Flow of a Suspension into a Channel, *Powder Technology* 1968/1969 **2** 278.

[67] Taulbee, P. B., and Yu, C. P., Simultaneous Diffusion and Sedimentation of Aerosols in Channel Flow, *J. of Aerosol Sci.* 1995 **6** 433.

[68] Thiagarajan, V., and Yu, C. P., Sedimentation from Charged Aerosol Flows in a Parallel-Plate and Cylindrical Channels, *J. Aerosol Sci.* 1979 **10** 405.

[69] Turner, J. R., Fissan, H. J., and Liguras, D. K., Particle Deposition from Plane Stagnation Flow: Competition between Electrostatic and Thermophoretic Effects, *J. Aerosol Sci.*1988 **19(7)** 87.

[70] Wallis, G. B., *One-Dimensional Two-Phase Flow*, McGraw-Hill, Inc., New York 1969.

[71] Wang, C., Gravitational Deposition of Particle from Laminar Flows in Inclined Channels, *J. Aerosol Sci* 1975 **6** 191.

[72] Ye, Y., et al., Theromophoretic Effect of Particle Deposition on a Free Standing Semiconductor Wafer in a Clean Room, *J. Aerosol Sci.*1991 **22(1)** 33.

[73] Yu, C. P., Theories of Electrostatic Lung Deposition of Inhaled Aerosols, *Ann. Occup. Hyg.*, 1985 **29(2)** 216.

[74] Yu, C. P., and Chandra, K., Precipitation of Submicron Charged Particles in Human Lung Airway, *Bulletin of Mathematical Biology* 1977 **39** 471.

[75] Zhou, L. X., and Soo, S. L., On Boundary Conditions of Particle Phase and Collection Efficiency in Cyclones, *Powder Technology* 1991 **64**.

[76] Zhu, C., and S. L. Soo, S. L., A Modified Theory for Electrostatic Probe Measurements of Particle Mass Flows in Dense Gas-solid Suspensions, *J. Appl. Phys.* 1992 **72(5)** 115.

[77] Zienkiewicz, O. C., *The Finite Element Method in Engineering Science*, McGraw-Hill, London 1971.